① Mechanics

② Machine Building and Machine Science

③ Information Technology, Computer Science, and Management

VESTNIK
of
DON STATE TECHNICAL UNIVERSITY

Vol. 20, № 2

*Founder and publisher ─ Federal State Budgetary Educational Institution of Higher Education
Don State Technical University (DSTU)*

Included in the list of peer-reviewed scientific editions where the basic research results of doctoral, candidate's theses should be published (State Commission for Academic Degrees and Titles List) in the following research areas:

01.02.01 – Analytical Mechanics (Engineering Sciences)
01.02.04 – Deformable Solid Mechanics (Engineering Sciences)
01.02.04 – Deformable Solid Mechanics (Physicomathematical Sciences)
01.02.06 – Dynamics, Strength of Machines, Gear, and Equipment (Engineering Sciences)
05.02.02 – Engineering Science, Drive Systems and Machine Parts (Engineering Sciences)
05.02.04 – Machine Friction and Wrear (Engineering Sciences)
05.02.07 – Technology and Equipment of Mechanical and Physicotechnical Processing (Engineering Sciences)
05.02.08 – Engineering Technology (Engineering Sciences)
05.02.10 – Welding, Allied Processes and Technologies (Engineering Sciences)
05.02.11 – Testing Methods and Diagnosis in Machine Building (Engineering Sciences)
05.13.11 – Software and Mathematical Support of Machines, Complexes and Computer Networks (Engineering Sciences)
05.13.17 – Foundations of Information Science (Engineering Sciences)
05.13.18 – Mathematical Simulation, Numerical Methods and Program Systems (Engineering Sciences)

CONTENTS

IN HONOUR OF THE SCIENTIST

21 June, 2020, professor Rudolf Anatolievich Neidorf, a remarkable scientist, engineer and organizer, Dr.Sci. (Engineering), died unexpectedly at the age of 76. He would have turned 76 years old 17 October.

Rudolf Anatolievich Neidorf was an expert in the field of automatic and automated systems, well-known in Russia and abroad. R.A. Neidorf embarked upon his scientific career at Novocherkassk Polytechnic Institute (SRSTU, Novocherkassk) as an expert in the automation of chemical technology processes, and he continued his activities at Rostov State Agricultural Academy and Don State Technical University (DSTU).

R.A. Neidorf's main area of expertise was the automatic control theory, in particular, development of the methodology for the structure synthesis of nonlinear automatic control systems. This is a complicated research area at the intersection of intuition, art and mathematics which requires nonstandard ideas and scientific courage to stand up for them. R.A. Neidorf's PhD and habilitational theses, monographs, scientific publications and scholary papers, as well as the dissertations of many of his disciples, are devoted to the research in this area. A wide range of scientific interests of R. A. Neidorf included also tasks and methods of mathematical modeling, optimization, and information processing. R.A. Neidorf developed these problems together with his graduate students. The joint research results were recorded in the publications and manuals.

The results of the theoretical and R&D work of Rudolf Anatolievich were tested at the major Russian and foreign scientific conferences and introduced into production. One of the examples is the method of experimental building of mathematical models of highly nonlinear systems proposed by R. A. Neidorf and a group of young scientists. The solution found application in the selection of structural elements of the MAAT transport system (Multibody Advanced Airship for Transport) (2012–2015). It was the basis for a scientific project on the theoretical underpinning of the method of experimental building of mathematical models and its implementation in scientific practice under a grant from the Russian Foundation of Fundamental Research.

R.A. Neidorf made a significant contribution to the development of engineering education in Russia, the improvement of the educational process, the training of engineering and scientific top-qualification brainpower. Two Dr.Sci. and more than twenty Cand.Sci. in the field of mathematical modeling, control theory, and operation research methods, trained by Rudolf Anatolievich, work at the universities and enterprises of the Rostov region.

R.A. Neidorf organized the training of engineering personnel majoring in "Management and IT in Engineering Systems", scientific brainpower majoring in "Information Systems Software and Administration" and "Software Engineering" in DSTU.

In 2002–2005 and 2006–2013, R.A. Neidorf was Head of the "Information and Control Systems" Department, Rostov State Agricultural Academy, and "Computer and Automated Systems Software" Department, DSTU. He made a great contribution to the scientific activities of the higher educational institutions, which later merged into a regional basic university, DSTU, and intensified R&D in the field of information control problems. R.A. Neidorf, in particular, developed optimization methods, control laws for various engineering systems, as well as search heuristic problem algorithms; he established the priority of R&D in this area.

At that time, he forged close links with the "Engineering Systems Control" Department, Kislovodsk Humanitarian Technical Institute, and the "Automated Information Systems" Department, Ukhta State Technical University, and organized visiting professorship. Lately, he had done a lot of work at the Center for Scientific Competence while developing methods for training top-qualification brainpower.

Since 1996, R.A. Neidorf headed the specialized Dissertation Board D.212.058.02. In 2010, he organized the annual seminar-conference "System Analysis, Management and Information Processing". Rudolf Anatolievich was a member of two editorial boards: "Vestnik of Don State Technical University" and the collection of research papers of the seminar-conference organized by him. R.A. Neidorf was author and co-author of more than 500 scientific publications including 5 monographs (3 foreign ones), 12 textbooks and teaching aids, more than 70 patents and copyright certificates.

Not many people know that Rudolf Anatolievich was a poet and editor of the monthly *Ataman News*, author of 158 poetical compositions.
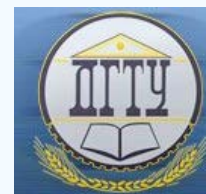
Vestnik of Don State Technical University. 2020. Vol. 20, no. 2, pp. 118–124. ISSN 1992-5980 eISSN 1992-6006

MECHANICS

UDC 539.3

https://doi.org/10.23947/1992-5980-2020-20-2-118-124

Transverse vibrations of a circular bimorph with piezoelectric and piezomagnetic layers

A. N. Solov'ev, Do Thanh Binh, O. N. Lesnyak
Don State Technical University (Rostov-on-Don, Russian Federation)

Introduction. Transverse axisymmetric oscillations of a bimorph with two piezo-active layers, piezoelectric and piezomagnetic, are studied. This element can be applied in an energy storage device which is in an alternating magnetic field. The work objective is to study the dependence of resonance and antiresonance frequencies, and electromechanical coupling factor, on the geometric parameters of the element.
Materials and Methods. A mathematical model of the piezoelement action is a boundary value problem of linear magneto-electro-elasticity. The element consists of three layers: two piezo-active layers (PZT-4 and $CoFe_2O_4$) and a centre dead layer made of steel. The finite element method implemented in the ANSYS package is used as a method for solving a boundary value problem.
Results. A finite element model of a piezoelement in the ANSYS package is developed. Problems of determining the natural frequencies of resonance and antiresonance are solved. Graphic dependences of these frequencies and the electromechanical coupling factor on the device geometrics, the thickness and radius of the piezo-active layers, are constructed.
Discussion and Conclusions. The results obtained can be used under designing the working element of the energy storage device due to the action of an alternating magnetic field. The constructed dependences of the eigenfrequencies of the resonance and antiresonance on the geometric parameters of the piezoelement provide selecting the sizes of the piezo-active layers for a given working frequency with the highest electromechanical coupling factor.

Keywords: energy storage device, piezoelectrics, piezomagnetics, finite element method, natural oscillation frequencies.

For citation: A. N. Solov'ev, Do Thanh Binh, O. N. Lesnyak. Transverse vibrations of a circular bimorph with piezoelectric and piezomagnetic layers. Vestnik of DSTU, 2020, vol. 20, no. 2, pp. 118–124. https://doi.org/10.23947/1992-5980-2020-20-2-118-124

Funding information: the research is done with the support from the RF Ministry of Education and Science (project part of state order no. 9.1001.2017/ПЧ) and the Government of the Russian Federation (contract no. 075-15-2019-1928).

Introduction. In the development of sensor and measuring systems, modern small-sized household appliances, cellphones and wireless sensor systems, powerful sources of energy are not required for monitoring and diagnosing the technical condition of various objects, but mobility and nonvolatility of the above devices are mandatory. Energy storage devices with piezo-active elements that directly convert the energy of mechanical vibrations into electrical energy are widely used to power this kind of apparatus. In [1-3], energy storage devices using piezoelectric generators under the action of mechanical loads are studied.

If the system is in an alternating magnetic field created by permanent magnets mounted on rotating parts of the machine, then the piezomagnetic layer is deformed along with the piezoelectric element. Due to this, an electric current is generated. In [7,8], Guo-Liang Yu and others discussed theoretical models of multilayer magnetoelectric composites for the magnetoelectric response at resonant frequencies corresponding to vibrations of the bending and extensional modes. A theoretical model of magnetic energy collectors using a functionally gradient composite cantilever was analyzed to improve the collecting ability and adjust the resonance frequency in [9]. In [10], Y.F. Zhanga and others studied bifurcations, periodic and chaotic dynamics of a tetrahedral composite multilayer piezoelectric rectangular plate

http://vestnik.donstu.ru

118

with simple supports. In [11], bending and free vibrations of a magnetoelectroelastic plate with surface effects were studied.

In this paper, axisymmetric vibrations of the device are considered. The effect of the radius and thickness of the piezoelectric and piezomagnetic plates on the frequency characteristics of the device (eigenfrequencies of resonance and antiresonance) and on the efficiency of the conversion of vibratory energy into electrical energy, which is characterized by an electromechanical coupling factor, is studied. As a method for solving the problem, the finite element method implemented in the ANSYS package is selected.
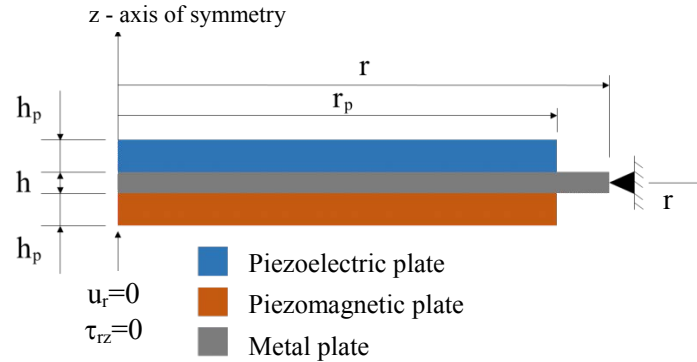
Fig. 1. Scheme of half axial section of piezoelectric generator

The energy storage device under consideration is an axisymmetric design, which consists of a metal disk (substrate) with two piezoelectric layers glued on it (Fig. 1). The top layer is piezoelectric; the bottom one is piezomagnetic. The flat surfaces of the piezoelectric layer are covered with electrodes that are connected to an external electrical circuit, or one of the electrodes is free while the other is set to zero electric potential. The piezomagnetic layer is affected by an alternating magnetic field according to the harmonic law; the outer radius of the substrate is pivotally fixed. The mathematical model of transverse steady-state vibrations of the described construction is the boundary-value problem of the linear theory of piezo-magnetoelectric elasticity [4]. The ANSYS package, which implements a piezoelectric model, is selected as a solution tool.

The boundary value problem for a piezo-magnetoelectric body consists of a system of equations and boundary conditions [4]:

$$\nabla \cdot \sigma + \rho f = \rho \ddot{u}, \quad \nabla \cdot D = \sigma_\Omega, \quad \nabla \cdot B = 0 \tag{1}$$

$$\sigma = c : \varepsilon - e^T \cdot E - h^T \cdot H$$
$$D = e : \varepsilon + \kappa \cdot E + \alpha \cdot H \tag{2}$$
$$B = h : \varepsilon + \alpha^T \cdot E + \mu \cdot H$$

$$\varepsilon = \frac{1}{2}\left(\nabla u + \left(\nabla u\right)^T\right), \quad E = -\nabla \varphi, \quad B = -\nabla \phi, \tag{3}$$

where σ and ε are tensors of mechanical stress and strain; D and E are vectors of electric induction and electric field strength; B and H are vectors of magnetic induction and magnetic field strength; ρ is density of the material; c is tensor of elastic modules; e is tensor of piezoelectric modules; h is tensor of piezomagnetic modules; κ is tensor of dielectric permeabilities; α is tensor of magnetoelectric modules; μ is permeability tensor; f is vector of the density of mass forces; σ_Ω is volume density of electric charges; u is displacement vector; φ and ϕ are electric and magnetic potentials.

Boundary conditions are specified for the mechanical, electrical, and magnetic components of the fields.

Mechanical boundary conditions. Let the surface S consist of two parts Γ_1 and Γ_2, so that $S = \Gamma_1 \cup \Gamma_2$, moreover $\Gamma_1 \cap \Gamma_2 = \varnothing$.

$$u = U \text{ on } \Gamma_1, \quad n \cdot \sigma = p \text{ on } \Gamma_2. \tag{4}$$

Electrical boundary conditions. Let the surface S consist of two parts Γ_3 and Γ_4, so that $S = \Gamma_3 \cup \Gamma_4$, moreover $\Gamma_3 \cap \Gamma_4 = \varnothing$.

$$\varphi = \varphi(x, t) \text{ on } \Gamma_3, \quad n \cdot D = -\sigma_0 \text{ on } \Gamma_4, \tag{5}$$

where σ_0 is surface-charge density. In addition, if the electrodes are connected to an external circuit, two conditions should be added:

Mechanics

119

$$\varphi\big|_{S_E} = v, \quad \iint_{S_E} \mathrm{n} \cdot \mathrm{D} dS = I, \tag{6}$$

where s_E is electrode area; v is unknown potential which is found from the second condition; I is current.

Magnetic boundary conditions. Let the surface S consist of two parts Γ_5 and Γ_6, so that $S = \Gamma_5 \cup \Gamma_6$, moreover $\Gamma_5 \cap \Gamma_6 = \varnothing$.

$$\phi = \phi(\mathrm{x}, t) \text{ on } \Gamma_5, \quad \mathrm{n} \cdot \mathrm{B} = \sigma_1 \text{ on } \Gamma_6 \tag{7}$$

where σ_1 is density of free surface currents along the boundary.

For the elastic layer, the first equations in the system (1)–(3) are used; the components of the displacement vector u are unknown. For the piezoelectric layer, the second equations are added to them; u and the electric potential φ are unknown. For the piezomagnetic layer, the third equations are added to the first equations, and the magnetic potential ϕ is added to the unknown displacements. In this case, the relations (2) are transformed through zeroing the corresponding constants.

Finite element modeling. The computer model of the device is built in the ANSYS finite element package. The metal substrate (steel) has thickness *h* and radius *r*. The piezo-active layers consist of one piezoceramic and one piezomagnetic plates which are polarized in thickness, have thickness h_p and radius r_p (Fig. 1).

In the finite element model, devices for the metal and piezoelectric layers are used as finite elements PLANE42 and PLANE13, respectively. In this work, the piezomagnetic layer is modeled by the finite element PLANE13, in which the piezoelectric properties of the material are replaced by piezomagnetic ones. This can be done for two reasons: the piezoelectric layers do not contact each other; qualitatively, the equations for the electric and magnetic potentials coincide.

The properties of the piezoelectric layers used in the calculations are presented in Tables 1–2: piezoceramics — PZT-4, piezomagnetic material — CoFe2O4 [5, 6], adhesive layers are not taken into account.

Table 1

Material properties of PZT-4 piezoceramics

C_{11}^E, Hpa	C_{12}^E, Hpa	C_{13}^E, Hpa	C_{33}^E, Hpa	C_{44}^E, Hpa	e_{31}, CL/m^2	e_{33}, CL/m^2	e_{15}, CL/m^2	k_{11}/ε_0	k_{33}/ε_0
139	77.8	74.3	115	25.6	−5.2	15.1	12.7	730	635

$\varepsilon_0 = 8.85 \times 10^{-12}$ F/m, PZT-4 piezoceramic density $\rho = 7500$ kg/m^3

Table 2

Material properties of CoFe$_2$O$_4$ piezomagnetic element

C_{11}^M, Hpa	C_{12}^M, Hpa	C_{13}^M, Hpa	C_{33}^M, Hpa	C_{44}^M, Hpa	Q_{31}, N/A m	Q_{33}, N/A m	Q_{15}, N/A m	λ_{11}, N s^2/Kl^2	λ_{33}, N s^2/Kl^2
286	173	170	269.5	45.3	580.3	699.7	550	5.9x10^{-4}	1.57x10^{-4}

CoFe$_2$O$_4$ piezomagnetic element density is $\rho = 5290$ kg/m^3

The elastic properties of the isotropic substrate material are characterized by the Young's modulus *E* and the Poisson's ratio ν, $E = 200$ Hpa, $\nu = 0.29$, density $\rho = 7860$ kg/m^3 (steel) were used in the calculations.

To achieve high accuracy in the calculations, the size of the final element of the metal layer is set to the value not higher than 1/5 its thickness; the size of the final element of the piezoelectric layers is automatically set. The finite element grid of the energy storage device is shown in Fig. 2.
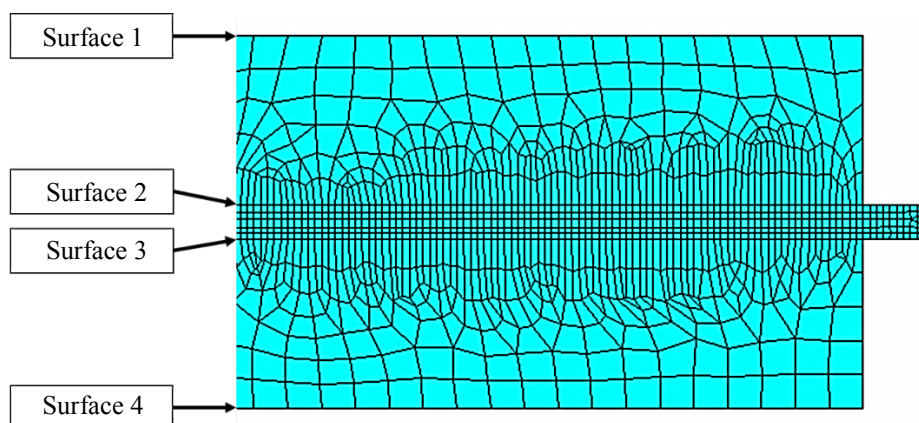
Fig. 2. The finite element grid of the energy storage device.
Surfaces 1, 4 are outer surfaces of piezoelectric layers;
surfaces 2, 3 are contact surfaces between piezoelectric layers and metal layer.

When analyzing the natural vibrations of a piezo-electromagnetic energy storage device, it is assumed that the following mechanical and electromagnetic boundary conditions are met. At the left end, symmetry conditions are specified, the right end is pivotally fixed (Fig. 1). To calculate the resonance frequency of the device, electric potentials are set on surfaces 1, 2; on surface 3, the magnetic potential is set; the magnetic-flux density is set on surface 4. In the case of calculating the antiresonance frequency of the device, the same boundary conditions as for calculating the resonance frequency are set on surfaces 1–4. However, the electric potential on surface 1 is unknown and is found from the condition (6).

Numerical results. The natural vibrations of a piezoelectric element are considered, the radius of which is r_p=9.8 mm, the thickness of the piezoelectric layers is h_p=0.5 mm, the radius of the substrate is r=10 mm, and the thickness of the substrate is h=0.1 mm. Table 3 presents the first three natural frequencies of antiresonance.

Table 3

Antiresonance natural frequencies

No.	Antiresonance frequency kHz	Distribution of vertical displacement on deformed state and distribution of electric and magnetic potential on undeformed sample
1	11.675	
2	56.748	
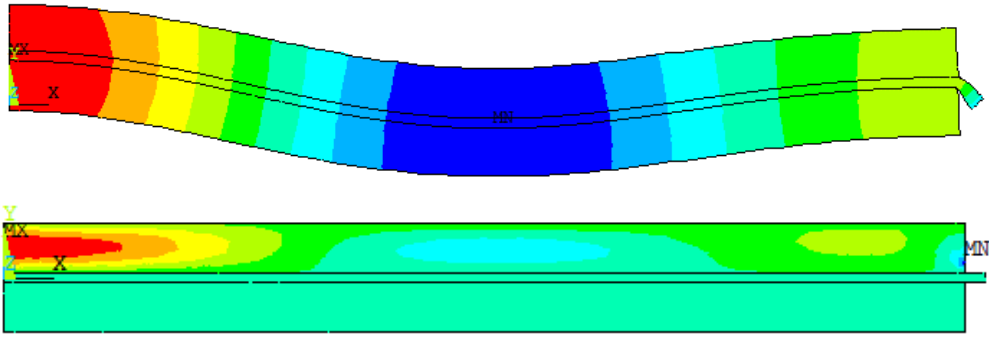
No.	Antiresonance frequency kHz	Distribution of vertical displacement on deformed state and distribution of electric and magnetic potential on undeformed sample
3	115.572	

Table 3 presents the distribution of vertical displacement, electric and magnetic potential while the latter are presented in a single scale, here, the display of the magnetic potential is not visual. To build an approximate theory of calculating the vibrations of the considered bimorph, an analysis of the stress-strain state, electric and magnetic fields, which shows that for lower bending modes, there can be accepted hypotheses about their distribution corresponding to the bending of the plates.

In the results of numerical calculations presented below, the dependence of the eigenfrequencies of resonance and antiresonance, and the electromechanical coupling factor on geometric parameters is investigated.

When the number of alternating piezoelectric and piezomagnetic layers becomes sufficiently large, it is possible to use an approach based on the effective properties of the piezo-magnetoelectric composite [5, 6]. In this case, all equations of the problem (1) - (3) are used.

The thickness value of the piezoelectric layers h_p varies in the range of $0.3 \div 0.7$ mm, and the radius value r_p – in the range of $6.8 \div 9.8$ mm.

a)   *b)*
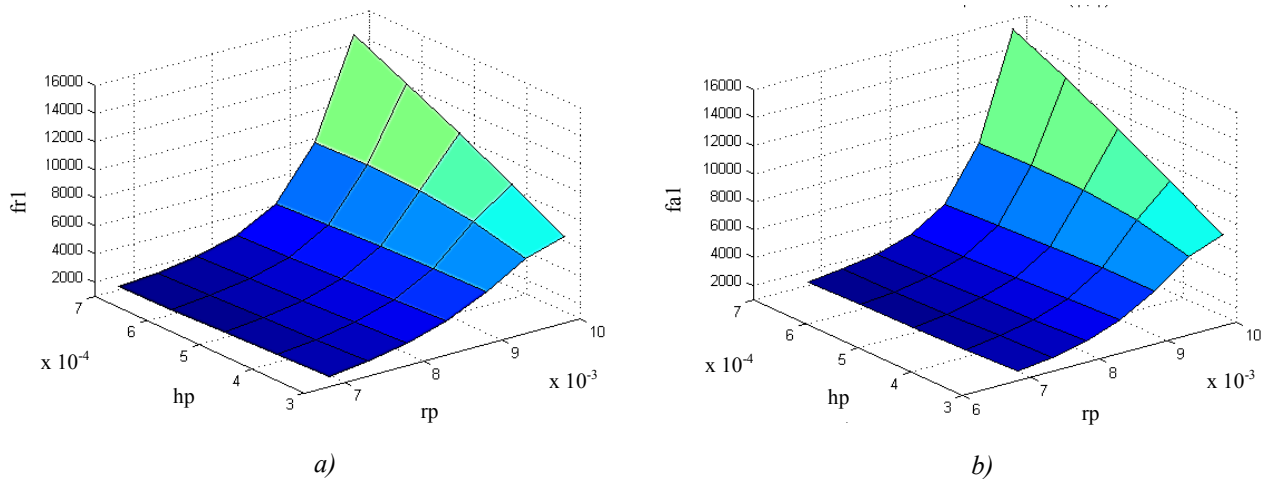
Fig. 3. Natural frequencies: a) resonance frequency,
b) antiresonance frequency

Fig. 3 shows the natural frequency dependences on the thickness h_p and the radius r_p of the piezoelectric layers. Fig. 3 shows that the values of the natural frequencies increase with increasing the radius.

Fig. 4 shows the dependence of the electromechanical coupling factor on the thickness h_p and the radius r_p of the piezoelectric layers. Fig. 4 shows that the value of the natural frequency increases with increasing the radius of the piezoelectric layers r_p, but decreases with increasing thickness h_p of the piezoelectric layers.
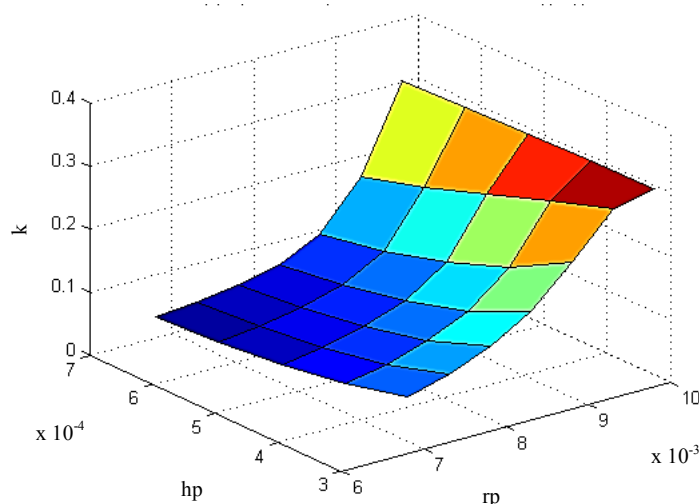
Fig. 4. Electromechanical coupling factor

Conclusion. An axisymmetric finite element model of an energy storage device based on round plates in the ANSYS package is considered. The active elements of the energy storage device are the piezoelectric and piezomagnetic plates fixed on a metal plate. The effect of the geometric characteristics of the piezoelectric layers under certain restrictions on the device dimensions, on the electromechanical coupling factor, which shows the efficiency of the energy storage device, is studied. The calculation results presented in the paper allow selecting rational sizes of piezoelectric elements operating at a certain frequency and having the greatest efficiency. This analysis shows that the maximum value of the electromechanical coupling factor is achieved when the thickness and radius of the piezoelectric layers take the largest and smallest values, respectively, within the considered limits.

References

1. Shevtsov SN, Soloviev AN, Parinov IA, et al. Piezoelectric Actuators and Generators for Energy Harvesting. Heidelberg: Springer; 2018.

2. Duong LV. Konechno-ehlementnoe modelirovanie p'ezoehlektricheskikh ustroistv nakopleniya ehnergii s uslozhnennymi fiziko-mekhanicheskimi svoistvami: diS…. kand. tekhn. nauk [Finite-element modeling of piezoelectric energy storage devices with complicated physical and mechanical properties: Cand.Sci. (Eng.), diss.]. Rostov-on-Don; 2014. 214 p. (In Russ.)

3. Duong LV, Pham MT, Chebanenko VA, et al. Finite Element Modeling and Experimental Studies of Stack-Type Piezoelectric Energy Harvester. International Journal of Applied Mechanics. 2017;9(6): 1750084. doi: 10.1142/S1758825117500843

4. Kurbatova NV, Nadolin DK, Nasedkin AV, et al. Finite element approach for composite magneto-piezoelectric materials modeling in ACELAN-COMPOS package. Analysis and Modelling of Advanced Structures and Smart Systems. Series "Advanced Structured Materials". Altenbach H, Carrera E, Kulikov G. (Eds.). Singapore: Springer. 2018;81(5):69-88.

5. Jin-Yeon Kim. Micromechanical analysis of effective properties of magneto-electro-thermo-elastic multilayer composites. International Journal of Engineering Science. 2011;49:1001–1018.

6. Challagulla KS, Georgiades AV. Micromechanical analysis of magneto-electro-thermo-elastic composite materials with applications to multilayered structures. International Journal of Engineering Science. 2011;49:85–104.

7. Guo-Liang Yu, Huai-Wu Zhang, Fei-Ming Bai, et al. Theoretical investigation of magnetoelectric effect in multilayer magnetoelectric composites. Composite Structures Journal. 2015;119:738–748. https://doi.org/10.1016/j.compstruct.2014.09.049.

8. Guo-Liang Yu, Huai-Wu Zhang, Yuan-Xun Li, et al. Equivalent circuit method for resonant analysis of multilayer piezoelectric-magnetostrictive composite cantilever structures. Composite Structures Journal. 2015;125:367–476. https://doi.org/10.1016/j.compstruct.2015.02.001.

9. Yang Shi, Hong Yao, Yuan-wen Gao. A functionally graded composite cantilever to harvest energy from magnetic field. Journal of Alloys and Compounds. 2017;693:989–999. https://doi.org/10.1016/j.jallcom.2016.09.242.

10. Zhang YF, Zhang W, Yao ZG. Analysis on nonlinear vibrations near internal resonances of a composite laminated piezoelectric rectangular plate. Engineering Structures Journal. 2018;173:89–106. https://doi.org/10.1016/j.engstruct.2018.04.100.

Mechanics

11. Ying Yang, Xian-Fang Li. Bending and free vibration of a circular magnetoelectroelastic plate with surface effects. International Journal of Mechanical Sciences. 2019;157-158:858–871. https://doi.org/10.1016/j.ijmecsci.2019.05.029.

About the authors:

Solov'ev, Arkadii N., Head of the Theoretical and Applied Mechanics Department, Don State Technical University (1, Gagarin sq., Rostov-on-Don, 344000, RF), Dr.Sci. (Phys.-Math.), professor, ResearcherID H-7906-2016, ScopusID 55389991900, ORCID: http://orcid.org/0000-0001-8465-5554, Solovievarc@gmail.com

Do Thanh Binh, postgraduate student of the Theoretical and Applied Mechanics Department, Don State Technical University (1, Gagarin sq., Rostov-on-Don, 344000, RF), ORCID : http://orcid.org/0000-0003-1002-2468, Dothanhbinh@mail.ru

Lesnyak, Olga N., associate professor of the Theoretical and Applied Mechanics Department, Don State Technical University (1, Gagarin sq., Rostov-on-Don, 344000, RF), ORCID : http://orcid.org/0000-0001-7410-0061, Lesniak.olga@yandex.ru

Claimed contributorship

A.N. Solov'ev: task formulation; discussion of the results. Do Thanh Binh: survey conducting; selection of a solution method for constructing a mathematical and computer model; computational analysis; discussion of the results. O.N. Lesnyak: discussion of the results.

All authors have read and approved the final manuscript.

MECHANICS

Investigation of crack propagation in the surface white layer of rail steel

A. Yu. Perelygina, V. Yu. Konyukhov, A. E. Balanovskii
Irkutsk National Research Technical University (Irkutsk, Russian Federation)

Introduction. The paper is devoted to the evaluation of cracking of white layers formed on the surface of the rail while in operation. Cracks are detected in the white layer of rail steel after one thousand test cycles. This is due to tensile and shear stresses on the surface of the wheel–rail contact spot. The paper presents the study results of the morphological characteristics of the white layer on the rail surface.

Materials and Methods. The object of study (rail surface after operation) was examined under a microscope. Then, a two-dimensional model of finite elements of the plane deformation was developed to simulate the dynamic characteristics of the white layer cracking. Mathematical models describing crack propagation are proposed. For this, we applied the criterion of the elastic plastic fracture mechanics, the *J*-integral method. The *SYSWELD* program performed numerical modeling of the formation of a white layer and the distribution of residual stresses.

Results. Optical images of the microstructure of the cross section of a white layer on the rail surface after operation are presented. Two different types of cracks were fixed at the trailing edge of the white layer of the samples studied. The *SYSWELD* program visualized fragments of simulating the mechanism of the white layer formation with the distribution of residual stresses, compression, and tension. The calculation results show that the values of the *J*-integral for all three cracks slightly decrease if the crack length reaches 10–50 μm.

Discussion and Conclusions. The results obtained are applicable to assess the wear resistance of rail steels and predict the direction of crack growth. Comparisons of *J*-integral maxima have shown that under identical load conditions, crack no. 1 is likely to grow faster than cracks nos. 2 and 3. With an increase in the length of the crack, the maxima of the *J*-integral of all three cracks decreased.

Keywords: rail steel, white layer, crack, elastic plastic fracture, *J*-integral method, distribution of residual stresses.

Introduction. It is known that parts of machines and mechanisms, various functional structures often experience catastrophic brittle fracture. Moreover, depending on the operating conditions, the metal may undergo plastic or brittle fracture [1-3]. Brittle fracture occurs due to the growth of cracks that suddenly become unstable and propagate in the material at sonic velocity. Cracks in the metal can be of technological origin or appear and grow during operation. White non-etching layer (*WEL*) is a phenomenon that occurs on the surface of an operated rail under the impact of wheels. *WEL* is formed due to strong multicycle plastic deformation. It has been established that due to fatigue from contact rolling on the rail surface, cracks bind to the white layer [4–6]. The layer is named because of its resistance to acid etching during metallographic preparation and the white "faceless" appearance (it looks like this under a microscope). A white layer is usually found in contact spots on the rail surface. Its depth is ~ 0.10–100 μm after several months of rail operation [4]. An important feature of the white layer is hardness. It reaches 1300 *HV* [5], but is usually in the range of 700–1200 *HV* [6]. This condition can cause the formation of brittle cracks in the white layer and subsequent propagation of fatigue cracks. The authors [4], having examined the rails after operation, found that cracks

were present in the white layer, but did not penetrate the interface with the base metal of the rail [4, 5]. Cracks developed on the surface and propagated along the interface between the *WEL* and the pearlite structure of the material causing severe wear. The mechanism of the formation of the white layer and its microstructure are studied by many authors [6–12].

The microstructure of the layer is identified as the following mixtures:

- martensite with residual austenite and pure martensite saturated with nitrogen and carbon;

- ferrite with martensite;

- residual austenite and martensite with tempered martensite;

- ferrite with cementite, carbide and nanocrystalline phase α-*Fe*.

It was found [6, 7, 9] that the white layer has a martensitic microstructure with a high dislocation density. The authors of [8–10] suggested that *WEL* consists of a nanocrystalline phase of α-*Fe* with grain sizes from 15 to 500 nm. According to [7], *WEL* consists of strongly deformed perlite, nanocrystalline martensite, austenite, and cementite. In [8], the results of X-ray measurements of residual compressive stresses in *WEL* are presented, and significant compressive stresses of the rail (~ 600 MPa) in both directions, longitudinal and transverse, are specified. An analysis of the papers [4–19] shows that cracks in the white layer of rail steel are detected after all tests, even those that were completed far just one thousand cycles. The reason for this is mixed tensile and shear stresses on the surface of the wheel – rail contact spot. After the appearance of a crack in the white layer, it grows rapidly due to the fragility of the martensite structure until it reaches the interface with the base metal of the rail having a perlite structure — here a different microstructure deflects the crack and slows its propagation. This deviation is caused by the orientation of the cementite plates in the pearlite structure [10–19], which are parallel to the rolling surface. According to [12], a decrease in rail fatigue resistance is associated with contact pressure and slip coefficient. The authors of [13] have found that the initiation of a crack in a white layer is caused by the traction force and the designed transverse shear load to the rail track surface. Two types of cracks are identified:

- leading defect crack in the contact spot (caused by a shift);

- back crack (brittle fracture in the form of a wedge).

The authors of [14] associated the short-wave dynamic interaction between the wheel and the rail with the beginning and growth of surface deformation. Under the conditions of contact rolling in rail steel under fatigue, three types of cracks were identified [15]:

1) perpendicular contact surfaces,

2) with a tilt angle,

3) parallel contact surfaces at various depths.

To determine the stress state near the crack tip under conditions of contact with rolling, the authors proposed a numerical method and recorded a change in the crack shape. In [16], the criteria for the direction of crack growth in the mixed mode were used to evaluate cracking behavior. It is shown that cracks grew in the direction of the plane of maximum shear stress, and not perpendicular to the plane. The authors of [17] developed a two-dimensional finite element model for simulating the crack behavior in the rolling contact (wheel and rail) with four short cracks. It was found that the shear stress plays a dominant role in the crack growth, a longer crack grows upward, and this causes a breakaway of the surface layer. Using a two-dimensional computational model, the authors of [18] found that the growth rate of cracks on the rail surface increases with increasing crack length and starts to decrease after a certain depth. In the study on the dynamic wheel and rail interaction [19], a three-dimensional model of finite elements was used and various cracking behavior was recorded due to the static and dynamic solutions. In [20], the residual stress effects were taken into account when studying the path and rate of crack growth. Many works including [21, 22] show the influence of a liquid on the further development of cracks. It is assumed that the liquid on the surfaces of the cracks significantly affects their opening (stress intensity factor of mode I). If the crack develops under dry conditions, then the

shear regime dominates [22]. Until now, linear mechanics of elastic fracture has been widely used under the numerical simulation of the contact of wheels and rails [23, 24]. This approach evaluates the resistance to unstable crack propagation, or the crack resistance of metals, under static loading according to one or more fracture criteria:

- force (critical stress intensity factor K_{1c});
- deformational (critical opening at the crack tip);
- energy (the critical value of the *J*-integral, the work of plastic deformation and fracture).

In practice, materials near the contact area can be plastically deformed due to the high axial load [3–6]. To obtain a more accurate solution, calculations using elastoplastic fracture mechanics or energy-based criteria should be used. In addition, cracks can be formed in areas adjacent to the white layer [7–12], and the mechanisms of their development are still not properly understood. Papers on the formation of a white layer and cracks [14, 15] are published; however, the behavior of the crack propagation in the area of the white layer is not studied in detail. Moreover, in relation to the situation under consideration, the impact of loading conditions, friction, and other interaction parameters is not described. This paper presents results of the study on the morphological characteristics of the white layer on the rail surface.

Materials and Methods. At first, the object of study was examined under a microscope. Then, a two-dimensional model of finite elements of plane deformation was developed to simulate the dynamic characteristics of cracking of the white layer. According to the hypothesis put forward, the contact area on the rail surface was plastically deformed under the interaction of the wheel and the rail; therefore, the energy-based *J*-integral criterion was introduced to evaluate the crack propagation behavior.

Samples containing white layers on the surface of the railhead were cut from the rail, which used to be operated on the East Siberian Railway. The rail was made of pearlite steel in accordance with GOST51685-2013. This is grade 76KhF steel: *C* 0.78%, *Si* 0.54% and *Mn* 0.8%, *Cr* 0.40%, *V* 0.035%. The mechanical properties of the rail were determined:

- yield strength was 944 kN,
- temporary resistance was 1287 kN,
- elongation was 11.5%,
- relative reduction was 31%,
- impact strength was 18 J/cm^2.

The test temperature was +20°C. Brinell macrohardness on the rolling surface in places without white layers was 435, 485, 445, 465 and 494. This does not meet the requirements of GOST 51685-2013 (should be 352–405 according to Brinell). Hardening of the railhead surface during operation is due to the combined action of a number of physical mechanisms [4–16]. For the calculation, the Young's modulus E = 206 GPa was adopted, the shear modulus was 80 GPa, and the density was 7850 kg/m^3 [3–10]. The standard metallographic procedure was performed after sectioning the samples in the direction parallel to the motion direction. After cutting, the sample was poured into resin, polished with silicon carbide sandpaper (grain size 1200–3000) and polished with 0.5 μm microsilica. The cross section was observed under an optical microscope after etching with a 2% alcohol solution of nitric acid for 7 seconds. The mechanism of a white layer formation was investigated through the *SYSWELD* program, which uses an analytical model of the volumetric heat release of Goldak double ellipsoid. Three types of heat source are prescribed: 2D Gaussian, double ellipsoid and 3D conical Gaussian. After the geometric parameters of the heating model are determined and the maximum volumetric heat release value is set, an approximate calculation with constant thermophysical characteristics is performed. All material properties necessary for modeling are set in the form of piecewise linear functions. In the *SYSWELD* program, simultaneously with the heat problem, the metallurgical problem is solved. In the latter case, the calculations are based on the Leblond model, which describes the metallurgical transformation of one phase into another. The solution to the mechanics problems is reduced to the determination of thermal deformations. To do this,

you need to specify in the program the following: elasticity modulus, Poisson's ratio, thermal-expansion coefficient, as well as hardening curves for metallurgical phases. When cracking in a white layer under the moving contact conditions, observations were performed using ANSYS/LS-DYNA software, which is intended for finite element modeling. In studies on the dynamics of railway crews, the well-known algorithm of the named software *FASTSIM* with an elliptical contact area is widely used [25]. Compared with the geometric dimensions of the wheel and rail, the contact area is quite small (not more than 15 mm^2 [25]). Therefore, the model of wheel – rail contact can be simplified to the condition of deformation of the 2D plane [26, 27]. White layers in the form of an arc 2 mm long and 0.2 mm thick were constructed on the longitudinal section (the parameters were obtained as a result of the analysis of *WEL* studies on the rail surface [4–15]). In order to reduce computational costs and ensure accuracy in the model, the adaptive grid method was used. In the region of the white layer, very fine grids were used (Fig.1).
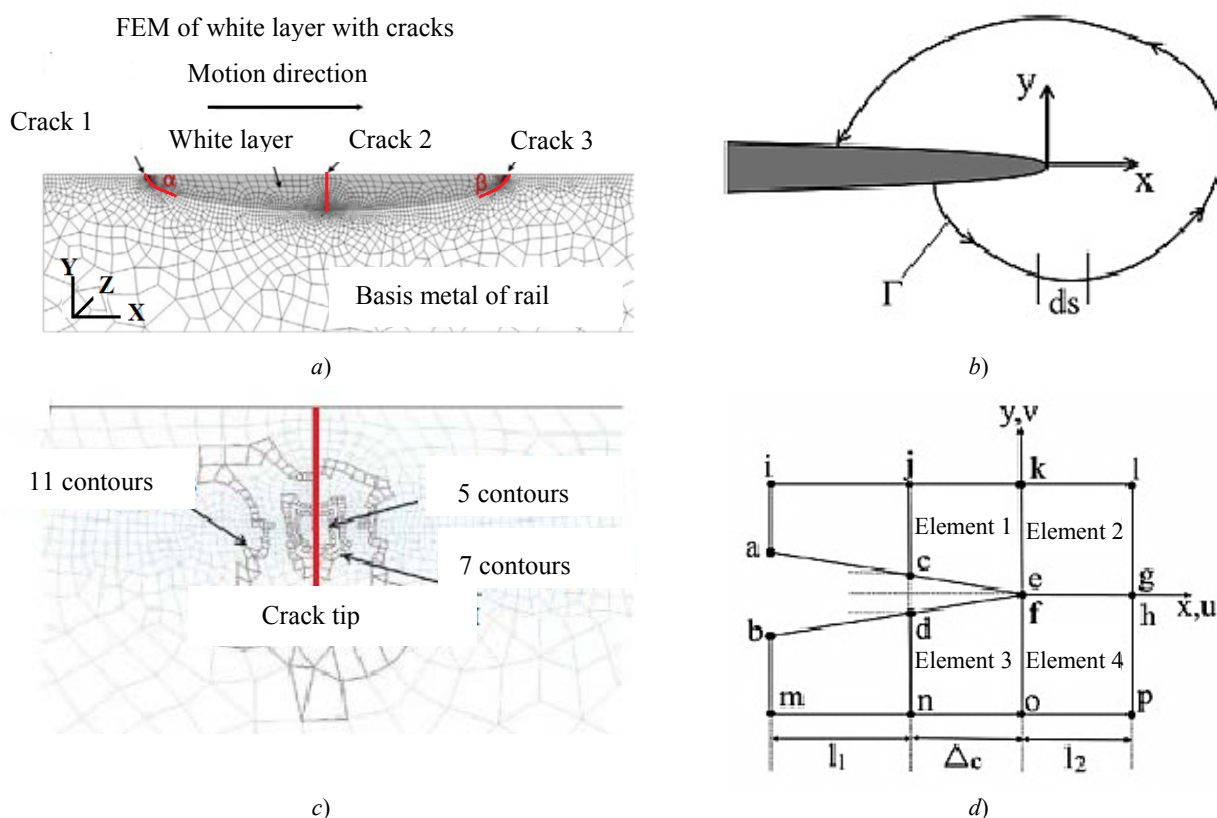
Fig. 1. Finite element modeling (FEM) of white layer with three cracks (a) and transformation of element contour integral into surface contour integral: arbitrary contour around the crack tip (b); different contours of elements selected to represent independence from the calculation path of J-integral (c); basic diagram of 2D virtual crack closure method for calculating stress intensity factor (d)

The established minimum element size was 0.02×0.02 mm^2. The elements had a higher grid density with a set minimum element size of 0.01×0.01 mm^2 at the tips and faces of cracks. This enabled to accurately capture the stress gradients. Outside the cracking zone, larger grids were used with a minimum element size of 0.1×0.1 mm^2 in the wheel – rail contact surfaces. They gradually increased towards the far sections of the field. At first, the rail was combined into 776,919 elements with 789,084 nodes, which changed during the simulation due to the use of the adaptive grid method. Such a model size is acceptable for obtaining accurate calculations of contact with rolling [19, 20, 28]. A constant vertical loading force of 13,000 N was applied to the wheel, which corresponded to the equivalent maximum Hertz pressure of ~ 1.2 GPa [25]. The wheel was set to a rotation speed of ω 43.5 rad/s, which equals a travel speed of 72 km/h with a friction coefficient of 0.3. It was studied how the properties of cracks in a white layer are affected by their length, changes in the angle of inclination, load pressure, and friction coefficient.

The crack growth that destroys the surface was analyzed under the assumption of linear elastic fracture mechanics [1–3, 17–19]. For a more accurate solution, we used the criterion of elastic-plastic fracture mechanics, the *J*-integral method, which is applicable for both linear and elastic plastic solutions [29]. It was introduced to study crack propagation behavior. For numerical calculations, the *J*-integral can be obtained from the solution in the far zone [29]. In the scope of work with finite elements, the element contour integral should be transformed into the surface contour integral, as shown in Fig. 1*b*, where Γ is the contour of the curve that defines the boundary of the *J*-integral, and it is directed counterclockwise from the lower edge of the crack to the upper one. The *J*-integral can be additionally estimated as:

$$J = \int (w \, dy - T_i \, \frac{du_i}{dx} ds),$$

where w is strain energy density; T_i is the thrust vector; u_i is the component of the displacement vector; ds is the length increment along the contour Γ [29].

The *J*-integral evaluation is implemented in *LS-PrePost* as a post-processing tool. This application is also suitable for 2D modeling of plane deformation [30]. To calculate the *J*-integral around the crack tip, various contours of the elements were selected (see Fig. 1*c*). It is important to note that the unloading conditions for a path-independent *J*-integral are not proposed in accordance with the fracture mechanics [31]. The principle of expanding the *J*-integral methodology beyond the admissibility of linear elastic fracture mechanics was to idealize elastoplastic deformation as a nonlinear elastic deformation. The identity of the load characteristics — the deformation for elastoplastic and nonlinear elastic materials is known [30, 31]. The elastic-plastic material follows a linear unloading path with a slope equal to Young's modulus. Non-linear elastic material gets unloaded in the same way as when loading. Thus, the analysis suggests that the nonlinear-elastic behavior is valid for an elastoplastic material. Unloading occurs near the crack tip after the wheel has passed along the rail. The calculated values of the *J*-integral can be valid only until maximum is reached. Therefore, only the maximum values of the *J*-integral are discussed in the present paper. The stress intensity factors within the framework of the finite element scheme were calculated by the 2D method of virtual crack closure [29–32]. The forces y and x needed to connect the nodes c and d (see Fig. 1*d*) are denoted by F_c and T_c, respectively.

It should be noted that the theory of linear elastic fracture mechanics is based on the assumption that there is no plastic deformation around the cracks. At the same time, according to [1–3], the use of the theory of linear elastic fracture mechanics is correct since the nonlinear deformation of the material is limited to a small area surrounding the crack tip. The reasoning that a plane problem can be considered in connection with a small contact area is incorrect. Under the plane deformation, this region is strip and infinite. And in this case, we are talking about an essentially three-dimensional problem. In [32], the complexity of the rail geometry and the boundedness of the region in which the main changes in the stress-strain state occur. The authors of this paper propose to consider a simplified axisymmetric problem for a multilayer coating in the form of a piecewise inhomogeneous layer. In [33], the stress-strain state of a multilayer coating was studied in the vicinity of the wheel – rail contact area. It was shown that the rigidity and thickness of the upper coating layer affect significantly the equivalent and contact stresses. At the fixed mechanical parameters of the coating, with an increase in the thickness of its upper layer, the values of maximum equivalent and contact stresses decrease. The authors of [34] applied thin multilayer coatings on the surface of a railway rail in the vicinity of the lateral wheel – rail contact. The stress-strain state of these coatings was investigated at various values of their geometric and mechanical parameters during rotary movements.

Research Results. Fig. 2 shows optical images of the microstructure of the cross section of a white layer on the rail surface.

Mechanics
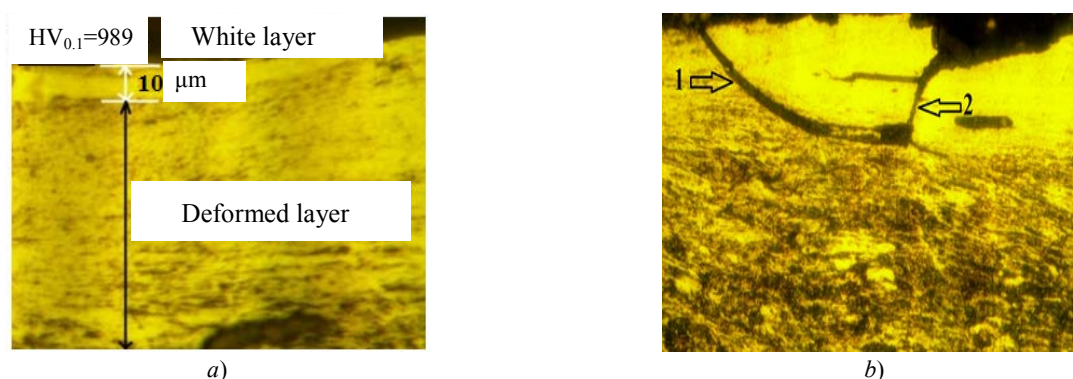
Fig. 2. Features of cracks in white layer on rail surface detected through optical microscopy: general view of white and deformed layer at 200-fold magnification (*a*); 1 - front edge crack, 2 - mid-position crack at 500x magnification (*b*)

Fig. 2*a* shows a segment of a white layer on the surface. Its depth is 10 μm. The microhardness value in the white layer is $HV_{0.1} = 989$. This corresponds to the *WEL* features presented in [4–15]. The *WEL* thickness can reach 200–300 μm depending on the operating conditions [4–6]. The image shows a sharp boundary between the white layer and the deformed pearlite structure of the basis rail metal. The depth of the plastic deformation zone between *WEL* and the basic rail material is ~ 70 μm. According to the estimates [5–10], on the pearlitic rails in operation, in the spot of the wheel – rail contact, plastic deformation has a high concentration creating a thin shear zone of 502,180 μm. At the same time, hardness tests show that due to volume contact, the depth of plastic deformation can reach 1–10 mm [4–9, 27–30]. This causes an important evolution of the microstructure on a narrower scale, i.e., to bend or rupture of cementite plates, to reduction of the inter-plate distance. The mechanical properties also change since the tensile strength increases and the fracture toughness decreases for cracks parallel to the aligned cementite plates. Two different cracks are located at the leading edge of the *WEL* (see Fig. 2*b*). They can originate and propagate at the interface between the *WEL* and the deformed pearlite microstructure. A detailed study on other samples showed that an inclined crack appeared on the leading edge of the *WEL* following the flow direction of the rail material. Then the crack went down into the rail material along the layer boundary. Fig. 2*b* shows a crack propagating vertically in the mid-position within the *WEL*. In the samples studied, two different types of cracks are observed at the trailing edge of the *WEL*. They are obtained from different *WEL* sections, but are located on the same rail sample and are very close to each other. The first-type crack originates and propagates along the boundary between the white layer and the plastic deformation zone (see Fig. 2*b*). The second-type crack crosses the interface with a deformed microstructure, but shows a tendency to curvature along the line in the direction of perlite shear strain. Such behavior of cracks is described in [4–7]. Indeed, the cracks studied by us are located in the same white layer; therefore, they were subjected to the same loads. However, their growth and development rates are different. This indicates a change in the state of stress in the leading, middle and rear position in the white layer. This means that the mechanism for the subsequent crack propagation (i.e., behind it) should be different. As shown in [35, 36], the plastically deformed structure of the pearlite region directly below the white layer can play a significant role in effecting the crack propagation. Cracks that are formed due to fatigue when in the rolling contact can be divided into two categories according to the place of their origination: beneath the surface and on the surface.

Typically, cracks beneath the surface result from a strong vertical load in conjunction with material defects. Most cracks originate on the surface due to the wheel – rail interaction, as well as the transfer of a large load to a small contact area. The contact area is elliptical. It is relatively small, and at the same time, it supports the entire wheel load. Cracks, that arise as a result of fatigue when in the rolling contact and are the result of intense shear stress in the wheel – rail contact area, will grow when these stresses exceed the allowable tensile strength of the rail. It is also possible that cracks will advance to the top of the rails. According to [11, 12, 23], the heating rate of the surface layer of the rail,

which occurs during the passing of a train, can exceed 10^6°C/s and reach the temperature at which austenite is formed. After passing the train under rapid cooling, austenite turns into martensite. The wheel – rail contact time is extremely short (milliseconds). In this case, the steel of the eutectoid composition is heated from room temperature to 727°C at a rate of 10^6°C/s.

Thus, it is practically impossible to measure actual temperature changes during the period under consideration. On the other hand, fast heating and hardening can be modeled and controlled in the *SYSWELD* program. For this, heating rates of 20–1000°C/s were used, which were obtained due to the parameter of the velocity of the heat source moving along the rail surface in the speed range 5–100 mm/s.

Fig. 3 shows a fragment of modeling the mechanism of formation of a white layer in the *SYSWELD* program.

a)   *b*)
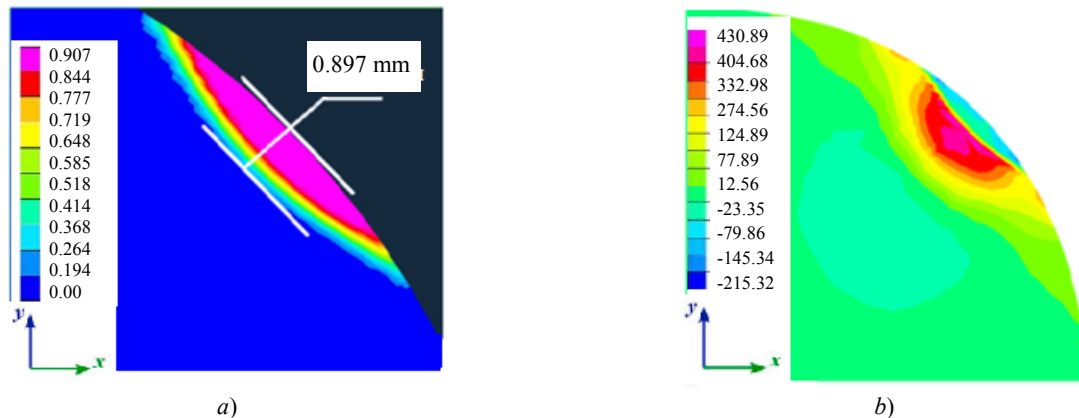
Fig. 3. Simulation results of white layer formation on the rail head surface in SYSWELD program: martensite fraction in the white layer, % (a); distribution of residual stresses in the white layer, MPa (b).

According to Table 1, we can judge how the level of residual stresses depends on the parameters of the path and the hardening rate.

Table 1

Residual stresses value (compression and tension) along the path width

and depth at a hardening speed of 15 mm

Distance along the center of the path axis (depth), mm	0	0.65	0.77	0.86	0.96	1.22	1.54	2.5	3.0
Residual stress, MPa	–43	–87	–15	323	445	347	396	274	176
Centre distance from path axis (width), mm	0	0.14	1.65	1.92	2.19	2.59	3.16	3.91	5.2
Residual stress, MPa	–43	–92	–140	–189	–116	30	200	249	128

The white layer modeled in the program consists of martensite. The layer morphology is similar to that observed in the studied rail (see Fig. 2). The hardness of the simulated *WEL* is 670–810 *HV*. This is slightly lower than in rails (*WEL* ~ 725–1050 *HV*). However, current simulations represent only one phase transformation cycle. From one to five repeated heat treatment cycles were simulated on the surface of the rail head. It is found that hardness increases to 700–850 *HV*. Obviously, martensite with the same hardness as in the white layer of the rail can be obtained after several passes of the wheels. When modeling the formation of the white layer, it turned out that the temperature change during the wheel – rail contact and the distribution of residual stresses play an important role in this process.

Fig. 4 shows *J*-integral maxima at the tips of the simulated crack.
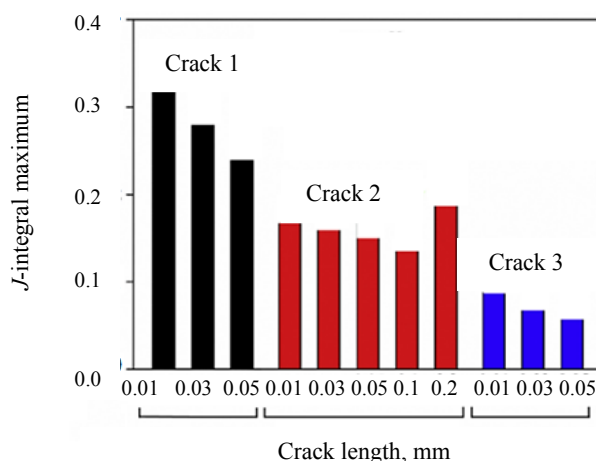
Fig. 4. Maximum values of *J*-integral at crack tips in the leading, middle, and trailing edges of *WEL*
(crack length for calculation is chosen as 0.01 mm; 0.03 mm; 0.05 mm; 0.1 mm and 0.2 mm, separately)

It should be noted that the length of the crack is measured from the rail surface to the *WEL* depth. In the presented simulation version, cracks no. 1, 3 originate at an angle α and β (83.13°), the maximum load pressure is 1.2 GPa. At this, all three cracks have a length of 10 μm. At the top of crack no. 1, the value of the *J*-integral reaches a maximum of 0.321 N/mm. The maximum values of the *J*-integral for cracks nos. 2 and 3 are much smaller — 0.18 N/mm and 0.088 N/mm, respectively. The analysis of Fig. 4 shows that crack no. 1 at the leading edge of *WEL* is likely to grow compared to cracks in the mid-position and at the trailing edge. This fact is in agreement with rolling fatigue experiments [10–18]. It is shown that the boundary (beginning) of the white layer on the rail surface and the basis metal has the lowest resistance to the formation of a contact-fatigue defect, while the fatigue life at the end of the *WEL* is approximately 3 times higher than in the center and at the starting point. Fig. 4 shows that the maxima of the *J*-integral around the crack tips show a tendency to decrease with increasing length or depth. This phenomenon is more significant for crack no. 1 than for nos. 2 and 3. As the crack length increases, the maximum value of the *J*-integral for all three cracks decreases, respectively, from 0.3214 *N*/mm to 0.222 *N*/mm; from 0.18 *N*/mm to 0.14 *N*/mm and from 0.088 *N*/mm to 0.062 *N*/mm. This is consistent with the results of [19] since the deeper surfaces of the crack are less affected by normal and tangential contact loads. However, Fig. 4 shows that, for crack no. 2, when its length is 200 μm and corresponds to the *WEL* thickness, the *J*-integral maximum tends to the opposite, which has never been reported. In this case, the *J*-integral maximum is the largest in comparison with other short cracks no. 2. It can be assumed that crack no. 2 will rapidly propagate to the boundary between the *WEL* and the substrate. This is clearly seen in Fig. 2*b* (arrow 2). The significant difference is due to material irregularities between the perfectly elastic *WEL* and the elastic-plastic rail matrix. The calculation results show that for all three cracks the values of the J-integral decrease slightly when the crack length increases from 10 to 50 μm. If the deepening of crack No. 2 is from 50 to 100 μm, the change in the J-integral is relatively small. On the contrary, there is a significant increase in the maximum value of the J-integral if crack No. 2 propagates through the entire layer to the boundary between WEL and the rail matrix. The calculation results show that for all three cracks, the values of the *J*-integral decrease slightly when the crack length increases from 10 to 50 μm. If the deepening of crack no. 2 is from 50 to 100 μm, the change in the *J*-integral is relatively small. On the contrary, there is a significant increase in the maximum value of the *J*-integral if crack no. 2 propagates through the entire layer to the boundary between the *WEL* and the rail matrix.

The maximum value of the *J*-integral increases sharply with increasing load pressure from 0.8 to 1.5 GPa:

- from 0.27 N/mm to 0.53 N/mm for crack no. 1;
- from 0.17 N/mm to 0.47 N/mm for crack no. 2;
- from 0.04 N/mm to 0.1 N/mm for crack no. 3.

This suggests that cracks are more likely to propagate at high loads. The maximum principal stress around the crack tip can be used as an indicator to assess the fracture properties and the crack path [19–26]. For example, if no. 1 crack length is 10 μm, the maximum principal stress at the crack tip is 1589 MPa. For cracks nos. 2 and 3 with the same length, different stress concentrations are obtained around the crack tips and the maximum principal stresses are about 1506 MPa and 1261 MPa, respectively. An increase in length from 10 to 100 μm causes a decrease in the maximum principal stress from 1506 MPa to 1206 MPa. When a crack propagates down to the boundary of the white layer, a sharp increase in stress concentration can be observed. This is clearly seen from modeling the distribution of residual stresses along the depth of the layer (see Fig. 3). So, according to *J*-integral calculations, under the same load conditions, cracks in the leading edge of the white layer propagate with greater probability than in the mid-position and at the trailing edge. This is consistent with crack growth. In this case, due to the inhomogeneity of the material, a complex stress field arises when the middle crack propagates at the interface between the white layer and the base metal. This causes a high concentration of stresses and thereby accelerates the crack propagation. It should be mentioned that this work did not consider the anisotropic characteristics of the material caused by severe plastic deformation in the transition zone. It was shown in [4–10] that this type of shear deformation causes elongation and alignment of cementite colonies of the surface layer of the rail head (see Fig. 2*a*). It is revealed that shear bands and regions with a high density of defects are found in the transition zone of the white layer, and some cementite plates in this region are destroyed [4–8]. Although linear elastic fracture mechanics does not reflect the detailed physics of the situation [1-3], it helps to understand the directions of the observed crack growth. To obtain more detailed information on the dynamics of crack formation in the white layer on the rail surface, stress intensity factors should be taken into account. At the same time, rolling contact cracks experience a mixed load corresponding to a sequence of tensile stresses followed by a shear cycle [4–20]. Therefore, stress intensity factors in the direction of maximum tangential stress can also be used to predict the direction of the crack growth.

Discussion and Conclusions. It is established that cracks in the leading edge of the white layer (crack no. 1) propagate from the edge of the layer along the interface between the white layer and the basis metal of the rail. Cracks no. 2 (in the middle of the layer) grow vertically before reaching the plastically deformed matrix. Cracks no. 3 of the trailing edge show two developmental trends. In the first case, the crack extends along the interface; in the second case, it crosses the rail material and gradually aligns in the direction of deformation.

Comparisons of the *J*-integral maxima have shown that under identical load conditions, crack no. 1 is most likely to have a high growth rate compared to cracks nos. 2 and 3. With an increase in the crack length, the maxima of the *J*-integral of all three cracks decreased. A great impact of the load pressure on the development of all the considered types of cracks is established.

References

1. Kogaev VP, Makhutov NA, Gusenkov AP. Raschety detalei mashin i konstruktsii na prochnost' i dolgovechnost' [Calculations of machine parts and structures for strength and durability]. Moscow: Mashinostroenie; 1985. 224 p. (In Russ.)

2. Broek D. Osnovy mekhaniki razrusheniya [Fundamentals of Fracture Mechanics]. Moscow: Nauka; 1974. 288 p. (In Russ.)

3. Vitvitskii PM, Popina SYu. Prochnost' i kriterii khrupkogo razrusheniya stokhasticheski defektnykh tel [Strength and criteria for brittle fracture of stochastically defective bodies]. Kiev: Naukova dumka; 1980. 186 p. (In Russ.)

4. Clayton P, Allery MBP. Metallurgical aspects of surface damage problems in rails. The Canadian Journal of Metallurgy and Materials Science. 1982;21(1):31–46.

5. Baumann G, Fecht H, Liebelt S. Formation of White-Etching Layers on Rail Treads. Wear. 1996;191:133–140. doi.org/10.1016/0043-1648(95)06733-7.

6. Newcom SB, Stobbs WM. A transmission electron microscopy study of the white etching layer on a railhead. Materials Science and Engineering. A. 1984;66(2):195–204. doi.org/10.1016/0025-5416(84)90180-0.

7. Jirásková Y, Svoboda J, Schneeweiss O, et al. Microscopic investigation of surface layers on rails. Applied Surface Science. 2005;239(2):132–141. doi.org/10.1016/j.apsusc.2004.05.289.

8. Österle W, Rooch H, Pyzalla A, et al. Investigation of white etching layers on rails by optical microscopy, electron microscopy, X-ray and synchrotron X-ray diffraction. Materials Science and Engineering. A. 2001;303(1/2):150–157.

9. Lojkowski W, Djahanbakhsh M, Bürkle G, et al. Nanostructure formation on the surface of railway tracks. Materials Science and Engineering. A. 2001;303(1/2):197–208. doi.org/10.1016/S0921-5093(00)01947-X.

10. Zhang HW, Ohsaki S, Mitao S, et al. Microstructural investigation of white etching layer on pearlite steel rail. Materials Science and Engineering. A. 2006;421(1/2):191–199. doi.org/10.1016/j.msea.2006.01.033.

11. Chou YK, Evans CJ. White layers and thermal modeling of hard turned surfaces. International Journal of Machine Tools and Manufacture. 1999;39(12):1863–1881. doi.org/10.1016/S0890-6955(99)00036-X.

12. Clayton P. The relations between wear behavior and basic material properties for pearlitic steels. Wear. 1980;60(1):75–93.

13. Steenbergen M, Dollevoet R. On the mechanism of squat formation on train rails. Part II: growth. International Journal of Fatigue. 2013;47:373–381.

14. Li Z, Dollevoet R, Molodova M, et al. Squat growth — some observations and the validation of numerical predictions. Wear. 2013;271(1):148–157. doi.org/10.1016/j.wear.2010.10.051.

15. Olzak M, Stupnicki J, Wojcik R. Investigation of crack propagation during contact by a finite element method. Wear. 1991;146(3):119–128.

16. Bold PE, Brown MW, Allen RJ. Shear mode crack growth and rolling contact fatigue. Wear. 1991;144(1/2):307–317.

17. Ringsberg JW. Shear mode growth of short surface-breaking RCF cracks. Wear. 2005;258(7):955–963.

18. Seo J, Kwon S, Jun H, et al. Fatigue crack growth behavior of surface crack in rails. Procedia Engineering. 2010;2(1):865–872. doi.org/10.1016/j.proeng.2010.03.093.

19. Xin Zhao, Xiaogang Zhao, Chao Liu, et al. A study on dynamic stress intensity factors of rail cracks at high speeds by a 3D explicit finite element model of rolling contact. Wear. 2016;366–367:60–70 /doi.org/10.1016/j.wear.2016.06.001.

20. Trollé B, Baietto M-C, Gravouila A, et al. 2D fatigue crack propagation in rails taking into account actual plastic stresses. Engineering Fracture Mechanics. 2014;123:163–181. doi.org/10.1016/j.engfracmech.2014.03.020.

21. Bogdański S, Lewicki P. Experimental and theoretical investigation of the phenomenon of filling the RCF crack with liquid. Wear. 2005;258(7-8):1280–1287. doi.org/10.1016/j.wear.2004.03.038.

22. Makino T, Kato T, Hirakawa K . The effect of slip ratio on the rolling contact fatigue property of railway wheel steel. International Journal of Fatigue. 2012;36(1):68–79. doi.org/10.1016/j.ijfatigue.2011.08.014.

23. Dubourg MC, Lamacq V. A predictive rolling contact fatigue crack growth model: onset of branching, direction, and growth — role of dry and lubricated conditions on crack patterns. Journal of Tribology — Transactions of the ASME. 2002;124(4):680–688. DOI: 10.1115 / 1.1479698.

24. Benuzzi D, Bormetti E, Donzella G. Stress intensity factor range and propagation mode of surface cracks under rolling — sliding contact. Theoretical and Applied Fracture Mechanics. 2003;40(1):55–74. doi.org/10.1016/S0167-8442(03)00034-X.

25. Kalker JJ, Piotrowski J. Some New Results in Rolling Contact. Vehicle System Dynamics. 1989;18:223–242. doi.org/10.1080/00423118908968920.

26. Kato T, Sugeta A, Nakayama E. Investigation of influence of white layer geometry on spalling property in railway wheel steel. Wear. 2011;271(1):400–407. doi.org/10.1016/j.wear.2010.10.024.

27. Seo JW, Kwon S, Jun HK, et al. Numerical stress analysis and rolling contact fatigue of White Etching Layer on rail steel. International Journal of Fatigue. 2011;33(2):203–211. doi.org/10.1016/j.ijfatigue.2010.08.007.

28. Lian Q, Deng G, Juboori AA, et al. Crack propagation behavior in white etching layer on rail steel surface. Engineering Failure Analysis. 2019;104:816–829. doi.org/10.1016/j.engfailanal.2019.06.067.

29. Rice JR. A Path Independent Integral and Approximate Analysis of Strain Concentration by Notches and Cracks. Journal Applied Mechanics. 1968;35:379–386.

30. Rybicki EF, Kanninen MF. A finite element calculation of stress intensity factors by a modified crack closure integral. Engineering Fracture Mechanics. 1977;9(4):931–938. doi.org/10.1016/0013-7944(77)90013-3.

31. Chow WT, Atluri SN. Finite element calculation of stress intensity factors for interfacial crack using virtual crack closure integral. Computational Mechanics. 1995;16:417–425. https://doi.org/10.1007/BF00370563.

32. Danil'chenko SA, Nasedkin AV. Modelirovanie uprugogo indentirovaniya mnogosloinogo antifriktsionnogo pokrytiya rel'sa metodom konechnykh ehlementov [Modeling of elastic indentation of multilayer antifriction rail coating by the finite element method]. Izvestia RAS SamSC. 2011;13(3):1029–1032. (In Russ.)

33. Chebakov MI, Kolosova EM, Nasedkin AV. Modelirovanie kontaktnogo vzaimodeistviya tel s neodnorodnymi po glubine mekhanicheskimi svoistvami pri nalichii treniya v zone kontakta [Modeling of contact interaction of bodies with mechanical properties non-uniform in depth in the presence of friction in the contact zone]. Izvestia RAS SamSC. 2011;13(4):1252–1255. (In Russ.)

34. Nasedkin AV, Sukhov DYu, Chebakov MI. Modelirovanie kontaktnogo vzaimodeistviya zheleznodorozhnogo kolesa i rel'sa s tonkim trekhsloinym pokrytiem [Modeling of contact interaction between wheel and rail with thin triple-layered covering]. Vestnik RGUPS. 2010;2:11–16. (In Russ.)

35. Al-Juboori A, Wexlera D, Lia H, et al. Squat formation and the occurrence of two distinct classes of white etching layer on the surface of rail steel. International Journal of Fatigue. 2017;104:52–60. doi.org/10.1016/j.ijfatigue.2017.07.005.

36. Li S, Wu J, Petrov RH, et al. Brown etching layer: a possible new insight into the crack initiation of rolling contact fatigue in rail steels. Engineering Failure Analysis. 2016;66:8–18. doi.org/10.1016/j.engfailanal.2016.03.019.

About the authors:

Perelygina, Aleksandra Yu., acting head of the Engineering and Computer Graphics Department, Irkutsk National Research Technical University (83, Lermontov St., Irkutsk, 664074, RF), Cand.Sci. (Eng.), ResearcherID AAF-1094-2020, ORCID: https://orcid.org/0000-0001-7814-0431, perelygina@isru.edu

Konyukhov, Vladimir Yu., professor of the Automation and Management Department, Irkutsk National Research Technical University (83, Lermontov St., Irkutsk, 664074, RF), Cand.Sci. (Eng), professor, ResearcherID AAE-5296-2020, ScopusID 56769690400, ORCID: https://orcid.org/0000-0001-9137-9404, c12@ex.istu.edu

Balanovskii, Andrei E., associate professor of the Engineering Technologies and Materials Department Irkutsk National Research Technical University (83, Lermontov St., Irkutsk, 664074, RF), Cand.Sci. (Eng.), ResearcherID AAE-2964-2020, ScopusID 56375902200, ORCID: https://orcid.org/0000-0002-6466-6587, fuco.64@mail.ru

Claimed contributorship

A.Yu. Perelygina: literature analysis; research objective selection; task setting; planning and organization of joint work; development of a model of cracking in a white layer under conditions of moving contact using commercial *ANSYS / LS-DYNA* finite element modeling software; the paper writing. V. Yu. Konyukhov: the calculated data analysis; parametric identification of models based on graphical experimental distributions using statistical methods and *Excel* spreadsheets. A. E. Balanovskii: experimental work on materials science (cutting, testing, preparation, metallography, measuring the hardness of samples of rails with a white layer); development of a model for the formation of a white layer on the rail head using the *SYSWELD* program; the paper writing.

All authors have read and approved the final manuscript.

MACHINE BUILDING AND MACHINE SCIENCE

Stability of a nonlinear elastic plate under lateral compression

G. I. Volokitin

Don State Technical University (Rostov-on-Don, Russian Federation)

Introduction. Loss of stability and buckling of a round plate may be observed if the plate is loaded on the lateral surface. The solution to this problem is based on a bifurcation approach. In this case, a plate is considered as a nonlinear elastic body. It is important to choose the relation between stresses and deformations in sustainability problems of nonlinear elasticity. Simple laws of state (constitutive equations) were considered in early works devoted to this problem, for example, material of the "harmonic type" (Sensenig).

Materials and Methods. Equations of neutral equilibrium for round plates made of Murnaghan and Blatz-Ko materials are obtained. Assuming a uniform initial deformation on the plate, the stability problem is considered. Strict three-dimensional neutral equilibrium equations provide exploring related forms of equilibrium taking into account physical and geometric nonlinearity. Derivation of these equations is based on the application of the theory of superposition of small deformation on the final one.

Results. Progress in solution to the corresponding secular equation (with non-linear parameter entry) for practically important laws of elasticity of Murnaghan and Blatz-Ko is possible using the numerical methods only. The developed method for calculating bifurcation values of loading parameters makes it possible to analyze the effect of nonlinearity.

Discussion and Conclusions. The influence of physical and geometric nonlinearity on the upper critical value of the initial deformation parameter is explored. The results obtained can be used under the assessment of reliability of elastic third-order moduli for various physical materials. Data on these moduli is still scarce. The numerical research has shown that the constants given in some sources should be treated with caution. The use of elasticity moduli in the law of state of Blatz-Ko is also discussed.

Keywords: finite deformation, stresses, buckling, plate, stability.

*For citation***:** G. I. Volokitin. Stability of a nonlinear elastic plate under lateral compression. Vestnik of DSTU, 2020, vol. 20, no. 2, pp. 137–142. https://doi.org/10.23947/1992-5980-2020-20-2-137-142

Introduction. Currently, the study of new relatively simple and adequate laws of state for various materials that require considering nonlinear deformations is an actively developing area of continuum mechanics [1–10]. In the framework of the theory of superposition of small deformation on the finite one, three-dimensional equations of neutral equilibrium are derived for the materials of Murnaghan and Blatz-Ko. Based on these equations, an example of end buckling of a uniformly compressed round plate is considered [11, 12].

Materials and Methods

Equations of neutral equilibrium. Let r, φ, z be the cylindrical coordinates of a point in an undeformed state. We assume that the initial deformation of the body is determined by the radius vector R:

$$\mathrm{R} = R(r)\mathrm{e}_r + dz\mathrm{i}_3 , \qquad (1)$$

where $R(r) = ar$, parameters a, d are constants, e_r, e_φ, i_3 are basis vectors.

For the coordinates of this point in the initial deformed state, we have:

$$R = ar, \quad \Phi = \varphi, \quad Z = dz .$$

Therefore, the strain gradient, the Finger strain measure, and its principal invariants are determined through the relations:

$$\nabla \mathrm{R} = \nabla \mathrm{R}^T = a(e_r e_r + e_\varphi e_\varphi) + d\, i_3 i_3, \quad \mathrm{F} = \nabla \mathrm{R}^2 ,$$

$$I_1 = 2a^2 + d^2, \quad I_2 = a^4 + 2a^2 d^2, \quad I_3 = a^4 d^2 . \qquad (2)$$

From now on, ∇, $\tilde{\nabla}$ is the nabla operator in the metric of the undeformed and initial-deformed state:

$$\tilde{\nabla} = \nabla \mathrm{R}^{-1} \cdot \nabla .$$

Mechanics

We will use the neutral equilibrium equations proposed by A. I. Lurie [13]: $\tilde{\nabla}\Theta = 0$, where the tensor Θ is a linear differential operator over the vector of additional displacements W. The expressions of the components of this tensor concretized with account of the laws of state of Murnaghan and Blatz-Ko were obtained in [14, 15]. In the representations of the tensor Θ, the components are some functions defined as a result of solving the boundary value problem of the initial deformation.

Research Results. To consider the bending form of the plate equilibrium bifurcation, similarly to [11, 12], we accept the following additional displacement vector

$$\mathbf{W} = u(r,z)e_r + w(r,z)i_3 . \tag{3}$$

Considering (1), (2) and (3), Lurie tensor has the form:

$$\Theta = Ae_re_r + Be_\varphi e_\varphi + Ci_3i_3 + Gi_3e_r + He_ri_3 .$$

Here,

$$A = A_1 \frac{u}{r} + A_2 \frac{\partial u}{\partial r} + A_3 \frac{\partial w}{\partial z}, \ B = B_1 \frac{u}{r} + B_2 \frac{\partial u}{\partial r} + B_3 \frac{\partial w}{\partial z}, \ C = C_1 \frac{u}{r} + C_2 \frac{\partial u}{\partial r} + C_3 \frac{\partial w}{\partial z},$$

$$G = G_1 \frac{\partial u}{\partial z} + G_2 \frac{\partial w}{\partial r}, \ H = H_1 \frac{\partial u}{\partial z} + H_2 \frac{\partial w}{\partial r} .$$

We note that the structure of these operators is typical in the stability problems of cylindrical nonlinear elastic bodies. Omitting the expressions of the remaining coefficients, we give, for example, formulas for A_1. In the case of Murnaghan law of the state [13, 14] A_1 is expressed through the relation

$$A_1 = \frac{a}{d}\left(\lambda - \frac{3v_1 + 4v_2}{2} + \frac{v_1}{2}d^2 + (v_1 + 2v_2)a^2\right).$$

Henceforward, λ and μ are Lame elasticity moduli, v_1, v_2, v_3 are the third-order elasticity constants. For Blatz-Ko material [15]:

$$A_1 = \frac{2\mu(1-\beta)}{a\sqrt{I_3}}\left(I_3^{\lambda/2\mu} + \frac{\beta}{1-\beta}I_3^{-\lambda/2\mu}\right),$$

where β is the refining elasticity modulus.

The equation of neutral equilibrium is equivalent to the system of differential equations with respect to the components of the vector $\mathbf{W}$:

$$\begin{cases} A_2\left(\frac{\partial^2 u}{\partial r^2} + \frac{1}{r}\frac{\partial u}{\partial r} - \frac{u}{r^2}\right) + \left(A_3 + \frac{a}{d}G_2\right)\frac{\partial^2 w}{\partial r\partial z} + \frac{a}{d}G_1\frac{\partial^2 u}{\partial z^2} = 0, \\ \left(A_3 + H_1\right)\frac{\partial}{\partial z}\left(\frac{\partial u}{\partial r} + \frac{u}{r}\right) + H_2\left(\frac{\partial^2 w}{\partial r^2} + \frac{1}{r}\frac{\partial w}{\partial r}\right) + \frac{a}{d}C_3\frac{\partial^2 w}{\partial z^2} = 0. \end{cases} \tag{4}$$

Assuming that the plate is loaded with uniform pressure along the lateral surface, we supplement the differential equations (4) with the equilibrium conditions at the boundary:

$$u(r,z)\big|_{r=r_u} = 0, \quad \Theta_{rz}\big|_{r=r_u} = 0.$$

At the ends, i.e., at

$$z = \pm\frac{h}{2} \quad \Theta_{zr} = 0, \quad \Theta_{zz} = 0 . \tag{5}$$

We apply the substitution

$$\begin{cases} u = X_n(z)J_1(k_nr), \\ w = Z_n(z)J_0(k_nr). \end{cases} \tag{6}$$

Here, $n = 1, 2, \ldots$, J_0, J_1 are Bessel functions of zero order and first kind, and numbers k_nr_u are null functions $J_1(x)$.

Let us assume $x = k_nr$ and use the equations

$$\frac{dJ_1(k_nr)}{dr} = k_nJ_1'(x), \quad \frac{d^2J_1(k_nr)}{dr^2} = k_n^2 J_1''(x), \quad \frac{dJ_0(k_nr)}{dr} = k_nJ_0'(x) = -k_nJ_1'(x),$$

and well-known identities for Bessel functions

$$J_1'' + \frac{1}{x}J_1' - \frac{1}{x^2}J_1 = -J_1, \quad J_0'' + \frac{1}{x}J_0' = -J_0 .$$

Having completed the above steps, we obtain that the variables in the Lurie differential equations (4) and under the boundary conditions (5) are separated. We arrive at the following boundary value problem for ordinary differential equations:

$$\begin{cases} X_n'' - k_n^2 \dfrac{A_2}{H_2} X_n - k_n \dfrac{G_2 + C_2}{G_1} Z_n' = 0, \\ Z_n'' - k_n^2 \dfrac{G_1}{C_3} Z_n + k_n \dfrac{G_2 + C_2}{C_3} X_n' = 0. \end{cases} \tag{7}$$

$$\begin{aligned} k_n C_1 X_n \left(\pm h/2 \right) + C_3 Z_n' \left(\pm h/2 \right) = 0, \\ k_n G_2 Z_n \left(\pm h/2 \right) - G_1 X_n' \left(\pm h/2 \right) = 0. \end{aligned} \tag{8}$$

Two homogeneous linear ordinary differential equations (7) and four boundary conditions (8) result in the eigenvalue problem with a nonlinear occurrence of the parameter. In this problem, such a parameter is the quantity $(1-a)$. The system (7) is ended in the standard form:

$$\begin{cases} y_1' = y_2, \\ y_2' = k_n^2 \dfrac{A_2}{H_2} y_1 + k_n \dfrac{G_2 + C_2}{G_1} y_4, \\ y_3' = y_4, \\ y_4' = k_n^2 \dfrac{G_1}{C_3} y_3 - k_n \dfrac{G_2 + C_2}{C_3} y_2. \end{cases}$$

The following notations are accepted here: argument $t \equiv z$, $\left(y_1; y_2; y_3; y_4 \right)^T \equiv \left(X_n; X_n'; Z_n; Z_n' \right)^T$. Let the fundamental system of solutions be the following four vectors $y_i \equiv \left(y_{1i}; y_{2i}; y_{3i}; y_{4i} \right)^T$. Then, the general solution to the system is given by $\left(X_n; X_n'; Z_n; Z_n' \right)^T_{общ.} = \sum_{i=1}^{4} \xi_i y_i$, where ξ_i are arbitrary constants. For example, we set the initial data for $z = -h/2$ by the columns of the fourth-order unity matrix. Then we solve numerically the Cauchy problem with these initial conditions. As a result, on the right-hand side, we obtain the values of the basis functions, i.e., vectors $y_i(+h/2)$. Using the boundary conditions (8), we arrive at a homogeneous system of linear algebraic equations with respect to ξ_1, ξ_2, ξ_3, ξ_4:

$$\sum_{j=1}^{4} a_{ij} \xi_j = 0, \text{ where } i = 1, 2, 3, 4.$$

Here, the coefficients are the elements of matrix A :

$$a_{1j} = k_n C_1 y_{1j} \left(-h/2 \right) + C_3 y_{4j} \left(-h/2 \right), \; a_{2j} = k_n C_1 y_{1j} \left(h/2 \right) + C_3 y_{4j} \left(h/2 \right),$$
$$a_{3j} = k_n G_2 y_{3j} \left(-h/2 \right) - G_1 y_{2j} \left(-h/2 \right), \; a_{4j} = k_n G_2 y_{3j} \left(h/2 \right) - G_1 y_{2j} \left(h/2 \right).$$

The homogeneous system has a nontrivial solution if the condition is met

$$\det A = 0. \tag{9}$$

The determinant expression includes the load parameters a, d, Bessel null-functions, as well as the elasticity moduli λ, μ, v_1, v_2, v_3 (for the Murnaghan material) or λ, μ, β (for the Blatz-Ko material).

The parameters a, d, which set the initial deformation, are interconnected. The axial force acting on the cross-sectional area is determined by the relation [13]: $Q = 2\pi \int_0^{R_u} \sigma_Z R dR$, where σ_Z is the physical component of the stress tensor. Since the initial deformation is assumed in the form (1), the Cauchy stress tensor T and the Finger strain measure F are coaxial.

Moreover, the stress tensor is constant:

$$T = \frac{2}{a^2 d} \left(c^{(0)} \left(a^2 (e_r e_r + e_\varphi e_\varphi) + d^2 i_3 i_3 \right) - c^{(1)} \left(a^4 (e_r e_r + e_\varphi e_\varphi) + d^4 i_3 i_3 \right) + c^{(-1)} \left(e_r e_r + e_\varphi e_\varphi + i_3 i_3 \right) \right).$$

The ends of the plate are free of load, therefore $\sigma_Z = 0$. This implies the condition relating the coefficients of the Finger law

$$c^{(0)} - c^{(1)} d^2 + \frac{c^{(-1)}}{d^2} = 0. \tag{10}$$

Considering the law of state, we can write a specific expression of the condition (10), which establishes a connection between *a* and *d*. So, for the Murnaghan material, we get the condition:

$$\left(\frac{v_1}{4} + \frac{3v_2}{2} + 2v_3 \right) d^4 + \left(\lambda + 2\mu - \frac{3v_1}{2} - 5v_2 - 4v_3 + (v_1 + 2v_2) a^2 \right) d^2 -$$

$$-3\lambda - 2\mu + \frac{9v_1}{4} + \frac{9v_2}{2} + v_3 + (2\lambda - 3v_1 - 4v_2 - \frac{3v_3}{4})a^2 + (v_1 + v_2 - \frac{15v_3}{8})a^4 = 0 .$$

In particular, if $v_1 = v_2 = v_3 = 0$, then we get

$$d^2 = 1 + \frac{2\lambda}{\lambda + 2\mu}\left(1 - a^2\right).$$

When considering the Blatz-Ko law of state, d is expressed by the formula

$$d = a^{-2/3} .$$

Thus, through setting the elasticity moduli and Bessel null-functions, we find the bifurcation values of the initial strain parameter a_* from (9).

Note that the value $\Lambda \equiv 1 - a_*$ is a small parameter for relatively thin disks. So, in the classical theory of plate buckling, the critical value of a_* is determined by the formula

$$a_* = 1 - \frac{(3,8317)^2}{12(1+v)}\left(\frac{h}{r_{_H}}\right)^2 ,$$

where v is the Poisson's ratio, and 3.8317 is the first root of the Bessel function $J_1(x)$.

When solving the initial boundary value problem, it is assumed that the Signorini's perturbation method can be applied. At this, we assume that the coefficients of the operator Θ depend on a small parameter Λ in a power-law manner. This means that the boundary conditions for the incremental displacement components Λ are specified by the matrix $A = A(\Lambda)$. In this problem, a partial eigenvalue problem — the determination of the lowest eigenvalues — has physical meaning. The higher degrees Λ , which contain the matrix elements, slightly affect the values of the smallest roots of the secular equation (9). If we restrict ourselves to the linear theory under solving the initial problem, then $A(\Lambda)$ is a regular binomial [16].

Numerical experiments under studying the stability of nonlinear elastic bodies of not too large relative thickness confirm this conclusion. Therefore, a characteristic equation with non-linear occurrence of parameter (9) can be replaced by the characteristic equation of the linear operator. Iterative processes that converge to one eigenvalue, where a number close to the value in the theory of plates is chosen as the null approximation, can be applied.

Discussion and Conclusions. Using the equations obtained above, a numerical analysis of the influence of physical and geometric nonlinearity on the value of the upper critical parameter a_* is performed. The calculations are implemented in the Matlab environment for various options of specifying elasticity moduli, relative plate thickness, and waveformation number n . It is found that in all cases of loss of disk stability, the first-mode buckling that corresponds to the minimum critical value of the parameter, which corresponds to the root of the Bessel function 3.8317 [17], answers the smallest critical parameter value a_* .

Table 1 shows the critical parameter values a_* for plates with a relative thickness of 0.05; 0.1; 0.15; 0.2; 0.25; and 0.3.

Table 1

Critical parameter values a_* for plates of various relative thicknesses

$h/r_{_H}$	Relative plate thickness					
	0.05	0.1	0.15	0.2	0.25	0.3
1	0.9922	0.9869	0.9800	0.9660	0.9530	0.9330
	0.9972	0.9867	0.9735	0.9549	0.9300	0.8914
2	0.9977	0.9908	0.9801	0.9664	0.9504	0.9332
	0.9967	0.9869	0.9690	0.9410	—	—
3	0.9976	0.9907	0.9800	0.9662	0.9502	0.9330
	0.9965	0.9856	0.9665	0.9372	—	—
4	0.9977	0.9907	0.9798	0.9659	0.9497	0.9324
	0.9881	—	—	0.9965	0.9613	0.9861
5	0.9914	0.9865	0.9783	0.9668	0.9520	0.9350
	0.9929	0.9729	0.9341	0.9114	—	—
6	0.9978	0.9912	0.9800	0.9675	0.9520	0.9340
	0.9985	0.9941	0.9871	0.9775	0.9651	0.9539
7	0.9985	0.9941	0.9859	0.9735	0.9560	0.9320
	0.9985	0.9941	0.9863	0.9749	0.9594	0.9396

The following numbers indicate the materials listed below.

1. Steel Rex 535 ($\lambda = 1.09$, $\mu = 0.818$, $v_1 = -1.75$, $v_2 = -2.40$, $v_3 = -1.69$).

2. Steel 50HGSM2F ($\lambda = 1.129$, $\mu = 0.803$, $v_1 = -2.8$, $v_2 = -2.7$, $v_3 = -1.87$).

3. Steel Hecla 37 ($\lambda = 1.11$, $\mu = 0.821$, $v_1 = -3.58$, $v_2 = -2.82$, $v_3 = -1.77$).

4. Steel Hecla ATV ($\lambda = 0.87$, $\mu = 0.716$, $v_1 = 0.34$, $v_2 = -5.52$, $v_3 = -1.0$).

5. Beryllium bronze ($\lambda = 1.042$, $\mu = 0.49$, $v_1 = -4.0$, $v_2 = -1.7$, $v_3 = -0.6$).

6. Organic glass ($\lambda = 0.39$, $\mu = 0.186$, $v_1 = -0.078$, $v_2 = -0.07$, $v_3 = 0.047$).

In the first six cases, the Murnaghan law of state is considered. The last option presents the results for the material of Blatz-Ko. The top number in the table cell refers to the case in which physical non-linearity is not taken into account, i.e., $v_1 = v_2 = v_3 = 0$ in the Murnaghan law; $\beta = 0$ in the Blatz-Ko law. The second (lower) number takes into account physical nonlinearity. In the Murnaghan law, data were used for the third-order elasticity moduli from [14] in units $10^{12} \dfrac{dyne}{cm^2}$.

In the last row of Table 1, there are the results for the Blatz-Ko law, which was chosen in a simplified version (the Knowles-Sternberg equation): the Poisson's ratio was taken equal to 0.25, and the refining module $\beta = 0.45$. A dash means no critical value a_* was found.

The analysis of the results provides drawing some conclusions. At small relative thicknesses of the disk, the exact theory and the linear theory of plates give the same critical parameter values a_*. Geometric nonlinearity has marked impact at relative thicknesses greater than 0.1. Physical nonlinearity is even more pronounced. However, care should be exercised in choosing third-order elasticity moduli. For example, in the fourth version (Hecla ATV steel) and for thin plates, no reliable critical values of the parameter a_* were found; although acceptable values indicating a loss of stability are observed for the same Lame elasticity moduli. As in the stability problem for a nonlinear elastic sphere made of Blatz-Ko material [15], the constant β weakly affects the critical value a_*.

References

1. Azarov AD, Azarov DA. Description of non-linear viscoelastic deformations by the 3D mechanical model. Physics, Mechanics of New Materials and Their Applications. In: Proc. Int. Conf. devoted to the 100th Anniversary of the Southern Federal University. Parinov IA, Shun-Hsyung, Topolov VYu. (Eds.) New York: Nova Science Publishers; 2016. Ch. 49:367–375.

2. Azarov DA, Zubov LM. Mekhaniko-geometricheskoe modelirovanie v nelineinoi teorii uprugosti [Mechanical-geometrical modeling in nonlinear theory of elasticity]. Izvestiya vuzov. Severo-Kavkazskiy region. Natural Sciences. 2016;3(191):5–12. (In Russ.)

3. Kalashnikov VV, Karyakin MI. Ispol'zovanie modeli materiala Murnagana v zadache ploskogo izgiba uprugogo sterzhnya [Using Murnaghan material model in the problem of plane bending of elastic rod]. Trudy RGUPS = Transaction of RSTU. 2006;2(3):56–65. (In Russ.)

4. Rogovoi AA. Opredelyayushchie sootnosheniya dlya konechnykh uprugo-neuprugikh deformatsii [Defining relations for finite elastic-inelastic deformations]. Journal of Applied Mechanics and Technical Physics. 2005;46(5):138–149. (In Russ.)

5. Aidy A, Hosseini M, Sahari BB. A Review of Constitutive Models for Rubber-Like Materials. American Journal of Engineering and Applied Sciences. 2010;3(1):232–239.

6. Gent AN. Engineering with rubber. München: Carl Hanser Verlag & Co. KG; 2012. 451 p.

7. Greaves GN, Greer AL, Lakes RS, et al. Poisson's ratio and modern materials. Nature Materials. 2011;10:823–837.

8. Marckmann G, Verron E. Comparison of hyperelastic models for rubber-like materials. Rubber Chemistry and Technology, American Chemical Society. 2006;79(5):835–858.

9. Azarov AD, Azarov DA. Trekhmernaya mekhanicheskaya model' dlya opisaniya bol'shikh uprugikh deformatsii pri odnoosnom rastyazhenii [3D mechanical model for description of large elastic deformations under uniaxial tension]. Vestnik of DSTU. 2011;11(2):147–156. (In Russ.)

10. Eremeev VA, Zubov LM. Mekhanika uprugikh obolochek [Mechanics of elastic shells]. Moscow: Nauka; 2008. 280 p. (In Russ.)

11. Sensenig CB. Instability of thick elastic solids. Communications on pure and applied mathematics. 1964;XVII:451–491.

12. Zubov LM. Vypuchivanie plastinok iz neogukovskogo materiala pri affinnoi nachal'noi deformatsii [Bulging of plates from neo-Hookean material with affine initial deformation]. Journal of Applied Mathematics and Mechanics. 1970;34(4):632–642. (In Russ.)

13. Lur'e AI. Nelineinaya teoriya uprugosti [Nonlinear theory of elasticity]. Moscow: Nauka; 1980. 512 p. (In Russ.)

14. Volokitin GI. Ustoichivost' nelineino-uprugogo tsilindra pri bokovom davlenii i osevom szhatii [Stability of a nonlinear elastic cylinder under lateral pressure and axial compression]. Journal of Applied Mathematics and Mechanics. 1982;42(2):289–295. (In Russ.)

15. Volokitin GI, Moiseev DV. Usloviya bifurkatsii ravnovesiya sfery [Conditions for bifurcation of sphere equilibrium]. In: Proc. XV Int. Conf. "Modern problems of continuum mechanics". Rostov-on-Don: SFU Publ. House. 2011;1:69–73. (In Russ.)

16. Gantmakher FR. Teoriya matrits [Theory of matrices]. Moscow: Nauka; 1968. 576 p. (In Russ.)

17. Yanke E, Ehmde F, Lesh F. Spetsial'nye funktsii [Special functions]. Moscow: Nauka; 1968. 352 p. (In Russ.)

About the author:

Volokitin, Gennadii I., associate professor of the Mathematics Department, Don State Technical University (1, Gagarin sq., Rostov-on-Don, 344000, RF), Cand.Sci. (Phys.-Math.), ORCID: http://orcid.org/0000-0002-1421-6414, ivolokitin@bk.ru

The author has read and approved the final manuscript.

MACHINE BUILDING AND MACHINE SCIENCE

Development of design methodology of technological process of ball-rod hardening with account for formation of compressive residual stresses

M. A. Tamarkin, E. E. Tishchenko, S. A. Novokreshchenov, S. A. Morozov
Don State Technical University (Rostov-on-Don, Russian Federation)

Introduction. The study results on the multicontact shock-vibrating machining using a ball-rod hardener are presented. Methods of surface plastic deformation processing, their advantages are described. The tool circuit diagram is given. Features, technological advantages, and the application area of the ball-rod hardening are specified.

Materials and Methods. When conducting theoretical studies on the processing, factors, which affect the quality of the surface layer of the machined parts, were established. Dependences are given for calculating the surface roughness, the hardened layer depth, and the deformation ratio under ball-rod hardening. While studying the generation of residual stresses, the dependence for calculating the residual stresses generated in the surface layer of the machined part was specified.

Results. The experimental findings of the processing requisite for verification of the adequacy of the theoretical models, as well as the routine of the experiments, are presented. A table and graphs clearly confirming good convergence of the theoretical and experimental data are given (the difference does not exceed 20%). Residual stresses in the surface layer are compressive which enables to predict high performance properties of the machined parts. The value of residual stresses on the workpiece surface is in the range of $130 \div 200$ MPa. The depth of compressive residual stresses is in the range of 0.9–1 mm. The fatigue characteristic variation, the ultimate stresses of the cycle in depth, which affects the endurance limit, is calculated. It has been established that the processing of workpieces by a ball-rod hardener provides increasing the ultimate cycle stress under repeated loading by 27–35%.

Discussions and Conclusions. The design methodology of technological process of ball-rod hardening can be used under the development of production at the machine-building enterprises. In accordance with the recommendations, the limits of the required quality parameters of the workpiece surface layer are set; the parameters of the ball-rod hardener, the interference fit and the radius of rod sharpening are selected. Quality parameters of the surface layer are calculated. Correction of the selected modes and re-calculation of the parameters of the machined surface are carried out until all the specified characteristics are located within the required limits.

Keywords: ball-rod hardening, surface roughness, hardened layer depth, deformation ratio, residual stresses.

Introduction. The quality of parts depends on many different parameters, one way or another manifested in the process of their manufacture and affecting their life cycle. A special role in the formation of surface quality is played by finishing processing methods, the use of which provide improving the basic operational properties of machine parts, such as contact stiffness, wear resistance, fatigue strength and durability, etc.

Surface plastic deformation (SPD) processing methods allow solving the problems of increasing the product life cycle for parts from various materials of any configuration. In addition, such methods provide localized processing, which can significantly reduce production costs. The characteristic surfaces of the parts processed through the local SPD hardening are stress concentration zones (holes, slots, bevels, sampling, screwthreads, fillets, grooves, etc.); unreinforced areas of the surface of parts that have undergone general hardening in vibration, shotblasting and others installations (under clamps, in pockets, holes and other difficult-to-access areas for the processing environment); places for mechanical refinement of parts, etc.

Machine building and machine science

Methods of processing SPD, including local ones, can significantly reduce the surface roughness of the workpiece and increase its physical and mechanical properties. In addition, the SPD methods make it possible to remove residual stresses generated by various defects in a part, which have a significant effect on the physicomechanical properties of the material from which the part is made. It is known that tensile residual stresses can significantly reduce the strength characteristics of a part, and vice versa, compressive ones can improve them.

To carry out the process of local processing of SPD parts of simple and complex configurations, including those having a small vertical difference in height, a special device, a ball-rod hardener (BRH), was invented at the Engineering Technology Department, Don State Technical University, under the guidance of Prof. Babichev A.P. BRH is a multi-contact vibro-impact tool, the processing of which is based on the surface-plastic deformation. This processing method has several advantages, such as the ability to handle stress concentrators of large-sized products, products of irregular shape, low-rigid products. The method combines the technological capabilities of vibratory finishing and hardening processing and embossing.

A pneumatic hammer, on which the hardener body is fixed, is used as a power drive. The striker of the power drive 1 hammers with a frequency of about 42 Hz on several layers of steel balls 4, which are transmitted to the set of round rods 2 installed in the collet clamp 6 (Fig. 1). Several layers of balls allow rods with a spherical sharpening of the working surface to copy the shaped profile of the workpiece 5.
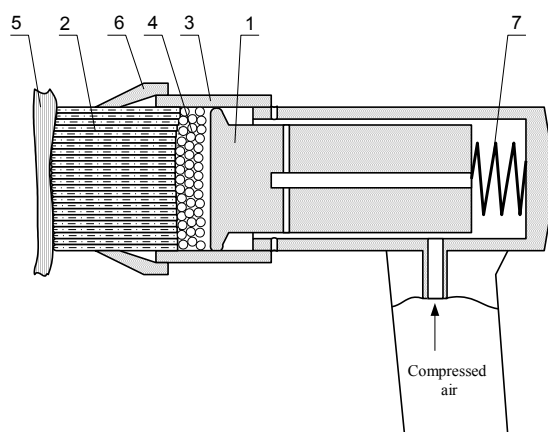
Fig. 1. Diagram of multi-contact vibro-impact tool (BRH):
1 - power drive, 2 - set of round rods, 3 - hardener body,
4 - steel balls, 5 - workpiece, 6 - collet clamp, 7 - elastic element

Main Part

The processing method under consideration is studied by a fairly large number of authors [1–10]. When studying the technological capabilities of the BRH processing, it was found that the impact energy of the drive, the diameter of the sharpening of the rods, the number of rods in the set, and the advance of the device along the working surface, have the greatest impact on the quality of the workpiece surface layer [1, 2]. In the work of Shcherba L.M. [1], a methodology for designing the process of treatment by a ball-rod hardener is developed.

Dependences are presented for determining the quality parameters of the surface layer: roughness of the treated surface, the degree of deformation, and the depth of the hardened layer. In the work of Isaev A.G. [2, 5], these dependences are refined and described below.

The surface roughness is determined by the formula

$$Rz = 0.03\sqrt{\frac{E_y \cdot \eta}{D \cdot N \cdot HB^{1,12}}} \, , \qquad (1)$$

where E_y is indenter impact energy; N is the number of rods in the set; HB is hardness of the work material according to Brinell; η is the device efficiency depending on a number of factors (interference during processing, the number of layers of balls, etc.), D is the diameter of the spherical sharpening of the hardener rod (indenter).

The deformation ratio is presented as:

$$\varepsilon = 1.13\sqrt[4]{\frac{E_y \cdot \eta}{D^3 \cdot N \cdot HB^{1,12}}} \, . \qquad (2)$$

The depth of the hardened layer is determined from the following relationship:

$$h_n = \sqrt[8]{\dfrac{\left(\dfrac{E_y \cdot \eta}{D \cdot N \cdot HB^{1,12}}\right)^3}{D}} \; . \tag{3}$$

In the study of Yu.R. Kopylov [3], the dependence of the determination of residual stresses for vibration finishing and hardening treatment is given. It seems possible to apply a similar technique to determine the residual stresses under the BRH processing through introducing the coefficient k_u that considers the features of the generation of internal stresses under the BRH processing. The coefficient k_u is determined during experimental studies. After transformations, the dependence will take the following form:

$$\sigma_0 = k_u k_\sigma \left(\dfrac{E_y}{\left(\dfrac{Dd}{2(D+d)}\right)^3}\right)^{\frac{1}{5}} \cdot \left(\dfrac{1-\nu_\partial^2}{E_\partial} + \dfrac{1-\nu_u^2}{E_u}\right)^{\left(-\frac{4}{5}\right)}, \tag{4}$$

where k_u is the coefficient that considers features of the generation of internal stresses during the BRH processing (determined experimentally); k_σ is the coefficient that takes into account the ability of the material to hardening; E_y is indenter impact energy; D and d are the diameters of the rod sharpening and the indent on the workpiece, respectively; ν_∂ and ν_u are Poisson's ratios for the workpiece and the rod; E_∂ and E_u are elasticity moduli for the workpiece and the rod, respectively.

To verify the adequacy of dependence (4), experimental studies on the generation of residual stresses under the BRH were carried out. Residual stresses were measured according to the standard method used by the factory laboratory, Rostvertol, Russian Helicopters JSC, using an automated test bench for residual stresses ASCON-3-KI on samples of B95 aluminum alloy. The rectangular samples 200×100×20 mm were processed under various modes with a tightness of 1.5 mm and 4.5 mm. Sets of rods with a radius of spherical sharpening of 4 mm and 8 mm were used. The residual stresses were determined according to the Davidenkov method through etching surface layers from plate samples cut from rectangular work samples. The measured values were compared to the theoretical values calculated from the formula (4). The calculation results are presented in Table 1.

The coefficient value k_u is determined from the results of preliminary experimental studies through comparing the magnitude of the residual stresses calculated by the dependence (4) and obtained experimentally. It varies in the range of 1.5–1.7. For calculations, the value of 1.6 is taken

Table 1

Comparison of the results of theoretical and experimental studies

Initial data		Theoretical values, MPa	Experimental data, MPa	Difference of theoretical data from experimental data, %
Rod sharpening radius	Interference			
4	4.5	141.6	168	15.7
4	1.5	137.3	135	1.7
8	4.5	124.1	130	4.5
8	1.5	118.74	126	5.6

Fig. 2 and 3 show graphs of the dependences of the residual stresses on the interference under processing. The solid line shows the theoretical curve. The squares indicate the results of experimental studies.
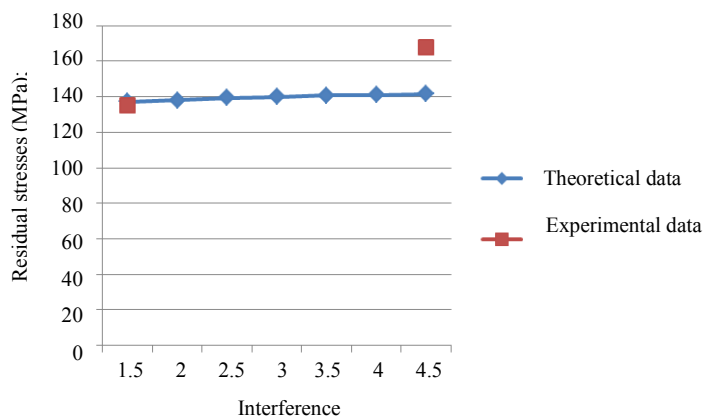
Machine building and machine science

Fig. 2. Dependence of residual stresses on interference under processing.
Spherical sharpening radius of the rod R = 4 mm
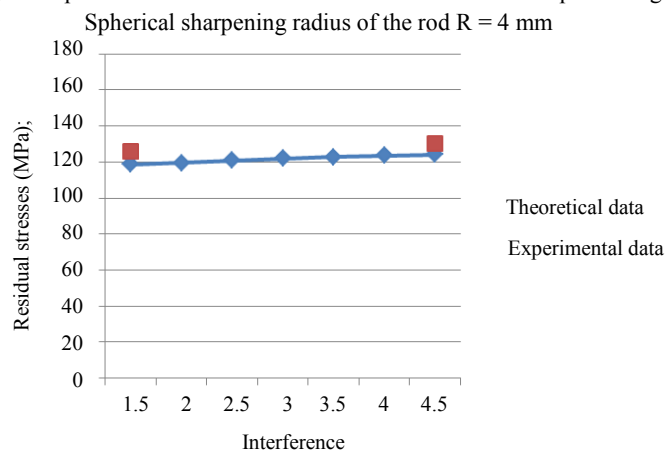
Fig. 3. Dependence of residual stresses on interference under processing.
Spherical sharpening radius of the rod R = 8 mm

For the values of residual stresses obtained as a result of studies, the changes in the fatigue characteristic, the ultimate stresses of the cycle in depth, were calculated using the formula given in [1]. It is known that the endurance limit value is affected by the value of the average stress of the cycle, which largely depends on the level of residual stresses of the surface layer.

The graphs are presented in Fig. 4–7. The solid line shows the ultimate stresses of the cycle, the dotted line shows the distribution of residual stresses.
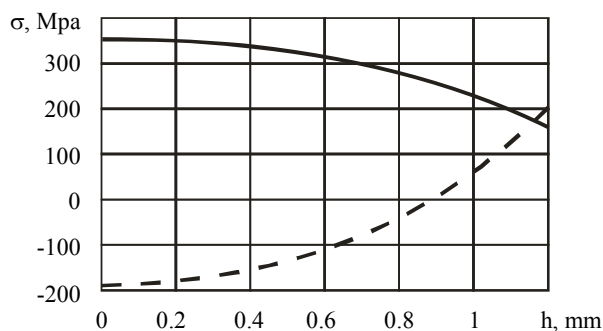
Fig. 4. Change in limiting stresses value of the cycle along the workpiece depth after BRH processing: R = 4 mm, interference is 4.5 mm
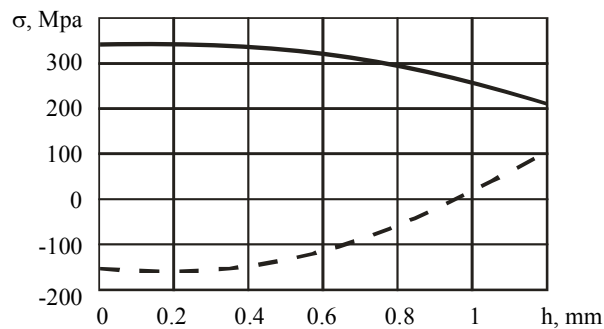
Fig. 5. Change in limiting stresses value of the cycle along the workpiece depth after BRH processing: R = 4 mm, interference is 1.5 mm
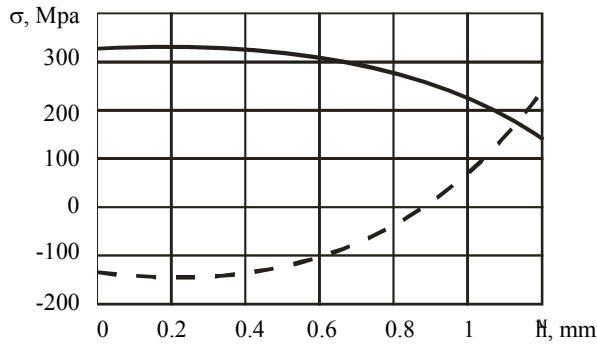
Fig. 6. Change in limiting stresses value of the cycle along the workpiece depth after BRH processing: R = 8 mm, interference is 1.5 mm
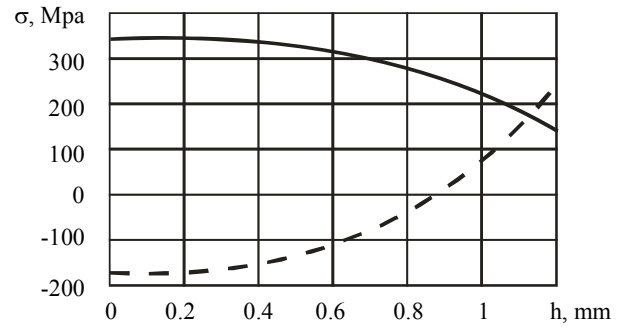
Fig. 7. Change in limiting stresses value of the cycle along the workpiece depth after BRH processing: R = 8 mm, interference is 4.5 mm

Conclusion

Based on the results of the research, the following conclusions can be drawn.

1. The residual stresses in the surface layer are compressive, which enables to predict high performance properties of the finished workpieces.

2. The magnitude of the residual stresses on the workpiece surface is in the range of 130–200 MPa, which, according to the data of Rostvertol PJSC, approximately corresponds to the magnitude of the residual stresses after the vibration hardening treatment.

3. The depth of the compressive residual stresses is in the range of 0.9–1 mm, which, according to the data of Rostvertol PJSC, is approximately two times greater than during the vibration hardening treatment.

4. BRH processing of workpieces provides increasing the ultimate stress of the cycle during cyclic loading of the workpiece by 27–35%.

5. Processing modes have a slight impact on the magnitude and depth of the residual stresses.

6. It is established that the difference between the results of theoretical and experimental studies does not exceed 20%, which indicates the adequacy of the obtained theoretical dependence for calculating the residual stresses under processing by a ball-rod hardener.

Studies on residual stresses with BRH are presented in the works of A. Shvedova [4, 6–9]. In [4], computer simulation of the process was performed using the Ansys software package. The obtained values of residual stresses correlate with the results of the above experiments.

Based on the research results, the following methodology for designing a ball-rod hardener treatment is proposed.

1. The limits of the required quality parameters of the workpiece surface layer are set.

2. A pneumatic hammer is selected. Then, a nozzle is selected considering those at the tooling engineer's disposal. For processing small areas, nozzles with a small number of rods are recommended; for processing areas of a large area – with a large number of rods. The number of layers of balls is selected depending on the height of the drops or the radius of curvature of the work surface.

3. Interference during processing and the radius of sharpening of the rod are selected. For harder materials, higher machining interferences and smaller sharpening radii are selected.

4. We assign a processing time of 10-15 seconds for the area of the bundle of rods. Considering the feed value recommended above, the number of tool passes along the workpiece surface is selected, and in most cases it is desirable to use single-pass machining. If there are several options for combinations of processing modes that enable to obtain the specified characteristics of the surface layer, the one, whose total processing time for a particular workpiece is shorter, is selected.

5. Then, the arithmetic average deviation of the surface roughness, the depth of the hardened layer, the deformation ratio, and the residual stresses are calculated according to formulas 1–4.

Machine building and machine science

147

6. Based on the calculation results, the selected processing modes are adjusted. Then, the parameters of the machined surface are calculated again, and so on, until all the specified characteristics are located within the necessary limits.

The above technique can be used under the production design of the BRH treatment.

The above engineering recommendations were used in the implementation of the BRH treatment at Rostvertol PJSC.

References

1. Tamarkin MA, Shcherba LM, Tishchenko EE. Proektirovanie tekhnologicheskikh protsessov vibroudarnoi otdelochnoi obrabotki shariko-sterzhnevym uprochnitelem [Design of technological processes for vibro-impact finishing treatment with a ball-rod hardener]. Strengthening Technologies and Coatings. 2005;7:13–20. (In Russ.)

2. Tamarkin MA, Chukarin AN, Isaev AG. Obespechenie akusticheskoi bezopasnosti tekhnologicheskogo protsessa obrabotki shariko-sterzhnevym uprochnitelem ploskikh detalei pri dostizhenii zadannykh parametrov poverkhnostnogo sloya [Ensuring acoustic safety of technological processing with a ball-rod reinforcer of flat details at achievement of the set blanket parameters]. Naukovedenie. 2016;6:28–35. (In Russ.)

3. Kopylov YuR. Dinamika protsessov vibroudarnogo uprochneniya: monografiya [Dynamics of vibro-impact hardening processes: monograph]. Voronezh: IPTs "Nauchnaya kniga"; 2011. 568 p. (In Russ.)

4. Shvedova AS. Povyshenie ehkspluatatsionnykh svoistv detalei pri obrabotke dinamicheskimi metodami poverkhnostnogo plasticheskogo deformirovaniya: dis. …kand. tekhn. nauk [Improving the operational properties of parts during processing by dynamic methods of surface plastic deformation: Cand.Sci. (Eng.) diss.]. Rostov-on-Don; 2016. 144 p. (In Russ.)

5. Tamarkin MA, et al. Povyshenie kachestva poverkhnostnogo sloya i bezopasnosti protsessa pri obrabotke detalei shariko-sterzhnevym uprochneniem [Improving the surface layer quality and process safety during the treatment of parts by ball-hardening]. Vestnik of P.A. Solovyov Rybinsk State Aviation Technical University. 2017;2(41):82–88. (In Russ.)

6. Tamarkin MA, Tishchenko EE, Shvedova AS. Optimization of Dynamic Surface Plastic Deformation in Machining. Russian Engineering Research. 2018;38(9):726—727.

7. Tamarkin MA, Shvedova AS, Tishchenko EE. Optimizatsiya protsessov obrabotki detalei dinamicheskimi metodami poverkhnostnogo plasticheskogo deformirovaniya [Optimization of parts processing by dynamic methods of surface plastic deformation]. STIN. 2018;3:26–28. (In Russ.)

8. Tamarkin MA, Shvedova AS, Tishchenko EE. Uvelichenie zhiznennogo tsikla detalei pri obrabotke dinamicheskimi metodami poverkhnostnogo plasticheskogo deformirovaniya [Increase in the life cycle of products when processing parts by dynamic methods of surface plastic deformation]. Contemporary Technologies in Automation. 2018;72(9):403–408. (In Russ.)

9. Tamarkin MA, Shvedova AS, Tishchenko EE. Metodika proektirovaniya tekhnologicheskikh protsessov obrabotki detalei dinamicheskimi metodami poverkhnostnogo plasticheskogo deformirovaniya [Methodic of technological processes designing of parts processing by dynamic methods of surface plastic deformation]. Vestnik Mashinostroeniya. 2018;4:78–83. (In Russ.)

10. Tamarkin MA, et al. Background technology of finish-strengthening part processing in granulated actuation media. Advances in Intelligent Systems and Computing. 2019;118-123.

About the authors:

Tamarkin, Mikhail A., Head of the Engineering Technology Department, Don State Technical University (1, Gagarin sq., Rostov-on-Don, 344000, RF), Dr.Sci. (Eng.), professor, ScopusID 6603762604, ORCID: https://orcid.org/0000-0001-9558-8625, tehn_rostov@mail.ru

Tishchenko, Ehlina E., associate professor of the Engineering Technology Department, Don State Technical University (1, Gagarin sq., Rostov-on-Don, 344000, RF), Cand.Sci. (Eng.), associate professor, ORCID: https://orcid.org/0000-0001-5156-5544, lina_tishenko@mail.ru

Novokreshchenov, Sergei A., postgraduate student of the Engineering Technology Department, Don State Technical University (1, Gagarin sq., Rostov-on-Don, 344000, RF), ORCID: https://orcid.org/0000-0002-7880-0783, Novokreschenov.sergej@yandex.ru

Morozov, Sergei A., external doctorate student of the Engineering Technology Department, Don State Technical University (1, Gagarin sq., Rostov-on-Don, 344000, RF), ScopusID 57211903915, ORCID: https://orcid.org/0000-0001-9937-7120, morozov-sergey@sssu.ru

Claimed contributorship

M. A. Tamarkin: academic advising; research objectives and tasks setting; correction of the conclusions. Eh. Eh. Tishchenko: research results analysis; text preparation; formulation of conclusions. S. A. Novokreshchenov: testing; computational analysis; the text revision. S. A. Morozov: basic research concept formulation; conducting of theoretical research; development of layout of experiments.

All authors have read and approved the final manuscript.

Machine building and machine science

MACHINE BUILDING AND MACHINE SCIENCE

Car integral performance index simulation

S. V. Teplyakova, A. A. Kotesova, N. N. Nikolaev
Don State Technical University (Rostov-on-Don, Russian Federation)

Introduction. The paper is devoted to the comparison and evaluation of the quality of a car using the method of mathematical simulation of the integral performance index. The work objectives were to develop a mathematical modeling technique for the integral performance index, to draw up a step sequence of quality assessment, to analyze most common brands of passenger cars on the domestic market, to sum up and validate the result obtained.

Materials and Methods. The sequence of simulating the integral performance index is proposed. Numerical modeling of the integral performance index is carried out on the example of six most common brands of passenger cars on the domestic market.

Results. A method of modeling the integral performance index is developed. A step sequence of the analysis is described. An additive form of determining the integral performance index which provides combining single, unrelated quality indices into a complex indicator in the process of comparison is proposed.

Discussion and Conclusions. The proposals presented can be used in the process of assessing and diagnosing the competitiveness of not only cars, but also of other products with a large set of independent quality indicators.

Keywords: modeling, integral index, quality requirements, motor car, performance specifications, additive method, weight coefficient.

Introduction. To obtain, systematize, describe and apply accumulated knowledge and information in any field of activity, a universal simulation technique is most widely used. Mathematical modeling is systematically supported and updated in many fields of science. Mathematical modeling provides combining accumulated knowledge and real processes including mental ones [1], combining the ability to reproduce the properties of a real or created object, process or phenomenon using another object, process or phenomenon.

Quality is a combination of consumer properties unrelated to each other through technical characteristics that must satisfy current and future needs [2]. At the same time, a close relationship between quality and requirements can be traced. Requirements are specific features and conditions that correspond to consumer preferences throughout the life of the product. Product requirements are laid at the design stage [3, 4].

However, quality and requirements have some inconsistency [5, 6]. This is most pronounced in the discrepancy between the declared technical qualities of the goods and the requirements of consumers. This is due to the constant change in consumer requirements depending on technology development, as well as the financial and cultural condition of the population.

Depending on the number of characterized properties and on their influence on the quality of the product, quality indices are divided into simple and complex. A simple index enables to characterize one property or one dependence of quality on the technical and operational characteristics, while a complex index combines several characteristics.

There is a concept of direct and inverse indices. An increase in direct indices causes an increase in quality; an increase in inverse indices causes a decrease [7].

After analyzing the classification of product quality indices (Fig. 1), we can conclude that the integrated index is a special case of a complex index. An integrated quality index characterizes the ratio of the overall useful effect during the operation of a given product to the cumulative costs of its purchase, operation or consumption [8].
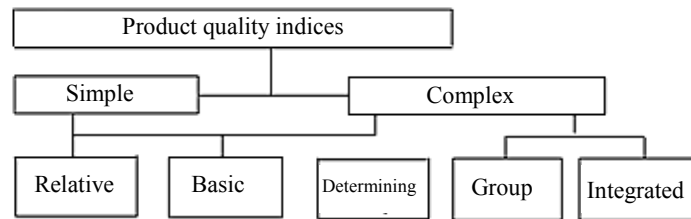
Fig. 1. Classification of product quality indices

Simulation technique for the integrated index of product quality.

The definition of a quality index by an example of a car is carried out in the sequence:

• goal setting;

• selection of prototypes for comparison and choice of the optimum alternative;

• selection of parameters characterizing the product from the standpoint of the consumer;

• determination of averages of quality indices;

• combining averages into one index for each brand;

• analysis of the integrated indices obtained for all prototypes;

• decision-making on product quality control.

The greatest difficulties are the selection of characteristics and obtaining the averages of these data [9] since there are no common techniques for forming a list of quality indices and transforming each index into a numerical form. To determine the integrated quality index, its additive form is widely used, i.e., the weighted average summation, which allows combining simple, unrelated quality indices into a complex index. It is used in cases when decisions are made on the economically best option if several prototypes are available on the market. That is, this technique is most suitable for modeling an integrated index of car quality.

The formula for calculating the complex integrated index [10]:

$$K_i = \sum_{i=1}^{n} \alpha_i \cdot \bar{X}_i,$$

where α_i is weight coefficient of the i-th parameter; $\bar{X}_i$ is the averaged quality index for the i-th parameter; n is the number of parameters to compare.

To determine the weight coefficient, an expert method is used according to the expression:

$$\sum_{i=1}^{n} \alpha_i = 1.0.$$

The algorithm of the calculations used can be traced on the example of choosing the best option for buying a car (Fig. 2).
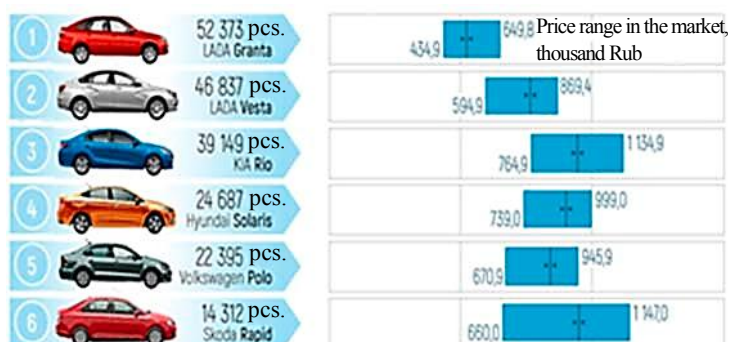
Fig. 2. Popular sedans at the domestic market

The analysis was carried out on the bestselling cars at the domestic market. The hierarchy is implemented by price characteristics.

Study Results. For the purity of the experiment, six sedan cars were compared in the same price category. There are several tens of quality indices; in the calculations, an integrated index was calculated for 6 groups of basic (from the consumer's point of view) quality indices. The initial data for the calculation are given in Table 1. In practice, the use of such quality assessments can take into account a different number of characteristics, even considering the fact that many of them have a rather contradictory effect on quality and, in their physical nature, are very difficult to quantify.

Table 1

Source Data

Car parameter	Model					
	Lada Granta	Hyundai Solaris	Skoda Rapid	Kia Rio	Lada Vesta	Volkswagen Polo
Price, thousand Rub	580	750	680	640	600	690
Mileage, thousand km	50	75	57	26	53	50
Fuel rate, l	7.2	8.3	8.5	6.4	8.7	8.0
Power, kWt	72.07	90.50	80.91	73.50	78.00	80.91
Clearance, mm	170	160	136	160	171	163
Acceleration time, s	11.5	11.0	10.0	13.1	12.8	11.7

An intermediate stage of the calculation is to obtain the averages of the 6 considered quality indices for each model. The weight coefficient is determined by the expert evaluation method, where the human factor (personal preferences) also plays an important role in the assessment and significantly affects the final value of the integrated quality index of the sedans compared. The calculation results are presented in Table 2.

Table 2

Calculation Results

Quality index	Model					
	Lada Granta	Hyundai Solaris	Skoda Rapid	Kia Rio	Lada Vesta	Volkswagen Polo
Rank by sales	1	4	6	3	2	5
Weight coefficient	0.11	0.15	0.25	0.15	0.14	0.20
Integrated quality index	0.32	0.32	0.71	0.48	0.33	0.49
Rank by quality index	5	5	1	3	4	2
Marketability	$55 \cdot 10^{-5}$	$42 \cdot 10^{-5}$	10^{-3}	$75 \cdot 10^{-5}$	$55 \cdot 10^{-5}$	$71 \cdot 10^{-5}$

Thus, the maximum quality integrated index belongs to Skoda Rapid and it is 0.71. At the same time, the values of the quality factor of the other compared cars that are in the same price range differ slightly. The values of the competitiveness indicator of the compared sedans are obtained by the ratio of the quality index and the cost of the car. This is also maximum estimator for Skoda Rapid, which is explained by the fact that the buyer of this car for one monetary unit gains more quality than buyers of the prototypes compared.

Discussion and Conclusions. Recording information about an object of research or design requires using mathematical simulation to store and transmit it in space or in time. The simulation is aimed at building, improving, studying and applying models of actually existing or designed objects for the subsequent assessment of their competitiveness. The integrated quality index is one of the unified indicators that can implement a comparison of indices even with a conflicting effect on quality.

References

1. Teplyakova SV, Cherpakov AV, Kosenko VV, et al. Matematicheskoe modelirovanie nadezhnosti mashin [Mathematical modeling of machine reliability]. In: Proc. Int. Conf. on "Physics and Mechanics of New Materials and Their Applications" (PHENMA 2016): Abstracts&Schedule, 19–22 July, 2016. Indonesia, Surabaya; 2016. P.268. (In Russ.)

2. Teplyakova SV, Cherpakov AV, Kosenko VV, et al. Analiz trebovanii dlya obespecheniya absolyutnoi bezotkaznosti mashin [Analysis of requirements to ensure absolute machine reliability]. In: Proc. Int. Conf. on "Physics and Mechanics of New Materials and Their Applications" (PHENMA 2016): Abstracts&Schedule, 19–22 July, 2016. Indonesia, Surabaya; 2016. P.267. (In Russ.)

3. Saati T, Kerns K. Analiticheskoe planirovanie. Organizatsiya sistem [Analytical planning. Organization of systems]. Moscow: Radio i svyaz'; 1991. 224 p. (In Russ.)

4. Teplyakova SV, Kotesova AA, Kopylov FS, et al. Opredelenie parametrov zakona Veibulla [Determination of the Weibull law parameters] Scientific Life. 2019;14(2):14–18. URL: http://www.sced.ru/ru/index.php? option=com_content&view=article&id=722:nauchnaya-zhizn-02-2019&catid=39& Itemid=156 (accessed 19.12.2019). (In Russ.)

5. Nedoluzhko AI, Smirnov II, Kotesova AA, et al. Ehffektivnost' diagnostiki avtomobilei s ehlektronnymi blokami upravleniya [Efficiency of diagnostics of cars with electronic control units]. In: Proc. 7th Int. Sci.-Pract. Conf. on "Quality in production and socio-economic systems". Kursk: Publ. House of South-West. University. 2019;2:9–12. URL: https://www.elibrary.ru/item.asp?id=37536406 (accessed 04.05.2020). (In Russ.)

6. Kas'yanov VE, Teplyakova SV. Metody obespecheniya absolyutnoi bezotkaznosti detalei mashin [Methods of reliability of machine parts]. Naukovedenie. 2013;3:139. URL: https://naukovedenie.ru/PDF/39trgsu313.pdf (accessed 04.05.2020). (In Russ.)

7. Fedyukin VK, Durnev VD, Lebedev VG. Metody otsenki i upravleniya kachestvom promyshlennoi produktsii: uchebnik dlya vuzov [Methods for assessing and managing the quality of industrial products]. Moscow: Filin" Rilant; 2001. 328 p. (In Russ.)

8. Fatkhutdinov RA. Konkurentosposobnost': ehkonomika, strategiya, upravlenie [Competitiveness: economics, strategy, management]. Moscow: INFRA-M; 2000. 312 p. (In Russ.)

9. Kas'yanov VE, Teplyakova SV. Teoreticheskie osnovy obespecheniya absolyutnoi bezotkaznosti detalei za zadannyi resurs [Theoretical foundations of ensuring absolute reliability of parts for a given resource]. Sovremennyi nauchnyi vestnik. 2015;1(2):59–70. (In Russ.)

10. Kolesov IM, Sycheva NA. Kachestvo i ehkonomichnost' produktsii [Product quality and economy]. Standards and Quality. 2000;9:70–72. (In Russ.)

Machine building and machine science

About the authors:

Teplyakova, Svetlana V., associate professor of the Transport Systems Operation and Logistics Department, Don State Technical University (1, Gagarin sq., Rostov-on-Don, 344000, RF), Cand.Sci. (Eng.), ORCID: https://orcid.org/0000-0003-4245-1523, ResearcherID: AAL-7931-2020, svet-tpl@yandex.ru

Kotesova, Anastasiya A., associate professor of the Transport Systems Operation and Logistics Department, Don State Technical University (1, Gagarin sq., Rostov-on-Don, 344000, RF), Cand.Sci. (Eng.), ORCID: https://orcid.org/0000-0001-7663-1288, ResearcherID: AAL-7301-2020, a.kotesova@mail.ru

Nikolaev, Nikolai N., associate professor of the Transport Systems Operation and Logistics Department, Don State Technical University (1, Gagarin sq., Rostov-on-Don, 344000, RF), Cand.Sci. (Eng.), ORCID: https://orcid.org/0000-0003-2087-0233, ResearcherID: AAL-7111-2020, nnneks@yandex.ru

Claimed contributorship

S. V. Teplyakova: basic concept formulation; research objectives and tasks setting; computational analysis; data acquisition, analysis and interpretation. A. A. Kotesova: text preparation; formulation of conclusions and of the first version of the paper. N. N. Nikolaev: analysis of the research results; the release paper version revision.

All authors have read and approved the final manuscript.

MACHINE BUILDING AND MACHINE SCIENCE
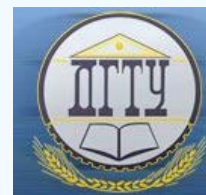
Mobile machine design through dynamic load simulation on their drive units

S. A. Partko, L. M. Groshev, A. N. Sirotenko
Don State Technical University (Rostov-on-Don, Russian Federation)

Introduction. The mobile machine design is impossible without considering the vibration parameters of their units. This requires the development of specialized dynamic models that take into account the probabilistic nature of these parameters. The root cause for the occurrence of vibration effects is the profile irregularity of the mobile machine path, and the variability of physicomechanical characteristics of the soil. Problems that consider these features are solved linearly with sufficient accuracy; but in multidimensional dynamical systems, such an approach is unacceptable due to the presence of a large number of interrelationships. The work objective is to conduct a comparative analysis of the efficiency of existing calculation methods of statistical characteristics of uncorrelated external actions as applied to a mobile machine presented as a multidimensional dynamic system with actions having different correlations.

Materials and Methods. External actions in the multidimensional dynamical systems are considered in a matrix form. When calculating statistical characteristics, intercouplings in the spectral density matrices are taken into account. The elements of the main and secondary diagonals are determined; the correlations between the effects are taken into account. These features significantly complicate the calculations. So, to get matrices of uncorrelated actions, the matrix of external actions is reduced to a diagonal form.

Results. A numerical comparison of spectral densities and intensity of the mobile machine oscillations under variation of speeds and nature of the soil fertility microprofile was carried out using various methods of calculation. Certain characteristics of spectral densities and oscillations of mobile machines of agroindustrial complex enabled to develop recommendations on the practical application of the presented dependences for designing this machinery.

Discussion and Conclusions. The results of solving the matrix of spectral densities of external actions by various methods are presented on the diagram of spectral oscillation velocities. The analysis of characteristic curves has shown that the identical results, regardless of the calculation method, are obtained only for machines with weak functional relations under the uncorrelated external action of the soil fertility. For some cases, the resonance machine speeds are set. The effect of irregularities of the soil fertility on the oscillation intensity of the machine units and the dispersion of loads on the units is shown in the graphical representation.

Keywords: multidimensional dynamic system, spectral density matrix, uncorrelated external influences, inverse matrix, attached matrix.

Introduction. When designing reliable mobile equipment, both static dynamic loads should be considered. Vibrations of the machine and its components affect significantly the characteristics of dynamic loads. Accounting and determination of vibration parameters require the development of specialized dynamic models that consider these

parameters as regards to probabilistic analysis. The root reason for the vibration effects is due to the uneven profile of the mobile machine path and the inconsistency of the physical and mechanical characteristics of the agricultural background. Problems that consider these features are solved linearly with sufficient accuracy, which is unacceptable when solving multidimensional dynamical systems with a large number of interconnections.

Materials and Methods. Quality of the technological process performed by a mobile agricultural machine is affected by both the characteristics of its working bodies [1–5] and the characteristics of the undercarriage system [6, 7], as well as the microrelief of the agricultural background [8, 9]. In general, external actions on a machine are considered as a system with n functions. The processes of changing the microroughness of the path (or changing the soil density) are denoted as functions $q_1(t) \ldots q_n(t)$ [9, 10].

If the statistical description of external actions admits a stochastic orthogonal representation, then the following equation is valid:

$$q_i(t) = m[q_i(t)] + \int_{-\infty}^{\infty} Q_i(\omega) \cdot \phi_i(t, \omega) d\omega,$$

where $Q_i(\omega)$ is a system of random functions ω; $\varphi_i(t,\omega)$ is a system of nonrandom functions t and parameter ω; $m[q_i(t)]$ is mathematical expectation.

Mobile agricultural machines are systems with delayed actions [2, 6, 9], which are characterized by many parameters of uneven field microrelief or soil hardness [2, 8, 9]. These are one-type parameters, and they can be shifted in time t_0. In addition, the design of the machine (front and rear axle wheels) affects the relationship between the actions. Given these features and the assumption that the mathematical expectation of external actions is zero, the matrix of spectral densities of external actions is described as follows [11, 12]:

$$S_q(\omega, j\omega) = \begin{Vmatrix} S_h(\omega) & S_h(\omega)e^{-j\omega t_0} & c_{13}S_{h\psi}(j\omega) \\ S_h(\omega)e^{j\omega t_0} & S_h(\omega) & c_{23}S_{h\psi}(j\omega) \\ c_{31}S_{\psi h}(j\omega) & c_{32}S_{\psi h}(j\omega) & S_\psi(\omega) \end{Vmatrix}, \tag{1}$$

where $c_{13} = t; c_{23} = e^{-j\omega t_0}; c_{31} = 1; c_{32} = e^{j\omega t_0}$ — for front drive axle; $c_{13} = e^{-j\omega t_0}; c_{22} = 1; c_{31} = e^{j\omega t_0}; c_{32} = 1$ — for rear drive axle.

To simplify the calculation of statistical characteristics, we reduce the matrix to a diagonal form to obtain a matrix of uncorrelated external actions. We introduce the characteristic matrix and reduce the matrix (1) to the form:

$$S_q(\omega, j\omega) - \lambda(j\omega) \cdot E = \begin{Vmatrix} S_h(\omega) - \lambda(j\omega) & S_h(\omega)e^{-j\omega t_0} & c_{13}S_{h\psi}(j\omega) \\ S_h(\omega)e^{j\omega t_0} & S_h(\omega) - \lambda(j\omega) & c_{23}S_{h\psi}(j\omega) \\ c_{31}S_{\psi h}(j\omega) & c_{32}S_{\psi h}(j\omega) & S_\psi(\omega) - \lambda(j\omega) \end{Vmatrix}, \tag{2}$$

where λ is a characteristic function; E is an identity matrix.

The characteristic equation can be represented as:

$$a\lambda^3(j\omega) + b\lambda^2(j\omega) + c\lambda(j\omega) + d = 0. \tag{3}$$

The characteristic functions $\lambda_1(j\omega), \lambda_2(j\omega), \lambda_3(j\omega)$ were defined using Cardano formulas [13].

The matrix of transition to a new basis constructed from the coordinates of the vectors $\lambda_i(j\omega)$ (at i=1, 2, 3) defined from the equation (3), has the form:

$$T(j\omega) = \begin{Vmatrix} \eta_{11} & \eta_{21} & \eta_{31} \\ \eta_{12} & \eta_{22} & \eta_{32} \\ \eta_{13} & \eta_{23} & \eta_{33} \end{Vmatrix}. \tag{4}$$

In this case, the inverse matrix has the form:

$$T^{-1}(j\omega) = \frac{\tilde{T}(j\omega)}{|T(j\omega)|}, \tag{5}$$

where $\tilde{T}(j\omega)$ is an adjoint matrix; $|T(j\omega)|$ is a matrix determinant.

The desired matrix was determined from the expression:

$$S_d(j\omega) = T^{-1}(j\omega) \cdot S_q(\omega, j\omega) \cdot T(j\omega) = diag \|S_1(j\omega) \cdot S_2(j\omega) \cdot S_3(j\omega)\|, \tag{6}$$

where S_1, S_2, S_3 are spectral densities of uncorrelated effects of complex-variable functions.

Finding the diagonal matrix (6) is simplified through solving a planar problem. In this case, external actions can be represented as:

$$S_q(\omega, j\omega) = \left\| \begin{matrix} S_h(\omega) & S_h(\omega)e^{-i\omega t_0} \\ S_h(\omega)e^{i\omega t_0} & S_h(\omega) \end{matrix} \right\|. \tag{7}$$

Then the characteristic matrix is determined from the expression:

$$S_q(\omega, j\omega) - \lambda(\omega) \cdot E = \left\| \begin{matrix} S_h(\omega) - \lambda(\omega) & S_h(\omega)e^{-i\omega t_0} \\ S_h(\omega)e^{i\omega t_0} & S_h(\omega) - \lambda(\omega) \end{matrix} \right\|. \tag{8}$$

In turn, the characteristic equation can be represented as:

$$\lambda^2(\omega) - 2S_h(\omega) \cdot \lambda = 0. \tag{9}$$

From which, the roots of the equation are: $\lambda_1(\omega) = 0, \lambda_2(\omega) = 2S_h(\omega)$.

At the root $\lambda_1(\omega) = 0$, the system of equations for determining the coordinates of the eigenvectors has the following form:

$$S_h(\omega)\eta_{11}(j\omega) + S_h(\omega)e^{-j\omega t_0} \cdot \eta_{12}(j\omega) = 0. \tag{10}$$

Given $\eta_{11} = e^{-j\omega t_0}$, we find $\eta_{12}(j\omega) = 1$.

At root $\lambda_2(\omega) = 2S_h(\omega)$, we get the system of equations:

$$\begin{cases} -S_h(\omega) \cdot \eta_{21}(j\omega) + S_h(\omega)e^{-j\omega t_0} \cdot \eta_{22}(j\omega) = 0 \\ S_h(\omega)^{j\omega t_0} \cdot \eta_{21}(j\omega) + S_h(\omega) \cdot \eta_{21}(j\omega) = 0 \end{cases}. \tag{11}$$

Then the matrix of transition to a new basis takes the following form:

$$T_1(j\omega) = \left\| \begin{matrix} e^{-j\omega t_0} & e^{j\omega t_0} \\ -1 & e^{2j\omega t_0} \end{matrix} \right\|. \tag{12}$$

Through transforming the expression (8), we find spectral densities of uncorrelated effects:

$$S_1(j\omega) = S_h(\omega) \cdot (1 + e^{-j\omega t_0}) = 0.$$

$$S_2(j\omega) = S_h(\omega) \cdot (1 + e^{j\omega t_0}) = 0. \tag{13}$$

If we assume that the profile of the agricultural background in the longitudinal and cross section is determined by uncorrelated random processes [8, 9], then we can imagine the third element of the diagonal matrix as $S_\omega(\omega)$. In this case, the matrix (13) takes the form:

$$S_d(j\omega) = diag \left\| S_h(\omega) \cdot (1 + e^{-j\omega t_0}); \quad S_h(\omega) \cdot (1 + e^{j\omega t_0}); \quad S_\psi(\omega) \right\| \tag{14}$$

Spectral densities of vibrations were determined through solving the matrix (1), together with the matrix (14) and with account of formulas describing uncorrelated actions. The result is the expression:

$$S_z(\omega) = S_h(\omega) \left[\Phi_{11}^2(\omega) + \Phi_{12}^2(\omega) \right] = 0. \tag{15}$$

Machine building and machine science
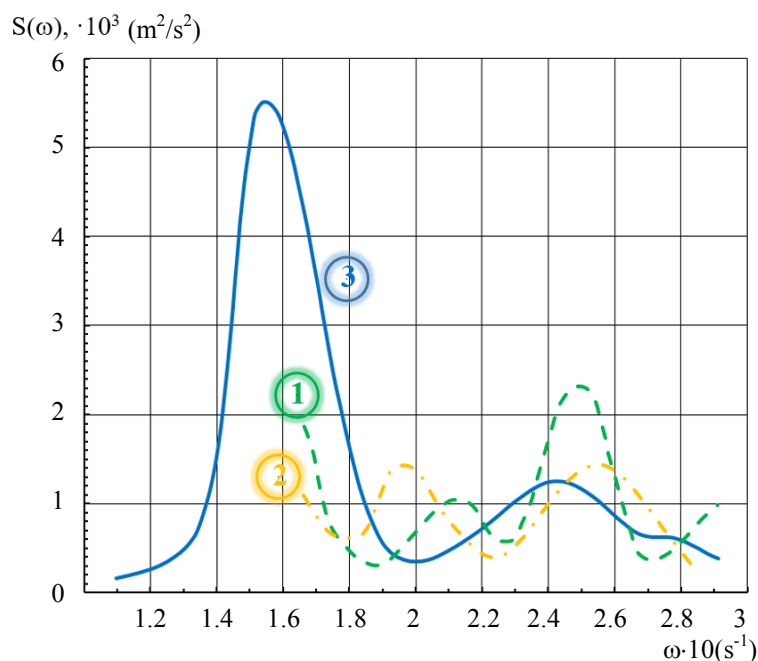
Fig.1 Spectral velocities of vibrations in the solution using:
curve 1— matrix (1); curve 2 — matrix (6); curve 3—matrix (15).

Research Results. Fig. 1 shows graphs of spectral densities of vertical velocities of the front part of the thresher of "Vector" line harvester. Obviously, the dynamic parameters of the machine affect the vibration spectrum (Fig. 1). The narrowband spectrum is typical for conditions of close coincidence of the frequencies of natural vibrations of the combine axles with the reaper (Fig. 1). The width of the spectrum is also affected by the delay in the actions of the wheels of the combine axles.

The results of calculating the intensity of vibrations using matrices (1), (6), (15) are diagrammatized in Fig. 2, which confirms the dependence of functional relationships in the machine on the nature of external actions.
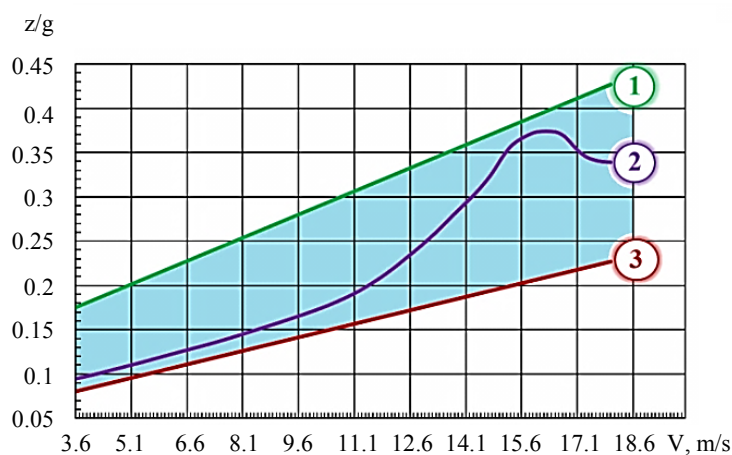
Fig. 2. Diagrams of vibration intensity when the machine moves along microprofile with different nature of irregularities:
1 and 2 — along the furrow; 3 — across the furrow

Solving the systems, which are uncorrelated external actions on a moving machine with weak functional relationships, gives close results regardless of the methods used.

Identical results, when using various calculation methods, are obtained only for machines with weak functional relationships when moving along the field microprofile that generates an uncorrelated external action.

The dynamic characteristics of the combine harvesters were evaluated according to the following formula:

$$W_{ke} = \frac{1}{\pi} \int_{\omega_1}^{\omega_2} S_{ke}(\omega) \cdot d\omega, \qquad (16)$$

where ω_1, ω_2 are spectrum frequency boundaries.

The vibration intensity for various conditions determined using the formula (16), is presented in Fig. 3.
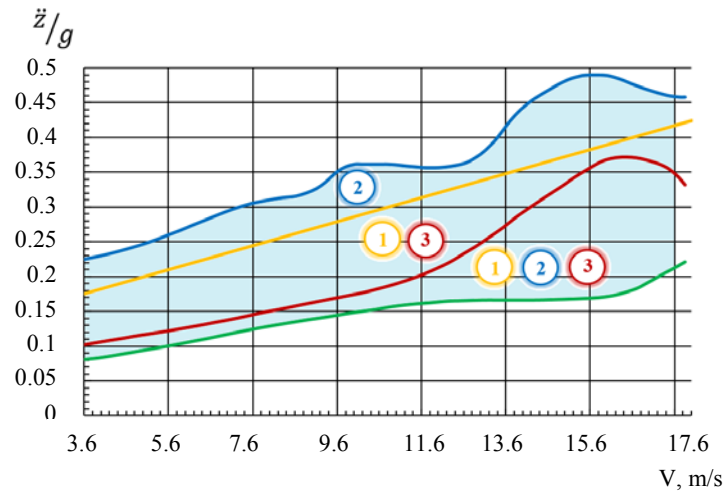
Fig. 3. Engineering assessment results of the harvester dynamics

Fig. 3 shows the dependence of overloads $\ddot{z}/g$ on the combine harvester velocity. Obviously, the different spectral composition of the irregularities of the agricultural background microprofile affects the intensity of vibrations of the machine nodes. There are resonant speeds in the range from 10 to 15 km/h. The graphical dependences obtained (Fig. 2, 3) provide estimating the load spread on the units.

The shaded area illustrates their scattering and enables to estimate the coefficients of variation of $V(z)$. The table shows parameters of the distribution of loads at medium speeds of the machines [2].

Table 1

Dynamic load parameters of mobile machines of agroindustrial complex

Machine type	Work mode	Motion speed m/s	$z_{cк}/g$
Combine harvester Vector	operational	0.840	0.332
	transport	2.781	0.835
Tractor K-700A, trailer 2 PTS-4	operational	3.352	0.474
	transport	8.323	0.510
Tractor T-150A, combine KKU	operational	1.247	0.364
	transport	3.527	0.382
Tractor T-150A, plow PR-2,7	operational (tillage)	0.752	0.346

Results and Discussion. The analysis of the calculation results of the spectral densities of vibrations according to formulas (1), (6), (15) is diagrammatized in Fig. 2, 3. From the graphical dependences, it can be seen that the spectrum of the effects of the loads and their dynamics affect the calculation error.

The calculation of dynamic multidimensional systems and the assessment of machine vibrations are automated and performed using a specialized software product[1].

---

[1] Groshev LM, Partko SA, Lukonin AYu. Calculation of random vibrations of the housing of Don line combine harvester. Certificate of software registration no. 2012614015 Russian Federation. Applicant and proprietor, FSBEI of Higher Education "Don State Technical University". No. 2012611617; March 7, 2012; publ. 04.28.2012.

The program is used to select vibration parameters of the contours and units of mobile agricultural machines, to calculate the smoothness of combine harvesters, to design machine parts [14], and to assess the working conditions of the machine operator.

Before using a software product, you should select a dynamic model first, then to set the design parameters of the machine and its units, and to determine the mass-geometric and elastic-dissipative characteristics of the system.

Conclusions. The expressions (1), (6), (15) are acceptable for the design calculations of spectral densities of impacts on machine components. The use of the formula (6) is unacceptable when designing machines with a mode of movement along irregularities of an agricultural background with a low-frequency spectral composition and for machines with a low correlation of vibrations of the undercarriage and the steering.

References

1. Zharov VP. Dinamika mekhanizmov sel'skokhozyaistvennykh mashin pri znachitel'nom razbrose parametrov v protsesse proizvodstva [Dynamics of agricultural machinery mechanisms with significant parameter spread during production]. Vestnik of DSTU. 2011;11(10):1925–1927. (In Russ.)

2. Partko SA, Groshev LM, Sirotenko AN, et al. Osobennosti spektrov nagruzok na agregaty mobil'nykh mashin APK v polevykh usloviyakh pri zapazdyvanii vneshnikh vozdeistvii [Features of the spectra of loads on the units of mobile agricultural machines in the field when delay in external influences]. Tractors and Agricultural Machinery. 2019;2:56–60. (In Russ.)

3. Antipas IR, D'yachenko AG, Savostina TP. Issledovanie protsessa obmolota tangentsial'no-aksial'nym separiruyushchim ustroistvom v zavisimosti ot raspredeleniya zernovoi massy po zonam [Research of the threshing process with tangential-axial breaking unit in dependence of grain mass zone division]. Science Review. 2016;23:87–91. (In Russ.)

4. Antipas IR, Savostina TP, Saed BI. Vliyanie parametrov molotil'no-separiruyushchego ustroistva na obmolot [Effect of threshing-separating device parameters on threshing]. Vestnik of DSTU. 2017;17(2):108–115. (In Russ.)

5. Groshev LM, Partko SA, Sirotenko AN. Vliyanie prodol'no- uglovykh kolebanii molotilki zernouborochnogo kombaina na plavnost' khoda zhatki [Effect of longitudinal-angular oscillations of the harvester-thresher separator on smooth motion of the reaper]. Vestnik of DSTU. 2017;17(2):131–135. (In Russ.)

6. Zharov VP. Dinamika i modelirovanie transportno-tekhnologicheskikh mashin dlya sel'skogo khozyaistva [Dynamics and modeling of transport technological machines for agriculture]. Vestnik of DSTU. 2011;11(9):1586–1589. (In Russ.)

7. Groshev LM, Partko SA, Sirotenko AN, et al. Sravnenie parametrov razgona mobil'noi mashiny s mekhanicheskim i gidromekhanicheskim privodom [Comparison of acceleration parameters of a mobile car with a mechanical and hydromechanical drive]. In: Proc. 6th Int. Sci.-Pract. Conf. on "State and prospects of agricultural machinery development" within framework of the 16th Int. Agroindustrial Exhibition "Interagromash-2013". Rostov-on-Don: DSTU Publ. House; 2013. P. 74–76. (In Russ.)

8. Partko SA, Groshev LM, Sirotenko AN. Finding stable region of torsional vibrations of agro-industrial rotary cultivators. In: Proc. 5th Int. Conf. on Industrial Engineering (ICIE 2019). Lecture Notes in Mechanical Engineering. Springer. 2019;I:839–845.

9. Partko SA. Optimizatsiya kolebatel'nykh parametrov khodovoi sistemy uborochnogo kombaina [Vibratory parameters optimization of harvester's running gear system]. Vestnik of DSTU. 2008;8(2):141–144. (In Russ.)

10. Sveshnikov AA. Prikladnye metody teorii sluchainykh funktsii [Applied methods of the theory of random functions]. 3rd ed. St.Petersburg: Lan'; 2011. 464 p. (In Russ.)

11. Lur'e AV. Statisticheskaya dinamika sel'skokhozyaistvennykh agregatov [Statistical dynamics of agricultural aggregates]. Moscow: Kolos; 1981. 382 p. (In Russ.)

12. Kamke, E. Spravochnik po obyknovennym differentsial'nym uravneniyam [Handbook on Ordinary Differential Equations]. Moscow: Nauka; 1971. 575 p. (In Russ.)

13. Khimmel'blau D. Analiz protsessov statisticheskimi metodami [Process Analysis by Statistical Methods]. Moscow: Mir; 1973. 957 p. (In Russ.)

14. Androsov AA, Galadzheva MR, Groshev LM, et al. Issledovaniya otkazov i nadezhnosti mobil'nykh mashin [Research of refusals and reliability of the mobile machines]. Vestnik of DSTU. 2010;10(1):102–105. (In Russ.)

About the authors:

Partko, Svetlana A., associate professor of the Machine Design Principles Department, Don State Technical University (1, Gagarin sq., Rostov-on-Don, 344000, RF), Cand.Sci. (Eng.), ScopusID 57202051755, ORCID: http://orcid.org/0000-0002-8568-0716, parlana@rambler.ru

Groshev, Leonid M., professor of the Theoretical and Applied Mechanics Department, Don State Technical University (1, Gagarin sq., Rostov-on-Don, 344000, RF), Dr.Sci. (Eng.), professor, ScopusID 57204647515, ORCID: http://orcid.org/0000-0002-9517-610X, groshev_lm@rambler.ru

Sirotenko, Andrei N., associate professor of the Machine Design Principles Department, Don State Technical University (1, Gagarin sq., Rostov-on-Don, 344000, RF), Cand.Sci. (Eng.), ORCID: http://orcid.org/0000-0001-9956-1032, andsirotenko@yandex.ru

Claimed contributorship

S. A. Partko: basic concept formulation, research objectives and tasks setting; development of the mathematical model; computational analysis; text preparation; formulation of conclusions. L. M. Groshev: academic advising; analysis of the research results; correction of the text and conclusions. A. N. Sirotenko: implementation of the experimental validation; processing of the results; calculations; correction of the text and conclusions.

All authors have read and approved the final manuscript.

MACHINE BUILDING AND MACHINE SCIENCE
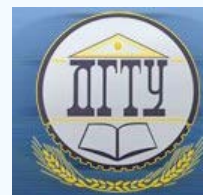
Effect of mass of parts on removal rate under vibroabrasive machining

V. I. Butenko, A. V. Stel'makh

Don State Technical University (Rostov-on-Don, Russian Federation)

Introduction. It should be noted that the study on the problem of the effect of the mass of parts on the vibration-abrasive processing is insufficient. In the works of A.P. Babichev and M.A. Tamarkin, the fact of such an effect is mentioned, but the degree and mechanism of the effect are not disclosed. In the metal removal formulas, only the number of interactions leading to microcutting is taken into account. The present work objective is to determine the effect of the mass of parts on the metal removal rate under vibroabrasive machining.

Materials and Methods. An empirical, i.e., experimental, approach is used. Parts from D16 and 30KhGSA materials which are widely used in the aviation industry were selected as samples. To change the mass, holes were drilled in the blanks; lead was poured into some samples, and plugs made of the same material as the blanks themselves were clogged into the others. Thus, experiments were carried out with solid, hollow, and weighted with lead samples. The working abrasive medium was scrap of grinding wheels of 40 × 80 mm, 25 grain size, and of trihedron prisms of 15 × 15 mm, 16 grain size. The experiments made it possible to clearly demonstrate the effect of grain size on the removal rate of the workpiece.

Results. The parameters of the effect of the mass of parts on the removal rate under vibroabrasive processing are determined. The results obtained show the removal per unit area. The data are approximated by the least squares method with a linear function. A version of its distribution is selected using the Fisher statistical criterion.

Discussion and Conclusion. It is shown how the workpiece mass determines the specific removal rate under the vibroabrasive machining. In the future, the database which is used to determine the effect of the work material characteristics on the process under consideration should be replenished. This will allow introducing a correction factor for the influence of mass in the metal removal formula, which will provide more accurate prediction of metal removal at the design stage of technological processes of vibration-abrasive machining.

Keywords: vibroabrasive machining, abrasive environment, finishing and clearing treatment, mass, specific removal rate, approximation, Fischer criterion, influence coefficient of weight, scrap of grinding wheels, grain size.

Introduction. Engineering has always faced the task of improving the quality of its products. With advances in technology, ways of its solution are improved. This requires methods for predicting the efficiency of finishing processes. Vibroabrasive processing provides the required quality parameters along with high productivity, processing complex parts, as well as multiple-workpiece machining. In order to solve the issues under consideration, the following are being studied:

- organization and development of processes and methods of affecting the working abrasive medium and the object to be processed;
- development of new media and processing techniques;
- reduction of energy costs;
- improving the quality of processing [1].

During vibroabrasive treatment, metal and its oxides are removed from the surface due to mutual collisions of medium particles and workpieces. This process is provided through vibration of the working chamber, in which the workpieces and the medium are located. The camera is mounted on spring supports, so it can vibrate in various directions. Oscillations are transferred from an inertial (or other type) vibrator with a frequency of up to 50–100 Hz and an amplitude of 0.5–5.0 mm or more [2]. The number of interactions on a unit of surface of the workpiece per unit time is of random nature [3– 10].

The study objective is to determine the effect of the mass of parts on the specific removal of metal under the vibroabrasive treatment.

Materials and Methods. The processing was carried out on a universal vibro-tumbling machine with four working chambers with a volume of 10 liters. The analytical balance AD 200 was used for mass measurements.

The working abrasive medium was scrap of grinding wheels of 40×80, grain size 25 [11] (Fig. 1), as well as trihedral prisms (TP) of 15×15 mm, grain size 16 (Fig. 2).

Fig. 1. Scrap of grinding wheels of 40×80, grain size 25

Fig. 2. Trihedral prisms, grain size 16

After a rough turning operation, the samples were processed in an environment of trihedral prisms for 10 minutes to remove burrs and smooth out roughness (Fig. 3).

Fig. 3. Processed parts from aluminum D16 and steel 30GSA

Then, processing was carried out in two stages of thirty minutes in the scrap of abrasive wheels. The working chamber vibrated with a frequency of 34.7 Hz and fluctuated with amplitude of 2.5 mm under continuous supply of process liquid (soda ash solution, 0.2%). The solution removed wear products (particles of metal and abrasive) from the surface of parts and the working medium. Then, processing was carried out in a TP medium (also in two stages of thirty minutes).

Research Results. As a result of the experiments, the desired values of mass m, g, and specific removal rate were obtained. Deviations of d from the theoretical model were estimated. The calculated and tabular values of the Fisher criterion were considered in comparison (Tables 1–4).

Table 1

Resulting data on mass and specific removal of samples from steel 30HGSA in TP environment

Weight, m, g	Removal rate, g/mm^2	d (deviation)
28.53175	2.18976E-06	−1.28317E-07
28.5348	1.73433E-06	−5.83836E-07
40.60125	2.8835E-06	2.10629E-07
40.6065	2.99742E-06	3.24395E-07
44.72755	2.98196E-06	1.87783E-07
44.73305	3.12387E-06	3.2954E-07
78.52885	3.29591E-06	−4.91895E-07
78.5414	4.01564E-06	2.27469E-07
96.7192	3.47528E-06	−8.4725E-07
96.48725	4.55972E-06	2.44012E-07
103.5209	4.14608E-06	−3.76394E-07
103.5378	5.42683E-06	9.03865E-07
Discrepancy	2.68051E-12	
Standard deviation	1.01462E-06	
Confidence interval 95 %	9.09679E-07	
Average	3.40253E-06	
Right class boundary	4.3122E-06	
Left class boundary	2.49285E-06	
F calculated	32.24585006	
F tabulated	3.105806516	
Angular coefficient a	2.93961E-08	
Free member b	1.47936E-06	

Table 2

Resulting data on mass and specific removal of samples from steel 30HGSA in wheel-scrap environment

Weight, m, g	Removal rate, g/mm^2	d (deviation)
28.55685	3.41274E-06	2.74176E-08
28.5631	3.55469E-06	1.69061E-07
40.6304	3.99566E-06	1.37735E-08
40.6367	3.59643E-06	−3.85769E-07
44.7538	4.08941E-06	−9.6225E-08
44.7618	4.54399E-06	3.57958E-07
78.58825	6.05373E-06	1.96296E-07
78.6054	5.48683E-06	−3.71445E-07
96.5534	6.59611E-06	−1.49006E-07
96.775	6.5642E-06	−1.91866E-07
103.5847	7.8442E-06	7.51664E-07
103.6058	6.77172E-06	−3.21859E-07
Discrepancy	1.21985E-12	
Standard deviation	1.5276E-06	
Confidence interval 95 %	1.3696E-06	
Average	5.20914E-06	
Right class boundary	6.57874E-06	
Left class boundary	3.83954E-06	

Weight, m, g	Removal rate, g/mm^2	d (deviation)
F calculated	8.4308727	
F tabulated	3.105806516	
Angular coefficient a	4.94112E-08	
Free member b	1.97429E-06	

Table 3

Resulting data of mass and specific removal of samples from aluminum D16 in TP environment

Weight, m, g	Removal rate, g/mm^2	d (deviation)
10.13095	1.36343E-06	3.59001E-07
10.13305	1.19318E-06	1.88631E-07
14.59555	1.10785E-06	−1,5278E-07
14.59835	1.5057E-06	2.44909E-07
27.98755	1.00601E-06	−1.02312E-06
27.9912	1.1657E-06	−8.63641E-07
34.66113	1.83039E-06	−5.81706E-07
34.73845	4.14834E-06	1.73181E-06
60.9715	3.36435E-06	−5.57569E-07
60.98585	4.57721E-06	6.54468E-07
Discrepancy	6.11719E-12	
Standard deviation	1.36499E-06	
Confidence interval 95 %	1.40279E-06	
Average	2.12622E-06	
Right class boundary	3.529E-06	
Left class boundary	7.23431E-07	
F calculated	13.93008274	
F tabulated	3.249835542	
Angular coefficient a	5.73851E-08	
Free member b	4.23063E-07	

Table 4

Resulting data of mass and specific removal of samples from aluminum D16 in wheel-scrap environment

Weight, m, g	Removal rate, g/mm^2	d (deviation)
10.12275	3.18169E-06	8.85432E-07
10.1236	2.31113E-06	1.47567E-08
14.58795	3.63568E-06	7.25513E-07
14.5936	3.20988E-06	2.98936E-07
27.97185	3.54486E-06	−1.20542E-06
27.9844	4.00792E-06	−7.44089E-07
34.43015	4.09858E-06	−1.53964E-06
34.43015	6.08322E-06	4.45003E-07
60.92935	1.10349E-05	1.75338E-06
60.99307	8.65641E-06	−6.33871E-07
Discrepancy	9.45129E-12	
Standard deviation	2.79828E-06	
Confidence interval 95 %	2.87576E-06	
Average	4.97643E-06	
Right class boundary	7.85219E-06	
Left class boundary	2.10066E-06	
F calculated	51.65197229	
F tabulated	3.249835542	

Weight, m, g	Removal rate, g/mm^2	d (deviation)
Angular coefficient a	1.37487E-07	
Free member b	9.04509E-07	

We approximate the tabular data by a linear dependence using the least-squares method. We take the approximating function in the form: $y = ax + b$. Then the discrepancy (sum of squared deviations) has the form: $S(a, b) = \sum_{i=1}^{n}(y_i - ax_i - b)^2$. In the least-squares method, discrepancy should be minimal. At the minimum point of the multivariable function, the partial derivatives of this function with respect to independent parameters are equal to zero; therefore, the minimum conditions are:

$$\begin{cases} \dfrac{\partial S}{\partial a} = -2 \sum_{i=1}^{n}(y_i - ax_i - b)x_i = 0, \\ \dfrac{\partial S}{\partial a} = -2 \sum_{i=1}^{n}(y_i - ax_i - b) = 0. \end{cases}$$

After transformations, we obtain the following system of two algebraic equations with two unknowns:

$$\begin{cases} a \sum_{i=1}^{n} x_i^2 + b \sum_{i=1}^{n} x_i = \sum_{i=1}^{n} x_i y_i, \\ a \sum_{i=1}^{n} x_i + bn = \sum_{i=1}^{n} y_i. \end{cases} \tag{1}$$

Denote the mass of parts by x, y is the specific removal of workpieces. We approximate the given tabular function by a linear dependence. To determine the best parameters a and b by the least-squares method, we solve the system (1). We solve the system using the matrix method in Microsoft Excel and obtain the values of a and b (see Tables 1– 4).

To check the adequacy of the results, we use the Fisher criterion and tabulate them (see Tab. 1–4). The calculated value of the Fisher criterion has the form:

$$F_{\text{расчет.}} = \frac{\sum(y_{i\ \text{расчет.}} - y_{\text{среднее расчет.}})^2}{t} \times \frac{n - t - 1}{\sum(y_i - y_{i\ \text{расчет.}})^2},$$

where t is the number of factors x affecting y; n is the number of observations.

Through comparing the calculated and tabulated values of the Fisher coefficient (see Tab. 1–4), we see that the calculated F significantly exceeds the tabulated F. Thus, we can conclude that the constructed dependence corresponds to the initial data with 95% confidence.

Substitute the obtained values of a and b.

For 30KhGSA samples in the TP environment, $y = 2.93961E - 08 \times x + 1.47936E - 06$, in the wheel-scrap environment, $y = 4.94112E - 08 \times x + 1.97429E - 06$.

For D16samples in the TP environment, $y = 5.73851E - 08 \times x + 4.23063E - 07$, in the wheel-scrap environment, $y = 1.37487E - 07 \times x + 9.04509E - 07$.

Graphically, the results are presented in Fig. 4–7.
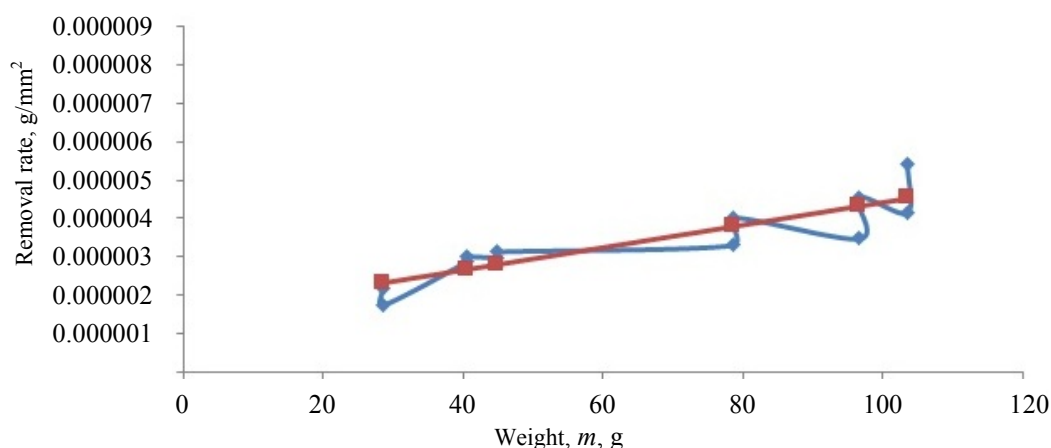
Fig. 4. Graph of dependence on specific removal mass of material of 30HGSA samples processed in TP
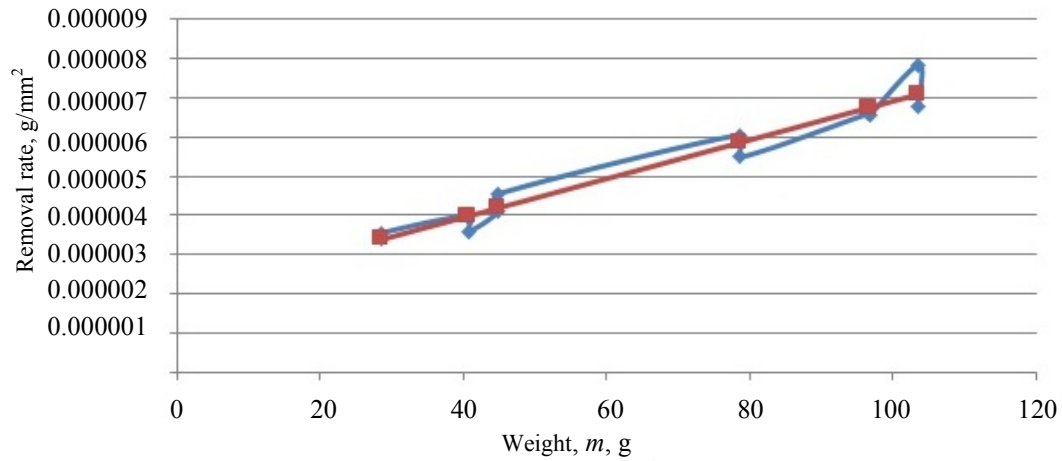
Fig. 5. Graph of dependence on specific removal mass of material of 30HGSA samples processed in wheel scrap
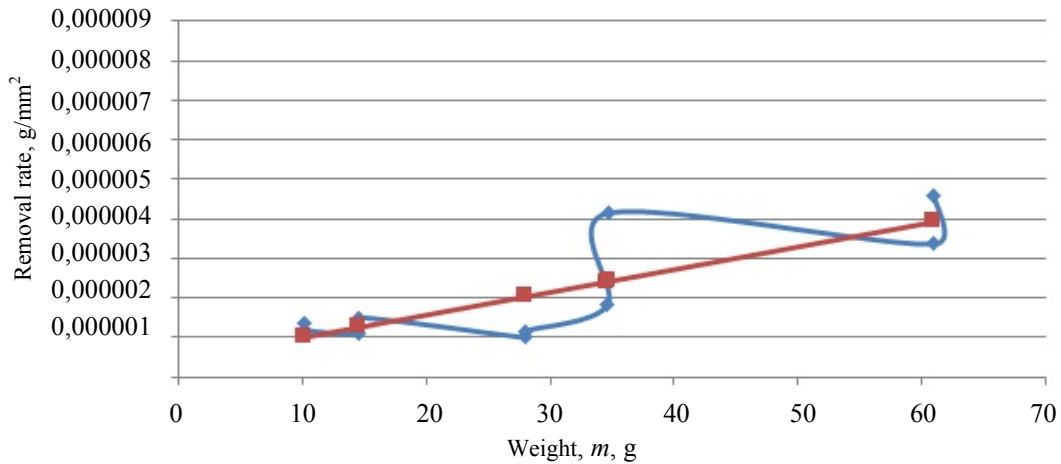
Fig. 6. Graph of dependence on specific removal mass of material of D 16 samples processed in TP
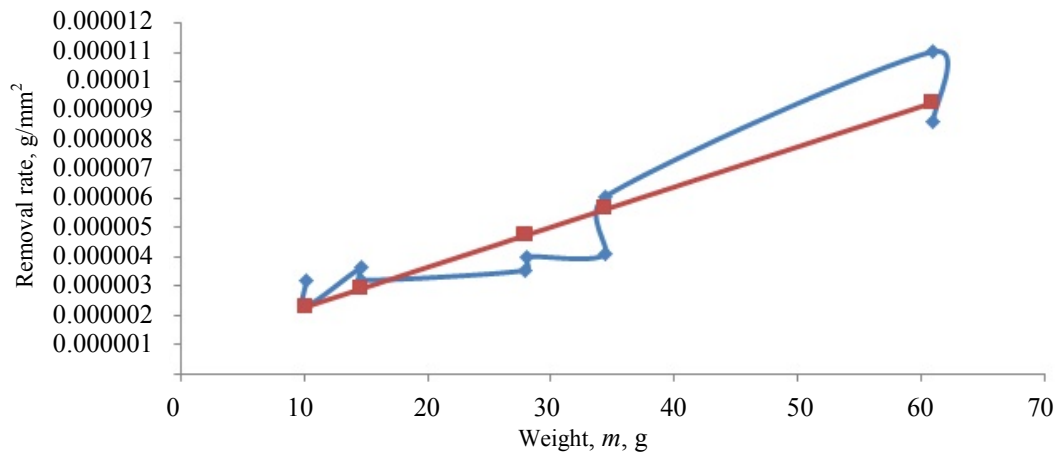
Fig. 7. Graph of dependence on specific removal mass of material of D 16 samples processed in wheel scrap

The graphs show that the specific removal rate varies significantly depending on the environment, as well as on the mass and material of the workpieces.

Conclusion. In analyzing Fig. 4–7, we can conclude that under machining workpieces of a larger mass, specific removal rate increases. This is due to changes in the momentum.

Since the momentum is equal to the product of the mass of the body and its speed, then with an increase in the mass of the workpiece, the momentum of the interaction of particles and the workpiece surface increases. With an increase in the mass of workpieces twofold, the specific removal rate increases by 1.5–2.2 times. When comparing the

Machine building and machine science

values of the angular coefficient *a* and the free term *b* between treatments, we can assume that they are affected by the parameters of the graininess of the media, as well as the characteristics of the processed material. The results obtained allow us to verify the theoretical dependences through introducing a coefficient to determine the impact of mass ratios. This will provide more accurate prediction of removal at the design stage of the vibration-abrasive processing. The results obtained replenish the database, which is used to determine the effect of the work material characteristics and the environment on the process under consideration.

References

1. Babichev AP, Babichev IA. Osnovy vibratsionnoi tekhnologii [Fundamentals of vibration technology]. 2nd ed. Rostov-on-Don: DSTU Publ. House; 2008. 3 p. (In Russ.)

2. Babichev AP, Motrenko PD, Ivanov VV, et al. Vibratsionnaya mekhanokhimiya v protsessakh otdelochno-uprochnyayushchei obrabotki i pokrytii detalei [Vibration mechanochemistry in the finishing and hardening processing and coating of parts]. Rostov-on-Don: DSTU Publ. House; 2012. 5 p. (In Russ.)

3. Martynov AN. Osnovy metoda obrabotki detalei svobodnym abrazivom, uplotnennym inertsionnymi silami [Fundamentals of the method of machining parts with a free abrasive compacted by inertial forces]. Saratov: Izd-vo Saratov. un-ta; 1981. 212 p. (In Russ.)

4. Babichev AP, Ryseva TN, Samadurov VA, et al. Naladka i ehkspluatatsiya stankov dlya vibratsionnoi obrabotki [Adjustment and operation of machines for vibration processing]. Moscow: Mashinostroenie; 1988. P. 12. (In Russ.)

5. Tamarkin MA, Krashenitsa SB. Vliyanie mikrorel'efa chastits rabochei sredy na proizvoditel'nost' vibroabrazivnoi obrabotki [Influence of the microrelief of working medium particles on vibroabrasive machining efficiency]. In: Progressive Hardening Technology. Rostov-on-Don: DSTU Publ. House; 1981. P. 12–15. (In Russ.)

6. Tamarkin MA. The optimization of technological processes of details processing by free abrasives. Key Engineering Materials. 2005;291/292:319–322.

7. Tamarkin MA, Tishchenko EE, Rozhnenko OA. Metal removal in the abrasive machining of complex surfaces. Russian Engineering Research. 2013;33(5):302–305.

8. Clark J, Massarsky ML, Davidson DA. Edge and Surface Conditioning for Improved Part Performance and Service Life. Products Finishing. November, 2016. P. 2.

9. Massarsky ML, Davidson DA. Turbo-Abrasive Machining and Finishing. Manufacturing Engineering. June, 2014. P. 22.

10. Massarsky ML, Davidson DA. Free Abrasives Flow for Automated Finishing. Manufacturing Engineering. May, 2013. P. 43.

11. Kashchuk VA, Vereshchagin AV. Spravochnik shlifovshchika [Handbook of the grinder]. Moscow: Mashinostroenie; 1988. P. 19. (In Russ.)

About the authors:

Butenko, Viktor I., professor of the Engineering Technology Department, Don State Technical University (1, Gagarin sq., Rostov-on-Don, 344000, RF),   Dr.Sci. (Eng.), professor, ScopusID 35972120700, ORCID: https://orcid.org/0000-0001-9260-1030, butenkowiktor@yandex.ru.

Stel'makh, Andrei V., graduate student of the Engineering Technology Department, Don State Technical University (1, Gagarin sq., Rostov-on-Don, 344000, RF), ORCID: https://orcid.org/0000-0002-8630-8748, andreystelmakh91@mail.ru.

Claimed contributorship

V. I. Butenko: academic advising; analysis of the research results; the text revision; correction of the conclusions. A. V. Stel'makh: basic concept formulation, research objectives and tasks setting; computational analysis; text preparation; formulation of conclusions.

All authors have read and approved the final manuscript.

MACHINE BUILDING AND MACHINE SCIENCE

Analytical determination of wear resistance criteria of a stamping tool for various loading conditions

S. D. Kolotienko, A.V. Zhuravlev, E.V. Roshchina
Don State Technical University (Rostov-on-Don, Russian Federation)

Introduction. The paper is devoted to the analytical determination of general criteria for predicting the wear resistance of heavily loaded friction couples, in particular, stamping tools, operating under various loading conditions. The proposed system of criteria is based on physical dependencies that link the basic wear index, i.e. the number of loading cycles N_F with crack resistance parameters *n* and *C*. The work objectives were the development and analytical foundation of the calculation technique that provides for predicting the wear resistance of the stamping tool for various loading conditions, as well as the predetermination of experimental verification of the efficiency of the developed methodology.

Materials and Methods. Mathematical models that link the key criterion of wear-resistance, the number of loading cycles N_F with crack resistance parameters *n* and *C*, are proposed. An analytical verification of the proposed models is carried out.

Results. Mathematical models are developed for predicting the wear resistance of a stamping tool operating under various loading conditions. In particular, for the following cases: under sliding and rolling friction of the tool on a plastically deformable metal, for conditions of thermo-mechanical contact fatigue, for high-cycle brittle contact damaging, for pulsating contact on a plastically deformable metal, as well as for combined types of frictional contact.

Discussion and Conclusions. The results obtained can be used in the design and structural optimization of the stamping tool operating under various loading conditions, as well as in predicting its life cycle.

Keywords: stamping tool, wear resistance criteria, loading conditions, contact damaging, crack resistance, sliding, rolling, surfacing materials.

Introduction. Experimental and theoretical studies on the wear processes of surfacing materials show that no material properties separately can determine the wear resistance under the frictional contact extreme conditions in a unique manner. Only a certain set of physical and mechanical properties with account of the frictional interaction features should be considered when determining the wear resistance of surfacing materials.

Wear resistance criteria should meet the conditions of specific tribocouplings. To determine the criteria, a single approach should be followed in each case. Obviously, for all the phenomena and types of contact damage, the principle condition should be taken into account: that material is considered more wear-resistant whose stage of fatigue crack growth is longer. Thus, the wear resistance criterion should take into account the duration of the process of destruction of the surface layer and separation of the first wear particle. In this case, the determination of the wear resistance criterion is reduced to evaluation of the cycle index N_F at which the surface layer destruction occurs.

In this case, the assignment of wear resistance criteria may consist not in calculating the contact endurance of materials, but in comparing and selecting surfacing materials for specific frictional contact conditions that are characteristic of heavy loaded friction couples. Thus, the criteria should provide adequacy of the wear resistance series for specific types of friction contacts.

In accordance with a unified approach, the following key points should be taken into account when determining the criteria. One type of crack should be considered in all types of frictional contact. Generically, the crack resistance parameters of materials that determine the kinetics of the development of fatigue microcracks should be taken into account. When comparing surfacing materials with each other according to the criteria, it is required to consider the possibility of developing a competing type of wear — low-cycle viscous damage as a result of the petal peeling.

Materials and Methods. For reversible sliding conditions on a plastically deformable metal, the author first proposed a method for analyzing wear resistance considering the basic properties of the material, which determine the surface layer destruction under friction [1].

It appears possible to determine the wear resistance criterion with account to the fracture toughness, yield strength, friction coefficient, and initial crack sizes. The studies [2–9, 11, 13, 15, 16] show that this approach is also promising for other frictional contact conditions characteristic of heavy loaded friction couples including a stamping tool.

V.V. Rubanov, assuming that the criterion proposed for reverse sliding in [1], and using the dependence of the yield strength on a number of characteristics of the structure of the material, proposed to determine the wear resistance of the material according to the criterion [4]:

$$K_u = \frac{\left(\sigma_{_M} l_i + 11Gb\frac{\phi}{1-\phi}\right) \cdot K_{1c}}{f^2 l_i^{3/2}}, \tag{1}$$

where $\sigma_{_M}$ is the ultimate mechanical stress in the material from the action of the matrix under which its destruction occurs; l_i is the average defect size; K_{1c} is fracture toughness; ϕ is the volume fraction of defects; G is the shear modulus; b is Burgers vector; f is the friction factor (from now on, the friction factor is applied on the ground of the Siebel law).

Given that for a number of alloys, there is the dependence K_{1c} on the tensile strength under bending $\sigma_{_{u32}}$, after a series of simplifications, V.V. Rubanov recommends the following criterion for assessing the wear resistance of surfacing materials:

$$K_u = \frac{G \cdot \phi \cdot \sigma_{_{u32}}}{f^2 \cdot (1-\phi) \cdot l_i^{3/2}}. \tag{2}$$

This approach has limited possibilities due to the following. The proposed criterion is common for various frictional contact schemes; and when determining the wear resistance of surfacing materials for sliding and rolling according to the criterion (2), differences in the contact damage mechanism are not taken into account under the conditions of contact interaction for sliding and rolling, both with tangential with effort or without it.

The wear resistance criterion (2) does not take into account the crack resistance parameters of materials that affect directly the rate of development of fatigue microcracks, and, therefore, determine the duration of contact damage processes.

Research Results. In the analytical definition of wear resistance criteria, the basic assumption should be made: the field of contact tensile stresses is uniform, and its value is equal to the maximum value that is determined on the surface. Thus, this assumption does not take into account the gradual attenuation of tensile stresses in the depth of the material and is a more stringent estimate. The studies [10] show that the errors arising in this case are small if the length of the cracks is less than the depth of the zone of compressive stresses.

The task of determining the criteria for the wear resistance of materials wearing under the contact damage conditions is as follows. It is required to analytically determine the time (the number of contact interaction cycles) of separating the particles of abnormal wear. In this regard, the stresses that act on the crack in a particular frictional contact should be used as tensile stresses.

Given the differences between low-cycle brittle contact damage and multi-cycle damage, the problem of determining the criteria for wear resistance is divided into two types. In the first case, when determining the contact fracture process time for low-cycle brittle contact damage, it is required to consider the possibility of reaching a critical crack. In the second case for low-cycle brittle contact damage, it was found that cracks do not reach critical values ($l_c \gg l_i$). Here, it is possible to use the maximum permissible size of spalling as the final crack length (it is established either from the requirements for wear tolerance of tribocoupling or from the requirements for limiting the size of contact damage on the edge of the working surface).

Wear resistance criterion for sliding on plastically deformable metal

The contact fracture process time is determined through integrating the Paris equation [17]. As a value of tensile stresses for this case of frictional contact, we should take [10]:

$$\sigma_{p\max} = \frac{4pf}{\pi}, \tag{3}$$

where p is the average pressure in contact.

In this case, the expression for the stress intensity factor takes the form:

$$\sigma_{p\max} = \frac{4pf}{\sqrt{\pi}}\sqrt{l} \ . \tag{4}$$

The fracture process time, and, consequently, the wear resistance criterion N_F, is defined as

$$N_F = \int_{l_i}^{l_k} \frac{dl}{CK^n l^{n/2}} = \frac{\pi^{n/2}}{C(4pf)^n} \int_{l_i}^{l_k} \frac{dl}{l^{n/2}} \ . \tag{5}$$

At $n \neq 2$, the expression (5) solution takes the form

$$N_F = \frac{2\pi^{n/2}}{(n-2)C(4pf)^n}\left(\frac{1}{l_i^{\frac{n-2}{2}}} - \frac{1}{l_c^{\frac{n-2}{2}}} \right). \tag{6}$$

From the basic principles of fracture mechanics, it is known that the critical crack length is the value at which the crack starts a supercritical self-motion. This moment determines uniquely the fracture toughness of the material K_{1C}. In the case of contact loading by a uniform stress field under sliding, the value of the critical crack length can be determined from the expression [10]:

$$l_c = \frac{\pi}{16p^2 f^2}K_{1c}^{f^2} \ . \tag{7}$$

After the corresponding replacement and transformations, we obtain

$$N_F = \frac{2\pi^{n/2}}{(n-2)C(4pf)^n}\left[\frac{1}{l_i^{\frac{n-2}{2}}} - \left(\frac{4pf}{\pi^{1/2}K_{1C}^f} \right)^{n-2} \right]. \tag{8}$$

This expression can be used as a criterion of wear resistance when sliding against a plastically deformable metal under the conditions of high contact pressures, when low-cycle brittle contact damage is realized. In this case, as follows from the expression (7), the wear resistance of surfacing materials is determined by the contact pressure, friction coefficient, fracture toughness, size of structural defects and crack resistance parameters n and C.

Wear resistance criterion for thermomechanical contact fatigue

The effect of heating-cooling cycles, which is characteristic primarily for a pulsating contact with a heated plastically deformable metal, on the friction surface causes the origination of periodic thermomechanical stresses in the surface layer. The expression of V. I. Dukhovchenko [12] for determining this type of stress is known as follows:

$$\sigma = \frac{\alpha E \Delta T}{1-v} \ , \tag{9}$$

where α is the thermal coefficient of linear expansion; E is the elasticity modulus; ΔT is the temperature difference of the heating-cooling cycle; v is the Poisson's ratio.

In this case, with regard to the expression (9), the solution to the integral for the Paris equation at $n \neq 2$ is determined from the formula:

$$N_F = \frac{2(1-v)^n}{(n-2)C\pi^{n/2}(\alpha E \Delta T)^n}\left(\frac{1}{l_i^{\frac{n-2}{2}}} - \frac{1}{b^{\frac{n-2}{2}}} \right). \tag{10}$$

If the limiting value $b_{\max}$, which is assigned as the tolerance on the limiting size of the centre of spalling of the working surface edges, is taken as l_c, we obtain

$$N_F = \frac{2(1-v)^n}{(n-2)C\pi^{n/2}(\alpha E \Delta T)^n}\left(\frac{1}{l_i^{\frac{n-2}{2}}} - \frac{1}{b_{\max}^{\frac{n-2}{2}}} \right) \tag{11}$$

or

$$N_F = \frac{2(1-v)^n \left(b_{\max}^{\frac{n-2}{2}} - l_i^{\frac{n-2}{2}} \right)}{(n-2)C\pi^{n/2}(\alpha E \Delta T)^n l_i^{\frac{n-2}{2}} b_{\max}^{\frac{n-2}{2}}} \tag{12}$$

This expression can be used as a criterion for the wear resistance of surfacing materials under thermomechanical fatigue. Under these conditions, wear resistance of materials also depends on the crack resistance parameters n and C, is determined by the tolerance for unit spalling, the elasticity modulus, the Poisson's ratio, and is inversely proportional to the coefficient of thermal expansion, the magnitude of the temperature difference and the size of the initial defects.

Wear resistance criteria for multi-cycle brittle contact damage

We consider $l_1 = l_i$ and take into account that when rolling with a tangential force and an elastic pulsating contact, the angle of crack development does not depend on the material properties and is close to 45°. Then, the following expression is obtained to determine the fracture process time under rolling with a tangential force:

$$N_F = \frac{2}{(n-2)C}\left[\frac{7.35}{(1+11f)\sigma_{z\,max}}\right]^n\left(\frac{1}{l_i^{\frac{n-2}{2}}} - \frac{1}{l_c^{\frac{n-2}{2}}}\right). \tag{13}$$

For rolling without tangential force

$$N_F = \frac{2}{(n-2)C}\left[\frac{4.62}{\sigma_{z\,max}}\right]^n\left(\frac{1}{l_i^{\frac{n-2}{2}}} - \frac{1}{l_c^{\frac{n-2}{2}}}\right), \tag{14}$$

Upon the pulsating contact

$$N_F = \frac{2}{(n-2)C}\left[\frac{6.65}{\sigma_{z\,max}}\right]^n\left(\frac{1}{l_i^{\frac{n-2}{2}}} - \frac{1}{l_c^{\frac{n-2}{2}}}\right). \tag{15}$$

Since, under conditions of multicycle brittle contact damage, the cracks do not reach a critical value during development, $l_c \gg l_i$, the expressions (13) - (15) can be transformed as follows:

– for tangential force rolling

$$N_F = \frac{2\cdot 7.35^n}{(n-2)C(1+11f)^n\sigma_{z\,max}^n l_i^{\frac{n-2}{2}}}. \tag{16}$$

– for rolling without tangential force

$$N_F = \frac{2\cdot 4.62^n}{(n-2)C\sigma_{z\,max}^n l_i^{\frac{n-2}{2}}}, \tag{17}$$

– for pulsating contact

$$N_F = \frac{2\cdot 6.65^n}{(n-2)C\sigma_{z\,max}^n l_i^{\frac{n-2}{2}}}, \tag{18}$$

The obtained criteria for wear resistance indicate that in this case, too, the critical impact is exerted by the parameters of crack resistance of materials n and C, the size of the defects; and, in addition, in the case of rolling with a tangential force, the friction coefficient should be taken into account.

Wear resistance criterion for rolling against plastically deformable metal

A feature of this frictional contact type is that the counterbody acquires intense plastic deformation. In this case, stresses in the contact zone cannot be estimated through the formulas for elastic contact, and the wear resistance criteria (16) - (18) are not applicable.

To solve this problem, we use the analogy for rolling against a plastically deformable metal and sliding under the same conditions. Then, the crack will be periodically affected by a plastically deformable rolling body. Considering that rolling under these conditions is accompanied by significant spalling, we use the expression (6) for the sliding contact. As the final crack length, the limit tolerance for unit spalling of the working surface edge should be used.

In this case, the number of cycles for the destruction of the surface layer can be determined through the expression:

$$N_F = \frac{2\pi^{n/2}}{(n-2)C(4pf)^n}\left(\frac{1}{l_i^{\frac{n-2}{2}}} - \frac{1}{b_{max}^{\frac{n-2}{2}}}\right). \tag{19}$$

After transformations, the expression (19) can be rewritten as follows:

$$N_F = \frac{2\pi^{n/2}\left(b_{max}^{\frac{n-2}{2}} - l_i^{\frac{n-2}{2}}\right)}{(n-2)C(4pf)^n l_i^{\frac{n-2}{2}} b_{max}^{\frac{n-2}{2}}}. \tag{20}$$

Thus, the wear resistance of surfacing materials when rolling against a plastically deformable metal is determined through the crack resistance parameters n and C, contact pressure, friction coefficient, limit tolerance on the size of the spalling and the sizes of the initial defects.

Wear resistance criterion for pulsating contact on plastically deformable metal

The characteristic features of this type of friction contact are extremely high contact pressures (up to 4000 MPa), which is associated with the dynamic nature of the application of the contact load. In this case, making use of the expression (18) for an elastic pulsating contact is also impossible.

For the maximum tensile stresses acting on the crack, we take the value that, at a first approximation, can be determined using the condition $\sigma_{z\,\max} \approx p$ from the formula:

$$\sigma_{p\,\max} = \frac{1-2v}{3}p \tag{21}$$

where p is average contact pressure.

The fracture process time is determined through the integration of the Paris equation for the given conditions of contact loading:

$$N_F = \int_{l_i}^{l_c} \frac{dl}{CK^n l^{n/2}} = \frac{3^n}{C\pi^{n/2}(1-2v)^n p^n} \int_{l_i}^{l_c} \frac{dl}{l^{n/2}} = \frac{2\cdot 3^n}{(n-2)\pi^{n/2}C(1-2v)^n p^n}\left(\frac{1}{l_i^{\frac{n-2}{2}}} - \frac{1}{l_c^{\frac{n-2}{2}}}\right). \tag{22}$$

Let us present the value of the critical crack length l_c through K_{1c}^f:

$$l_c = \frac{K_{1c}^f}{\pi\left(\dfrac{1-2v}{3}p\right)^2} \tag{23}$$

and we get after the transformations:

$$N_F = \frac{2\cdot 3^n}{(n-2)\pi^{n/2}C(1-2v)^n p^n}\left[\frac{1}{l_i^{\frac{n-2}{2}}} - \left(\frac{\pi^{1/2}(1-2v)p}{3K_{1c}^f}\right)^{n-2}\right]. \tag{24}$$

The given expression is a criterion for the wear resistance of surfacing materials for pulsating contact against plastically deformable metal. Under these conditions, wear resistance is determined by fracture toughness, crack resistance parameters, Poisson's ratio, contact pressure and the size of the initial defects.

Wear resistance criteria for integrated friction contact modification

Under the conditions of sliding friction against a heated plastically deformable metal, the tool working surface is subjected to alternating stresses from friction forces and thermomechanical stresses. In this case, according to the hypothesis of a linear summation of stresses, the stress intensity factor considering the expressions (3) and (4) can be represented as:

$$K = \sigma_{o6u} \sqrt{\pi l} = \left(\frac{4pf}{\pi} + \frac{\alpha E \Delta T}{1-v}\right)\sqrt{\pi l}\ . \tag{25}$$

Then, through integrating the Paris equation, we can obtain an expression for determining the number of cycles necessary for breaking:

$$N_F = \int_{l_i}^{l_c} \frac{dl}{C\left(\dfrac{4pf}{\pi} + \dfrac{\alpha E \Delta T}{1-v}\right)^n \sqrt{\pi l}} = \frac{2}{\pi^{1/2}(n-2)C\left(\dfrac{4pf}{\pi} + \dfrac{\alpha E \Delta T}{1-v}\right)^n}\left(\frac{1}{l_i^{\frac{n-2}{2}}} - \frac{1}{l_c^{\frac{n-2}{2}}}\right). \tag{26}$$

The critical crack length can be determined from the expression (25) given that the supercritical fracture point occurs at $K = K_{1c}^f$. Then

$$l_c = \frac{K_{1c}^f}{\pi\left(\dfrac{4pf}{\pi} + \dfrac{\alpha E \Delta T}{1-v}\right)^2}\ . \tag{27}$$

Substituting the value l_c into the equation (26), we can obtain an expression for the wear resistance criterion in the case of a combined effect on the sliding friction surface and thermomechanical stresses:

$$N_F = \frac{2}{\pi^{1/2}(n-2)C\left(\frac{4pf}{\pi}+\frac{\alpha E\Delta T}{1-v}\right)^n} \left(\frac{1}{l_i^{\frac{n-2}{2}}} - \frac{\pi^{\frac{n-2}{2}}\left(\frac{4pf}{\pi}+\frac{\alpha E\Delta T}{1-v}\right)^{n-2}}{K_{1c}^{f(n-2)}} \right). \tag{28}$$

A combined effect on the friction surface is possible under an elastic pulsating contact with the application of thermomechanical stresses. In this case, the equation (18) should be written as:

$$N_F = \frac{2}{(n-2)C}\left(\frac{6.65}{\sigma_{z\max}+\frac{\alpha E\Delta T}{1-v}}\right)^n \left(\frac{1}{l_i^{\frac{n-2}{2}}} - \frac{1}{l_c^{\frac{n-2}{2}}}\right). \tag{29}$$

Given that in this load case $l_c \gg l_i$, we obtain the expression for the wear resistance criterion for elastic pulsating contact with thermomechanical fatigue

$$N_F = \frac{2 \cdot 6.65^n}{(n-2)C\left(\sigma_{z\max}+\frac{\alpha E\Delta T}{1-v}\right)^n l_i^{\frac{n-2}{2}}}. \tag{30}$$

Discussion and Conclusions. Analytical dependences are obtained for calculating the wear resistance index N_F for various working conditions of a stamping tool based on general criteria describing the crack resistance parameters of materials n and C. The results can be used in the design and optimization of a stamping tool operating under various loading conditions, as well as under predicting its life cycle.

References

1. Kolotienko SD, Krasnichenko LV, Didovets AM. Kriterii kontaktnoi vynoslivosti naplavochnykh materialov pri kachenii [Criterion of contact endurance of surfacing materials under rolling]. In: Proc. All-Union Sci.-Tech. Conf. on "Theory and practice of creating, testing and operating tribotechnical systems". Moscow; 1986. P. 235–236. (In Russ.)

2. Rubanov VV, Kolotienko SD. Issledovanie iznosostoikosti naplavochnykh materialov pri trenii o plasticheski deformiruemyi metall [Investigation of the wear resistance of surfacing materials under friction against plastically deformable metal]. In: Proc. All-Union Sci.-Tech. Conf. on "Modern methods of surfacing and surfacing materials". Kharkov; 1981. P.103–104. (In Russ.)

3. Rubanov VV, Kolotienko SD, Didovets AM. Iznosostoikost' naplavochnykh materialov pri kachenii [Wear resistance of surfacing materials under rolling]. Dep. VNIITEHMR; 18 August, 1994. No. 249. (In Russ.)

4. Rubanov VV, Pastva K, Denishchenko MM. Kriterii iznosostoikosti naplavochnykh materialov v usloviyakh tyazhelogo nagruzheniya [Criteria of wear resistance of surfacing materials under heavy loading]. Mechanik. Poznan. 1991;36:119–124. (In Russ.)

5. Rubanov VV. Kriterii iznosostoikosti naplavochnykh tverdykh splavov [Wear resistance criterion for hardfacing cutting alloys]. Vestnik of DSTU. 2006;6(3):224–227. (In Russ.)

6. Rubanov VV, Kolotienko SD. Iznashivanie naplavochnykh materialov pri trenii skol'zheniya o plasticheski deformiruemyi metal [Wear coating materials in sliding friction about plastically deformable metal]. Progressive Technologies and Systems of Mechanical Engineering. 2016;2(53):201–206. (In Russ.)

7. Kolotienko SD, Didovets AM, Pivovarov AL. Kontaktnaya vynoslivost' naplavochnykh materialov pri kachenii [Contact endurance of surfacing materials under rolling]. In: Proc. All-Union Sci.-Tech. Conf. on "Application of new materials in agricultural engineering". Rostov-on-Don; 1985. P. 56–60. (In Russ.)

8. Kolotienko SD, Didovets AM, Pivovarov AL. Analiz protsessa kontaktnogo razrusheniya pri trenii kacheniya o plasticheski deformiruemyi material [Analysis of the contact fracture process under rolling friction against plastically deformable material]. In: Proc. All-Union Sci.-Tech. Conf. on "Optimization and intensification of finishing and cleaning hardening treatment processes". Rostov-on-Don; 1986. P. 103–105. (In Russ.)

9. Kolotienko SD, Didovets AM, Pivovarov AL. Issledovanie kontaktnoi vynoslivosti naplavochnykh materialov pri kachenii [Study on contact endurance of surfacing materials under rolling]. In: Proc. All-Union Sci.-Tech. Conf. on "Improving the finishing and hardening processing of parts". Rostov-on-Don; 1986. P. 114–118. (In Russ.)

10. Kolotienko SD. Issledovanie iznashivaniya naplavochnykh tverdykh splavov pri reversivnom trenii o

plasticheski deformiruemyi metal: diss. … kand. tekhn. nauk [Study on wear of hardfacing cutting alloys during reverse friction against plastically deformable metal: Cand.Sci. (Eng.), diss.]. Rostov-on-Don; 1978. 210 p. (In Russ.)

11. Kolotienko SD, Rubanov VV, Gordin YuA. Mekhanizm iznashivaniya litykh tverdykh splavov v tyazhelonagruzhennykh parakh treniya [Wear mechanism of cast hard alloys in heavily loaded friction pairs]. Vestnik of DSTU. 2003;3(3):5–16. (In Russ.)

12. Dukhovchenko VI. Issledovanie termonagruzhennogo sostoyaniya i razrabotka instrumenta dlya goryachei shtampovki osesimmetrichnykh detalei: dis. … kand. tekhn. nauk. [Study on thermally loaded state and development of a tool for hot stamping of axisymmetric parts: Cand.Sci. (Eng.), diss.]. Kramatorsk; 1982. 210 p. (In Russ.)

13. Suleimanov VN. Issledovanie iznashivaniya i povysheniya iznosostoikosti tyazhelonagruzhennykh kulakov kuznechnopressovykh mashin, rabotayushchikh v usloviyakh treniya kacheniya: dis. … kand. tekh. nauk [Study on wear and increase in wear resistance of heavily loaded fists of forging machines working under rolling friction conditions: Cand.Sci. (Eng.), diss.]. Rostov-on-Don; 1978. 150 p. (In Russ.)

14. Rubanov VV, Kolotienko SD. Ustanovka dlya issledovaniya iznashivaniya naplavochnykh materialov pri trenii kacheniya [Filler wear test facility under rolling friction]. Vestnik of DSTU. 2011;11(9):1646–1650. (In Russ.)

15. Netyagov PD, et al. Issledovanie tribotekhnicheskikh kharakteristik metallicheskikh pokrytii, nanesennykh naplavkoi, ehlektrodugovym i plazmennym napyleniem [Study on tribotechnical characteristics of metal coatings deposited by surfacing, electric arc and plasma spraying]. Journal of Friction and Wear. 1989;10(5):909–913. (In Russ.)

16. Shchipachev AM, Mukhin VS. Opredelenie predela vynoslivosti s uchetom parametrov kachestva poverkhnostnogo sloya [Determination of endurance limit taking into account the quality parameters of the surface layer]. Izv. VUZ. Aviatsionnaya Tekhnika. 1999;3:23–25. (In Russ.)

17. Kragel'skii IV, Dobychin MN, Kombalov VS. Osnovy raschetov na trenie i iznos [Fundamentals of calculations for friction and wear]. Moscow: Mashinostroenie; 1977. 526 p. (In Russ.)

18. Kolotienko SD, Zhuravlev AV, Roshchina EV. Raschetno-ehksperimental'nye metody prognozirovaniya vynoslivosti naplavochnykh materialov [Computational and experimental methods for predicting the endurance of surfacing materials]. Young Researcher of the Don. 2019;3(18):36–42. (In Russ.)

19. Savrai RA, et al. Kontaktnaya vynoslivoct' NiCrBSi pokrytii, poluchennykh metodom gazoporoshkovoi lazernoi naplavki [The contact endurance of NiCrBSi coatings obtained by gas powder laser cladding]. Obrabotka Metallov = Metal Working and Material Science. 2014;4:43–51. (In Russ.)

20. Stepnov MN, Zinin AV. Prognozirovanie kharakteristik soprotivleniya ustalosti materialov i ehlementov konstruktsii [Prediction of the fatigue resistance characteristics of materials and structural elements]. Moscow: Innovatsionnoe mashinostroenie; 2016. 392 p. (In Russ.)

21. Biserikan MV, Petrochenko SV, Averkov KV. Ehksperimental'noe issledovanie ustalostnoi dolgovechnosti vagonnogo kolesa povyshennoi tverdosti pri vzaimodeistvii s rel'som [Experimental study of fatigue life of wagon wheel of increased hardness when interacting with rail]. Omsk Scientific Bulletin. 2019;2(164):18–22. (In Russ.)

22. Guchinskii RV, Petinov SV, Siddik Sh, et al. Prognozirovanie ustalostnoi dolgovechnosti metallov s uchetom neodnorodnosti mikrostruktury [Fatigue life prediction based on finite-element modeling damage accumulation including material inhomogeneity]. St. Petersburg Polytechnic University Journal. 2015;4(231):134–143. (In Russ.)

23. Makhutov NA, Gadenin MM. Zakonomernosti nakopleniya malotsiklovykh povrezhdenii s uchetom ehkspluatatsionnykh parametrov protsessa nagruzheniya [Behavior of low-cycle damages accumulation taking into account loading service parameters]. PNRPU Aerospace Engineering Bulletin. 2019;56:45–57. (In Russ.)

24. Makhutov NA, Gadenin MM, Moskvichev VV, et al. Lokal'nye kriterii prochnosti, resursa i zhivuchesti aviatsionnykh konstruktsii [Local criteria for strength, resource and survivability of aircraft structures]. Novosibirsk: Nauka; 2017. 600 p. (In Russ.)

25. Pris NM, Bezmenova AV. Otsenka ustalostnoi dolgovechnosti pri deistvii stupenchatogo nagruzheniya [Evaluation of fatigue life under the action of step loading]. In: Proc. L Int. Sci.-Pract. Conf. on "Engineering - from theory to practice". 2015;9(45):34–40. (In Russ.)

26. Vorob'ev AA, Fedorov IV, Ivanov IA, et al. Metodika rascheta razmera kontaktno-ustalostnykh povrezhdenii zheleznodorozhnogo kolesa po rezul'tatam, poluchennym na model'nykh rolikakh [Method for calculating the size of contact-fatigue injuries of a railway wheel according to the results obtained on model rollers]. Bulletin of Research Results. 2018;1:18–24. (In Russ.)

About the authors:

Kolotienko, Sergei D., Head of the Construction Materials Engineering Department, Don State Technical University (1, Gagarin sq., Rostov-on-Don, 344000, RF), Dr.Sci. (Eng.), professor, ORCID: https://orcid.org/0000-0001-6724-5131 , spu-47.4@donstu.ru

Zhuravlev, Andrei V., associate professor of the Construction Materials Engineering Department, Don State Technical University (1, Gagarin sq., Rostov-on-Don, 344000, RF), associate professor, ORCID: https://orcid.org/0000-0002-9009-1844 , awj2001@yandex.ru

Roshchina Evgeniya V., Master's degree student of the Construction Materials Engineering Department, Don State Technical University (1, Gagarin sq., Rostov-on-Don, 344000, RF), ORCID: https://orcid.org/0000-0001-5729-4191 , ev_roschina@mail.ru

Claimed contributorship

S. D. Kolotienko: academic advising; basic concept formulation, research objectives and tasks setting. A. V. Zhuravlev: computational analysis; analysis of the research results; text preparation; formulation of conclusions. E. V. Roshchina: revision and final correction of the text and conclusions.

All authors have read and approved the final manuscript.

INFORMATION TECHNOLOGY, COMPUTER SCIENCE, AND MANAGEMENT

Algorithm of software package of intellectual decision support when designing cyber security system at the enterprise

E. A. Vitenburg, A. V. Nikishova
Volgograd State University (Volgograd, Russian Federation)

Introduction. To increase the decision-making efficiency at the enterprise, it is advisable to use a special software package of intellectual support. Such a product is necessary when designing an information security system and increasing its invulnerability during modernization or configuration changes. Research objectives are as follows: to develop an algorithm and a mathematical model of the software package for intellectual decision support.

Materials and Methods. The decision support method under designing an information security system is based on the use of a neural network (multilayer perceptron). For an objective assessment of the initial security of an information system (IS), a mathematical model for the analysis of security events is developed.

Results. The statistics of malicious attacks on the IS of enterprises is analyzed. The need for timely and accurate modernization of the information protection system is determined. Important characteristics of the designing an information security system are the speed at which the result is obtained and the reduction in the residual risk of IS. In this regard, the use of artificial intelligence systems in the process of determining the best set of protection subsystems is important. The threats to cyber security (CS) are classified. The main classes of security events are defined. A mathematical model of the neural network is developed; the input parameters of its operation are indicated. The current enterprise IS generates numerous events which necessitates the automatic collection and analysis of data from subsystems for registering IS objects. The process of analyzing security events is considered in detail since the adequacy of the generated design decisions depends on the correctness of the data obtained in this way. The algorithm of the software package is formed.

Discussion and Conclusions. The results can be used in the design of the information security system at the enterprise. In addition, CS administrators can use the developed software package to adjust the configuration settings of information security tools. The proposed solution will minimize the destructive influence of the developer of the security system which may and happen to be subjective.

Keywords: cyber security, information system, neural network engineering, multilayer perceptron, algorithm.

Introduction. With the development of industry in Russia, the number of enterprises classified as objects of critical information infrastructure (OCII) is growing. Statistics on the distribution of attacks from the Positive Technologies[1] vendor shows an increase in the number of successfully implemented malicious actions in this area. In 2019, 125 attacks on industrial information systems (IS) were recorded. This is more than three times (or by 212%) higher than the same indicator in 2018 (40 attacks). The diagram of the distribution of the number of attacks by quarters of the year (Q) is shown in Fig. 1.
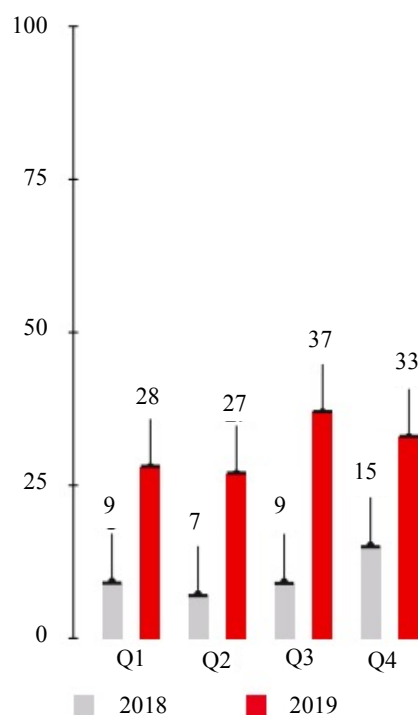

Fig. 1. Number of attacks on IS of enterprises in 2018 and 2019

Industrial IS are attacked mainly using malicious software (90% of attacks). This area is supervised by the Federal Security Service and the Federal Service for Technical and Expert Control. The need to ensure cyber security (CS) of industrial information systems is confirmed by statistics of the head research centers [1]. According to the regulatory legal acts of the Russian Federation[2], the owners of the OCII use a set of organizational and technical measures to ensure the safe operation of the information infrastructure. At the same time, the legislation provides for a periodic audit of the information protection system (IPS) performance, an assessment of its effectiveness. This results in prompt updating of the configuration settings of available tools or the retrofitting of the system with information security tools. A special role is played by the efficiency and accuracy of the decisions made, and the value of residual risk should not exceed the established indicators [2]. In this regard, it is proposed to automate the decision support process under designing the IPS at the enterprise.

Materials and Methods. To support decision-making in the design of IPS, a method based on a neural network (multilayer perceptron) was used [3]. Input data for the operation of a neural network were information security threats and security events. In addition, for an objective assessment of the initial information system security, a mathematical model of the analysis of security events was developed. Within this model, the calcu-

---

[1]Aktual'nye kiberugrozy: IV kvartal 2019 goda [Current cyber threats: Q4, 2019]. Positive Technologies. URL: https://www.ptsecurity.com/ru-ru/research/analytics/cybersecurity-threatscape-2019-q4 (accessed 24.02.2020).
[2]O bezopasnosti kriticheskoi informatsionnoi infrastruktury RF: feder. zakon ot 26.07.2017, № 187-FZ [On security of critical information infrastructure of the Russian Federation: Federal Law of July 26, 2017, no. 187-FZ]. RF State Duma, Federation Council. FSTEC of Russia. URL: https://fstec.ru/tekhnicheskaya-zashchita-informatsii/obespechenie-bezopasnosti-kriticheskoj-informatsionnoj-infrastruktury/285-zakony/1610-federalnyj-zakon-ot-26-iyulya-2017-g-n-187-fz (accessed 18.05.20).

lated measures of IS similarity are compared with one of the IS security levels. Weighted Manhattan Distance is used as a similarity metric.

Study Results. In the framework of this study, an approach to the design of a protection system based on the factors of the cyber security subsystem importance included in the IPS [4] is proposed. With these data, it is suggested to make a list of security tools for the most critical subsystems. This approach provides strengthening the IPS through neutralizing critical threats. Moreover, criticality should be specified through an automated analysis of security events [5, 6]. The vector of cyber security subsystem importance is generated according to the expression

$$V = S(Class\_Thr), \tag{1}$$

where $V = (V_1, \ldots, V_9)$ is the vector of IPS subsystem importance; $Class\_Thr = (Class\_Thr_1, \ldots, Class\_Thr_6)$ is the vector of criticality of threat classes; S is the functional relationship defined by a neural network.

For convenience, we divide set of CS threats Thr into classes $Class\_Thr$, which are defined as in [6]:

$$Class\_Thr = \{Thr\_Br, Thr\_L, Th\_Dist, Thr\_Loss, Thr\_B, Thr\_A\}, \tag{2}$$

where Thr_Br is the class of CS threats of the "cracking" type; Thr_L is the class of CS threats of the "leak" type; Th_Dist the class of CS threats of the "distortion" type; Thr_Loss is the class of CS threats of the "loss" type; Thr_B is the class of CS threats of the "blocking" type; Thr_A is the class of CS threats of the "abuse" type.

To generate the vector of IS CS threat criticality, it is proposed to form two matrices of compliance:

— set of threats to set of classes of threats — $MThr$,

— set of security events to threat classes — $MEvent$.

$MThr$ matrix:

$$MThr = Thr \times Class\_Thr = (mth_{ij}). \tag{3}$$

Here, mth_{ij} is determined from the formula:

$$mth_{ij} = \begin{cases} \frac{1}{n}, \text{if the threat belongs to the threat class,} \\ 0 \text{ if not.} \end{cases} \tag{4}$$

Here, n is the number of threat classes to which the threat belongs.

In this case, $\forall i, \sum_j mth_{ij} = 1$.

$MEvent$ matrix:

$$MEvent = Events \times CThr = (mev_{ij}). \tag{5}$$

Here, mev_{ij} is determined from the formula:

$$mev_{ij} = \begin{cases} 1, \text{if an event occurs when a class threat is implemented,} \\ 0 \text{ if not.} \end{cases} \tag{6}$$

To form the vector of the cyber security subsystem importance, it is proposed to use a neural network in a software package — a multilayer perceptron operating according to the formula given in [7]:

$$\begin{cases} In_{0k} = v_k \\ Out_{ij} = f(\sum_l w_{ijl} In_{ijl} - \theta_{ij}), \\ In_{ijl} = Out_{i-1l} \end{cases} \tag{7}$$

where In_{0k} is the k-th neuron of the input layer; v_k is the k-th element of the input vector; Out_{ij} is the output value of the j-th neuron of the i-th layer; f is the neuron activation function, which is determined by the functional dependence V (1); w_{ijl} is the weight of the l-th input of the j-th neuron of the i-th layer; In_{ijl} is the value of the l-th input of the j-th neuron of the i-th layer; θ_{ij} is the activation level of the j-th neuron of the i-th layer; Out_{i-1l} is the output value of the l-th neuron of the $(i-1)$-th layer.

At the stage of analyzing security events, the initial data are the security event logs created by the system and the application software of the enterprise IS. Set of the security *Events* include the following classes [8]:

$$\text{E}vents = \{EnterEv, ManagementSubEv, AccessObjEv, PolicyChangeEv,$$
$$\text{E}vents = \{EnterEv, ManagementSubEv, AccessObjEv, PolicyChangeEv,$$
$$UsePrivilegesEv, ISProcessesEv, LevelISEv\}. \tag{8}$$

Here, $EnterEv$ are events of the "subjects' log-on" class; $ManagementSubEv$ are events of the "subject management" class; $AccessObjEv$ are events of the "accessing objects" class; $PolicyChangeEv$ are events of the "system policy change" class; $UsePrivilegesEv$ are events of the "subject's using exclusive privileges" class; $ISProcessesEv$ are events of the "system processes running" class; $LevelISEv$ are events of the "system level" class.

Dangerous events are selected from the set. Matrices of compliance are used to compare the set of dangerous events to threat classes. The matrix developed in the framework of this study is presented in Table 1.

Table 1

Matrix of compliance of CS threats of enterprise IS

Security event class	Threat types						
	EnterEv	*ManagementSubEv*	*AccessObjEv*	*PolicyChangeEv*	*UsePrivilegesEv*	*ISProcessesEv*	*LevelISEv*
Thr_Br	+		+		+		
Thr_ L			+			+	
Th_Dist	+					+	
Thr_Loss			+			+	
Thr_B		+					+
Thr_A	+	+		+	+		+

Then the vector of urgent threat classes of CS IS threats is developed. After that, the subsystems of IPS are opposed to the urgent threat classes. Compliance is determined using a neural network with account for the functional dependence *V* in accordance with the formula (1).

Quite an important factor is the number of analyzed sets of events and their sources. It should be noted that the number of security events is directly proportional to the number of sources — information resources of the enterprise IS [8]. Given a large number of events generated by a working IS, it is valid to automatically collect and analyze data from the registration subsystems of IS objects that describe events. In this regard, it is worth considering in detail the analysis of security events since the adequacy of the generated design decisions depends on the correctness of the conclusions received at this stage.

According to [9, 10], at a given instant *T*, the current state of the enterprise IS $S_T \in State, State = \{Snorm, Sdang, Sanorm\}$ can be characterized as:

— normal (*Snorm*) — normal system operation in accordance with its tasks and as given in the documents regulating the work;

— dangerous (*Sdang*) — incorrect IS operation, when malfunctions associated with hacker attacks, crashes and failures of software and (or) hardware are recorded;

— abnormal (*Sanorm*) — temporary change in the normal IS operating mode and a surge in abnormal activity of users, programs and network traffic.

Information technology, computer science, and management

Dangerous and abnormal events require a more detailed analysis. A set of such events is the input to the stage of matching threat classes. Such events indicate the implementation of security threats.

Therefore, the results of monitoring and analysis of security events will be the input to the neural network (7).

Any $EventIS_i$ security event can be described by an attribute tuple [9]:

$$EventIS_i = \langle ID, Data, Level, Source, EventType, EventState, SecureParams \rangle, \tag{9}$$

где *ID* is the event ID; *Data* is the event generation time; *Level* is hazard level of the event; *Source* is the source of the event; *EventType* is the event type; *EventState* is event status; *SecureParams* is event security parameter vector.

$$SecureParams = \langle h, u, risk \rangle, \tag{10}$$

where *h* is an indicator for the generation of the event of a certain code relative to the total number of security events over the period ΔT; *u* is the severity of the consequences of the event (potential damage); *risk* is the IS information security risk.

Over the period ΔT, a set of IS events (*EventIS*) which should be evaluated to determine the level of IS security is generated in the information system.

The ratio of the number of events of one type or another to the total number is determined by the indicator *h*:

$$h = \frac{NEventID}{NEvent}, \tag{11}$$

where *NEvenID* is the number of events of a certain code, *NEvent* is the total number of events over the period ΔT.

The application software defines event codes differently. So, in the framework of this work, we have considered the encoding of the Windows OS Microsoft[3].

The IS information security risk is a function of the frequency of the event and the potential damage:

$$risk = h \times u. \tag{12}$$

The sum of private indicators determines the overall risk *RiskSum*:

$$RiskSum = \sum_{i=1}^{EventID} risk_i. \tag{13}$$

The set that provides the classification of events and the assessment of private indicators of IS security is described by subsets of elements:

$$PPS = \{\{EvType\}, \{EvState\}, \{ISState\}\}. \tag{14}$$

Here, *EvType is* a set of types of the events detected; *EvState is* a set of possible event states:

$$EvState = \{Ev^n, Ev^d, Ev^a\}, \tag{15}$$

where Ev^n — events of normal IS operation; Ev^d — IS CS threat events; Ev^a — abnormal events characterizing deviations of the IS from the normal mode of operation (additional analysis is needed).

To determine whether event $EventIS_i$ belongs to one of the three states *EvState*, the classification problem is solved — the set $SP = DamgeEv \cup NormEv$ is used, which is divided into two basic subsets. They are formed by an expert group on the basis of data on quick events of the normal IS operating mode and the previously detected CS attacks and incidents that describe the signature of IS quick and threat events:

— *DamgeEv* is a set of events that are known features of an attack or determine the scenario of an incident;

— *NormEv* is a set of events typical for the normal mode of IS operation.

---

[3]Opisanie sobytii sistemy bezopasnosti v Windows 7 i Windows Server 2008 R2 [Description of Security Events in Windows 7 and Windows Server 2008 R2]. Microsoft. URL: https://support.microsoft.com/ru-ru/help/977519/description-of-security-events-in-windows-7-and-in-windows-server-2008 (accessed 05.08.2019).

$F(EventIS_i(EvState) \rightarrow \{SP\}_j)$ are classified as follows:

$$EventIS_i(EvState) = \begin{cases} Ev^n, EventIS_i \in NormEv, \\ Ev^d, EventIS_i \in DamageEv, \\ Ev^a, EventIS_i \notin NormEv \cup DamageEv. \end{cases} \quad (16)$$

Here, $EventIS_i(EvState)$ are IS events with a status attribute, each of which corresponds to a set of connections SP_j with quick events from a set of templates of the normal mode and the mode with CS breach.

If the event is not present in the profiles of quick events or security breach events, it is determined to be abnormal. The reasons for its occurrence should be considered separately by the administrator of the IS system.

$ISState = \{ISnorm, ISdang, ISanorm\}$ is a set of IS statuses indicating a normal mode of IS operation. The IS status is determined from the formula:

$$ISState = \begin{cases} ISnorm, \forall EventIS_i \in EventIS | EvState = Ev^n, \\ ISdang, \exists EventIS_i \in EventIS | EvState_i = Ev^d, \\ ISanorm, ISnorm \cap ISdang, \end{cases} \quad (17)$$

where *ISnorm* is the mode of normal IS operation; *ISanorm* is the mode of IS operation with features of abnormal activity; *ISdang* is the mode with fixed IS security breaches (Fig. 2).
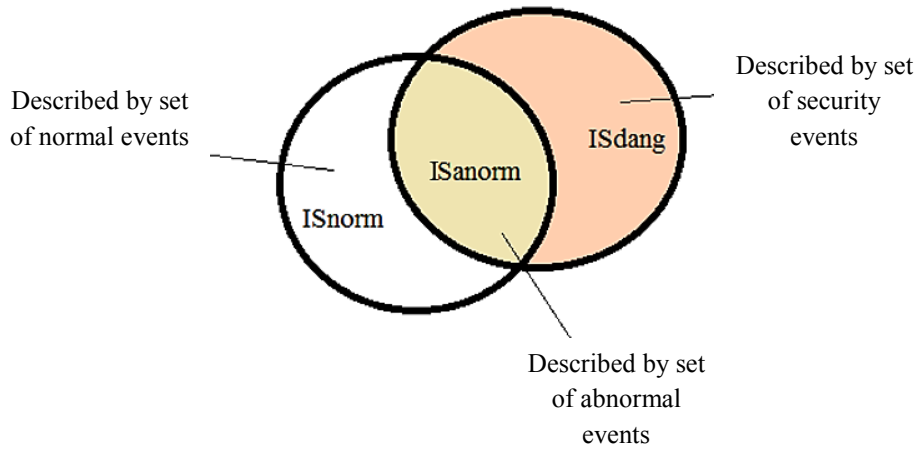

Fig. 2. Relationships of subsets of IS states

Based on the data obtained, a vector is formed that determines the IS status, the total risk, as well as the proportion of abnormal and security breaches:

$$IS = \langle ISState, RISKsum, NanalEv, NdandEv \rangle, \quad (18)$$

where *NanalEv* is the proportion of detected abnormal events, *NdandEv* is the proportion of events of CS breach of the enterprise IS.

To make a decision on whether to strengthen information security subsystems, the IS security level *SL* is calculated:

$$SL = \{safe, stable, abnormal, crisis, dangerous\}.$$

To determine the level of IS security, the designer of the CS system generates a vector that defines the reference indicator of the IS security *IS_Perf*. *SL* is formed according to the similarity of vectors *IS* and *IS_Perf*.

Five levels are accepted for evaluating the IS security within the framework of this mathematical model; therefore, when determining whether the IS belongs to one of the levels, the *k*-nearest neighbor method is used [10]. To this end, intermediate vectors corresponding to the remaining four security levels are compiled.

This operation is based on the values of the IS_Perf vector corresponding to the safe level of the IS status when multiplied by a scalar correction factor (the value is determined by experiment):

$$k \times RIS = \langle k \times ISState, k \times RISKsum, k \times NanalEvent, k \times\times \ NdandEvent \rangle. \tag{19}$$

Weighted Manhattan distance is used as a similarity metric [10]:

$$\rho(IS, RIS) = w \sum_{j=1}^{4} |IS_j - RIS_j|. \tag{20}$$

Based on the presented mathematical model, a generalized algorithm for the operation of a software prototype has been developed (Fig. 3).
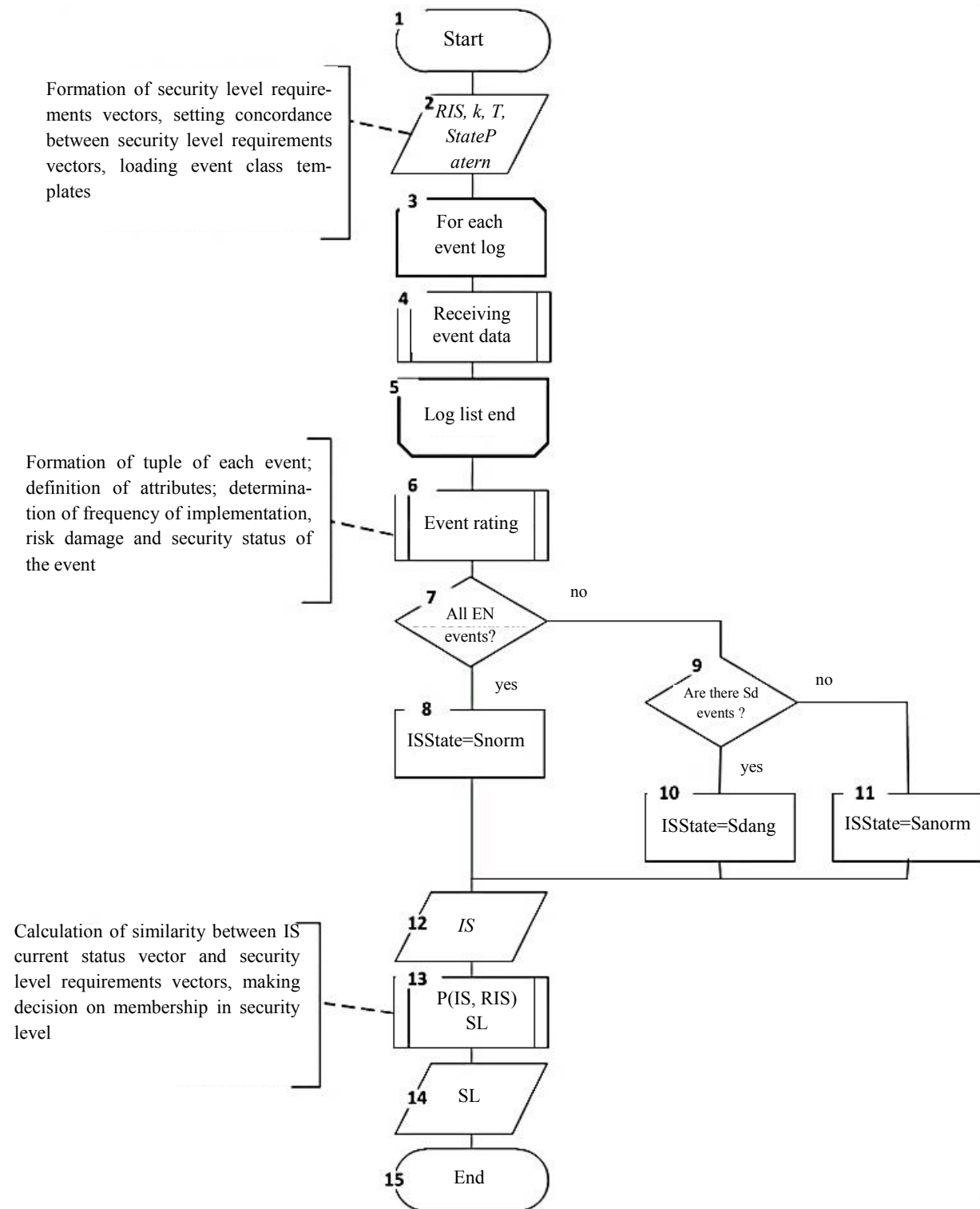

Fig. 3. Algorithm for software prototype of decision smartness complex when designing an information security system at the enterprise

Step 1 (blocks 1, 2). Launching a software prototype. The algorithm start. Input of data on the requirements vectors *IS_Perf* to the IS status of each security level. Enter the period over which monitoring will be conducted. Loading from the DB templates with sets of normal and dangerous events.

Step 2 (blocks 3–5). Monitoring OS event logs, receiving records on each event. Event listing.

Step 3 (block 6). Data analysis of the collected events, formation of the event tuple — the formula (8). Classification of events according to the formulas (14–15) into normal, abnormal, and dangerous ones. Calculation of the frequency of occurrence of events, potential damage and risk using the formulas (11–13).

Step 4 (blocks 7–11). Classification of IS states according to the formula (17) based on the event distribution data into a set of abnormal, normal, and dangerous ones (step 3).

Step 5 (blocks 12–14). Based on the calculated data and event tuple in the IS, the formation of the current status vector, calculation of similarity between *IS* and *IS_Perf* vectors: the formulas (19), (20). Decision-making on whether IS belongs to one of the five security levels.

Step 6 (block 15). The algorithm completion.

Discussion and Conclusion. In the framework of this study, an approach to modeling an information security system is proposed. Different qualitative and quantitative complex of security tools is taken into account depending on the actual threats to information security breaches. The presented method provides increasing the efficiency of the introduced cyber security system and reduces the likelihood of a designer mistake. The software package developed as part of this study has advantages that cannot be obtained under "manual" design:

- accounting of all data on the protected system,

- obtaining accurate results at the earliest.

References

1. Maiorova EV. Metodicheskie aspekty reagirovaniya na intsidenty informatsionnoi bezopasnosti v usloviyakh tsifrovoi ehkonomiki [Methodological aspects of responding to information security incidents in the digital economy]. Saint-Petersburg Economic Journal. 2020;1. URL: https://cyberleninka.ru/article/n/ metodicheskie-aspekty-reagirovaniya-na-intsidenty-informatsionnoy-bezopasnosti-v-usloviyah-tsifrovoy-ekonomiki (accessed 24.02.2020). (In Russ.)

2. Bratchenko AI, Butusov IV, Kobelyan AM, et al. Primenenie metodov teorii nechetkikh mnozhestv k otsenke riskov na-rusheniya kriticheski vazhnykh svoistv zashchishchaemykh resursov avtomatizirovannykh sistem upravleniya [Application of methods of theory of fuzzy sets to assess the risk of violations of critical properties protected resources automated control system]. Cybersecurity Issues. 2019;1(29). URL: https://cyberleninka.ru/article/n/primenenie-metodov-teorii-nechetkih-mnozhestv-k-otsenke-riskov-narusheniya-kriticheski-vazhnyh-svoystv-zaschischaemyh-resursov (accessed: 24.04.2020). (In Russ.)

3. Vitenburg EA. Matematicheskaya model' intellektual'noi podderzhki prinyatiya reshenii pri proek-tirovanii sistemy zashchity informatsii na predpriyatii [Mathematical model of intellectual decision support when designing an enterprise information security system]. In: Industrial Automatic Control Systems and Controllers. Moscow: Nauchtekhlitizdat; 2019. P. 54–60. (In Russ.)

4. Vitenburg EA, Levtsova AA. Vybor ehlementov kompleksa zashchity informatsionnoi sistemy predpriyatiya na osnove trebovanii normativno-pravovykh dokumentov [Selecting safety package components

of enterprise information system following requirements of standard legal documents]. Vestnik of DSTU. 2018;3:333–338. (In Russ.)

5. Stepanova ES, Mashkina IV, Vasil'ev VI. Razrabotka modeli ugroz na osnove postroeniya nechetkoi kognitivnoi karty dlya chislennoi otsenki riska narusheniya informatsionnoi bezopasnosti [Development of threats model on the basis of fuzzy cognitive maps contraction for information risk numerical estimation]. Izvestiya SFedU. Engineering Sciences. 2010;11(112):31–40. URL: https://cyberleninka.ru/article/n/razrabotka-modeli-ugroz-na-osnove-postroeniya-nechetkoy-kognitivnoy-karty-dlya-chislennoy-otsenki-riska-narusheniya-informatsionnoy (accessed 24.04.2020). (In Russ.)

6. Vitenburg EA, Levtsova AA. Model' ugroz informatsionnoi sistemy predpriyatiya [Model of threats of enterprise information system]. Industrial Automatic Control Systems and Controllers. 2018;9:46–50. (In Russ.)

7. Bova VV, Dukkart AN. Primenenie iskusstvennykh neironnykh setei dlya kollektivnogo resheniya intellektual'nykh zadach [Application of artificial neural networks for collective decision of complex intelligent problems]. Izvestiya SFedU. Engineering Sciences. 2012;7(132):131–138. (In Russ.)

8. Smolyak DS, Pulko TA. Monitoring sobytii informatsionnoi bezopasnosti tekhnogennykh ob"ektov [Monitoring of information security events of technogenic objects]. In: Reports of the Belarusian State University of Informatics and Radioelectronics. Minsk: BSUIR Publ. House; 2015. P. 43–47. (In Russ.)

9. Mashkina IV, Sentsova AYu, Guzairov MN, et al. Ispol'zovanie metodov sistemnogo analiza dlya resheniya problemy obespecheniya bezopasnosti sovremennykh informatsionnykh sistem [Use of system analysis methods for the solution of information protection problem of information systems]. Izvestiya SFedU. Engineering Sciences. 2011;12(125):25–35. (In Russ.)

10. Astrakhov AV, Klimov SM, Sychev MP. Protivodeistvie komp'yuternym atakam. Tekhnologicheskie osnovy [Countering computer attacks. Technological basis]. Moscow: Bauman University Publ. House; 2013. 70 p. URL: http://wwwcdl.bmstu.ru/iu10/comp-atak-techno.pdf (accessed 18.05.2020). (In Russ.)

About the authors:

Vitenburg, Ekaterina A., postgraduate student of the Information Security Department, Volgograd State University (100, Universitetskiy pr., Volgograd, 400062, RF), ResearcherID: N- O-8740-2017, ScopusID 57209346586, ORCID: https://orcid.org/0000-0002-1534-8865, e.vitenburg@ec-rs.ru

Nikishova, Arina V., associate professor of the Information Security Department, Volgograd State University (100, Universitetskiy pr., Volgograd, 400062, RF), Cand.Sci. (Eng.), ResearcherID: N-3217-2016, ScopusID 57201358403, ORCID: https://orcid.org/0000-0002-0919-2593, nikishova.arina@volsu.ru

Claimed contributorship

E. A. Vitenburg: basic concept formulation; research objectives and tasks setting; creation of a mathematical apparatus for processing security events; formulation of conclusions. A. V. Nikishova: academic advising; analysis of the research; development of a mathematical apparatus of intellectual decision support; correction of the conclusions.

All authors have read and approved the final manuscript.

INFORMATION TECHNOLOGY, COMPUTER SCIENCE, AND MANAGEMENT

Intelligent system for monitoring and controlling the technical condition of mechatronic process facilities

A. K. Tugengol'd[1], E. A. Luk`yanov[2], R. N.Voloshin[3], V. F. Bonilla[4]

[1,2,3] Don State Technical University (Rostov-on-Don, Russian Federation)

[4] University of Technology (Quito, Republic of Ecuador)

Introduction. Digital systems that control the maintenance of separate mechatronic process facilities (MPF) and sets of production machines are mainly considered. Numerous issues on maintaining the reliability of the condition and emerging malfunctions, as well as the multifactorial nature of the using the existing monitoring and diagnostic systems, are noted. In this regard, the relevance of the tasks of developing methods of processing equipment maintenance to make decisions under the data veracity and limitation is specified.

Materials and Methods. To analyze the criticality of the technical condition, an assessment of the efficiency of the autonomous control of the device state is formed. The method of the neuro-fuzzy system is used to determine the aggregate criterion of criticality. It is proposed to apply this approach to develop recommendations on equipping a production facility with the necessary means of maintaining overall performance and reliability.

Results. The solution provides predicting the development of the state of mechatronic process equipment, alerting personnel in case of emergency and other dangerous conditions, and, if necessary, updating or adjusting control programs. Provision is made for performing of some of the technical state maintenance functions by the mechatronic facility itself, i.e., equipment self-service. The concept of "autonomous management of the technical condition" is formulated. The system structure and control functions are considered. It is noted that the implementation of the systems under consideration will significantly increase the efficiency of the equipment use. The performance of the autonomous control of the device or MPF in general is evaluated in accordance with ISO 13381-1: 2004. Based on this standard and the data presented earlier, a neural network structure is built to assess the autonomy of state management. The system training efficiency is considered taking into account the standard deviation of the network outputs from the target values of the training sample.

Discussion and Conclusion. A list of the basic control functions at different levels of maintenance autonomy is presented: from alarm for failure prediction to complete maintenance autonomy without the direct involvement of an operator.

Keywords: digital systems, autonomous maintenance, technical condition management, critical condition.

Introduction. For more than 50 years, serious developments have been carried out in the field of machine maintenance, which focus on methods and standards for maintaining an operational condition of the equipment. New devices and techniques are being developed for determining emergency conditions, identifying faults, and predicting a remaining life. The condition control and monitoring are essential for production mechatronic facilities of the industrial enterprises, such as machines with computer numerical control (CNC), forging and foundry machines, automated flexible transfer lines, etc. Equipment maintenance methods take various forms [1, 2], each of which has pros and cons that affect the level of control of the production condition of the equipment. Such control and providing the reliability of

machines are urgent scientific tasks. Numerous studies are devoted to this topic. An example is the works [3–14]. Russian and foreign scientists mainly consider the creation of automated monitoring and diagnostic systems. When using artificial intelligence methods for automation, processor modules are developed; they have acquired a general name of "e-maintenance systems".

Digital systems of electronic service are implemented by a collection of hardware-software components, which are designed to receive sensory information and assess the equipment status realtime. They provide predicting state changes in the production equipment and its components, generating messages on the need for certain actions on the part of experts, and, in some cases, changing the equipment operation parameters. The systems under consideration are used for personal diagnostics and monitoring of the technical condition of separate mechatronic objects. In addition, they are involved in the service system of a group of production machines.

The focus of current research is the creation of programs and algorithms for service, and analysis of its results. Developments in the field of service quality and efficiency of the equipment utilization are aimed at this. In modern production sectors, such systems as Casip, Enigma, Icasame, RemoteDataSentinel, Intermor, INID, IPDSS, Proteus, MRPOS, WSDF, Telma, etc., are used for servicing [15–18].

It stands to mention multiplicity of issues on maintaining the reliability of the condition and arising faults, as well as the multifactority of the application of existing monitoring and diagnostic systems. In this regard, the tasks on the development of methods and techniques for the processing equipment maintenance, which provide decision-making under the conditions of data veracity and limitation, remain relevant.

In recent years, the basic functionality of control, monitoring and diagnostics systems, tools, methods and technologies for servicing, forecasting and analyzing equipment status has changed. They are reoriented from the analysis of the technical condition to the prevention and detection of malfunctions at the early operational stages. Such control methods are being developed that allow minimizing the impact of emerging malfunctions on the performance and downtime of the equipment, on the number of failed parts and the frequency of failures. Ultimately, new approaches reduce economic losses.

The urgent issue is the development of a new solution based on the intelligence of the system. It is about creating an automated autonomous service management and, as a consequence, about control over the autonomous technical condition of the equipment.

Autonomous maintenance (AM) [19] is a comprehensive definition. In relation to machines, it implies such an automatic performance of service and maintenance functions, in which the equipment independently maintains its operability (self-service). If human intervention in the maintenance is wanted, the service functions remain hand-driven by an operator, that is, the problems are fixed promptly, without involving external repair services and until the end of the production run.

The self-servicing of mechatronic process facilities (MPF) in the sense presented earlier is not yet an implemented solution, but a promising one. It is expected that the methods of artificial intelligence in the field of diagnostics and servicing will receive a level of knowledge equal to the level of staff.

Materials and Methods. At the present stage of technology development, we consider the concept of MPF AM in the following interpretation. The purpose of the solution is maintainability based on an assessment of the state of the component and the MPF in general. For this, an independent automated control purposefully displays the status and required impacts on the MPF components [20].

As noted earlier, the basic approach to creating and developing autonomy in managing the operability of the processing equipment is the application of artificial intelligence and intelligent control methods under the conditions of uncertainty and fuzziness of the knowledge provided [21].

Research Results. Under the conditions of uncertainty, we consider the control procedure as the dependence of the real state on the goal state (successful performance):

$$R^* = A \rightarrow B,$$

Information technology, computer science, and management

where *A* and *B* are expert reports on the real and goal state of MPF.

Presentation of the result of fuzzy inference *Y* depends on:

— observed data *X* obtained by the diagnostic system;

— knowledge system $A \rightarrow B$;

— coefficient *K*, which is responsible for a possible measurement error.

Therefore, the derivation of *Y* takes the form:

$$Y = X \times R^* + K = X \times (A \rightarrow B) + K,$$

where $Y = \{Y_1, Y_2, ..., Y_m\}$ are parameters responsible for the equipment state management and for log output for the operator; $X = \{X_1, X_2, ..., X_n\}$ are data on the input state of the equipment.

Using this interpretation of the maintenance autonomy, we consider the structure and functions of the MPF AM (Fig. 1).
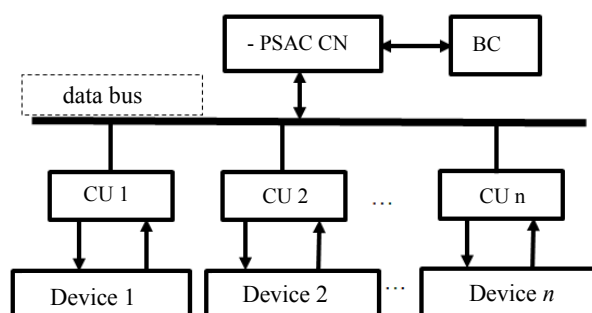

Fig. 1. Structure of the control system of the equipment technical condition

Here, signals from the diagnostic system sensors arrive at the control device not directly, but through the control unit of the technical state (TSCU) of the nodes.

Nodes of the control unit receive data from the central node of the autonomous control of the process system (PSAC CN), which:

— coordinates the operation and maintenance of all machine components;

— processes data received from diagnostic systems;

— on the basis of these data, analyzes the state, predicts the development of malfunctions and makes decisions on the required actions on smooth operation of the equipment.

In the proposed approach to the generalized functions for the MPF technical condition management, control methods using signaling about the risk of failures, emergency situations, the need for a fuzzy device working band, etc. [22], are considered.

An electronic service system (for example, e-Mind Machine) can provide information communication between the PSAC of an object through IS with equipment maintenance and repair units and enterprise management structures [23].

The autonomous control functions include decision-making on the system behavior in the event of a malfunction; consequently, the system should be trained during operation. Thus, diagnostic and monitoring methods are being improved, which provides eliminating previously unknown malfunctions.

The analytical methods are complicated (or impossible) in adequate presentation of the state and changes of MPF. This is due to the following maintenance features of this equipment:

— structural complexity of the mechatronic object consisting of a large number of nodes;

— variety of factors affecting the reliability and performance, accuracy and productivity of machines;

— wide range of properties of the materials from which the parts are made;

— variety of requirements for functionality, parametric characteristics and performance of units, modules and devices in accordance with their purpose, accuracy characteristics, implemented production tasks.

The e-MindMachine concept provides management based on data on the real state of the facility and operational history. In this case, the development of faults for each unit is predicted. The application of the gamma-percentile life of reliable operation is proposed if statistical data are available or a border health band is used [22–24].

When developing PSAC of process facilities, it is possible to provide a ranking of autonomy levels depending on the maintenance unit used at the enterprise [25, 26]. It also depends on the criticality of the machine in the overall production. In this case, criticality determines significance of one or another of its units for the enterprise. The higher the criticality, the more economic, physical or temporary losses an enterprise suffers from the downtime of this unit. Such data is based on the equipment usage statistics, the number of failures, downtime, the cost of spare parts and manufactured parts, the number of work shifts, etc.

When analyzing the criticality, it is also important to consider the future conditions of the machine, the degree of development of malfunctions, and the planning of the acquisition of spare parts. This is necessary to assess the residual life and to calculate the time before a possible failure under the conditions of uncertainty and stochasticity of data on the equipment status. Criticality assessment helps to find out the significance of the given equipment unit for the enterprise, and how much stop service and work resumption cost.

To analyze maximum number of parameters that affect criticality of failures, we construct a system for the generalized assessment of the MPF technical condition criticality. For the output aggregate criterion of criticality, we use an ANFIS-based neuro-fuzzy assessment in MATLAB. As an example, we consider the failure criticality of the spindle assembly of a HAAS SMM vertical milling machine (Fig. 2).
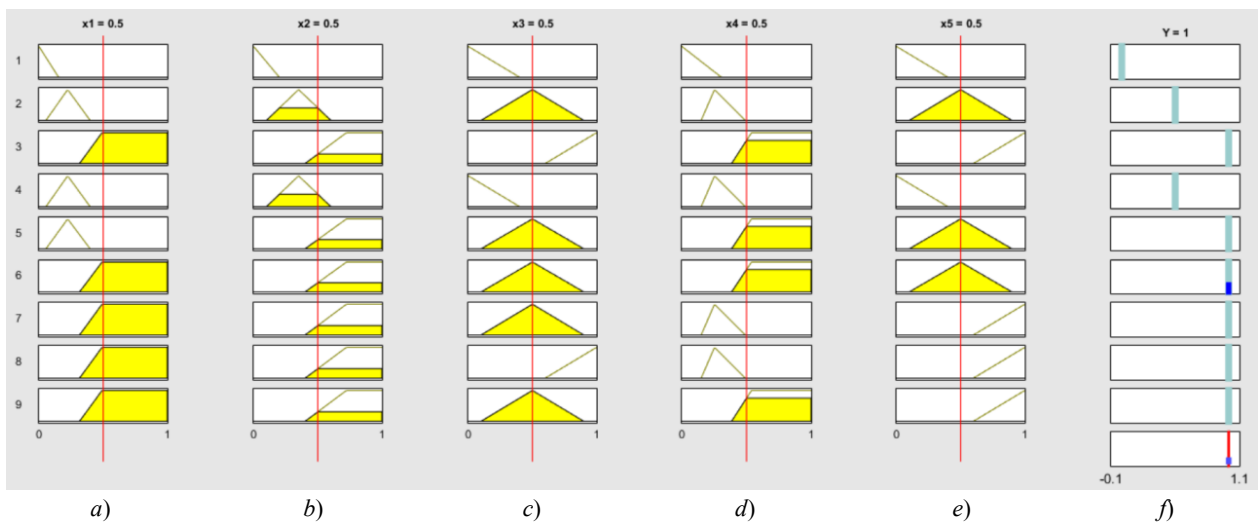

Fig. 2. Failure criticality assessment. Red vertical line is indicator 0.5:
(a) equipment performance and accuracy; (b) costs of equipment repair and spare parts; (c) equipment downtime; (d)
(b) number of equipment (unit) failures for a certain period; (e) time for fault identification and repair;
(c) (f) $Y = 1$ is full compliance to output parameters

Fig. 2 shows that the input actions in the neuron-fuzzy system are responsible for all the key aspects which concern the equipment operation at the enterprise [27]. As a result, when logging-out, we obtain a generalized criterion of criticality Y whose value can vary from 0 to 1. Here, $Y = 0$, the input parameters do not meet the production requirements. According to the monitoring data, the parameters went beyond $0 < Y < 1$, but an expert can make a conclusion on the availability of equipment (for example, at $Y = 0.75$). Using this criticality assessment technique, when determining the operability of the same type of equipment, it is possible to indicate a response range for emerging malfunctions and create a new decision-making system under uncertainty. Thus, the most significant (critical) equipment receives maximum response from the operator and maintenance personnel for its operability.

Fuzzy logic methods simplify the intelligent control system and evaluate immediately the state of an object. This is an autonomous management of the technical condition of the facility, so you need to understand how deep autonomy can be. A machine is considered together with an operator, which means that the equipment is automatically controlled by the actions of the operator as well. Management levels depend on the functions assigned to human.

Information technology, computer science, and management

191

Level 1. Control. It is determined by the presence or absence of an emergency malfunction, which causes equipment shutdown.

Level 2. Diagnostics. The data analysis on the equipment condition is carried out by the built-in or mounted sensors.

Level 3. Monitoring. The current level of performance is determined, operational or tactical decisions are made.

Level 4. The operator performs all basic functions without machine automation. They can be displayed as instructions.

Level 5. The operator performs part of the functions that do not require deviation from the production tasks.

Level 6. Autonomy of the MPF service without the intervention of an operator.

If it is necessary to maintain the equipment operability at a high level, it is advisable to use monitoring (level 3). The use of some automation at the 4th level seems to be a transition to the creation of intelligent service systems.

The implementation of the systems under consideration increases significantly the equipment efficiency. The productivity of the autonomous control of a device or MPF is generally evaluated in accordance with ISO 13381-1: 2004. Based on this standard and the data presented earlier, we construct the structure of a neural network for assessing the autonomy of state control (Fig. 3).
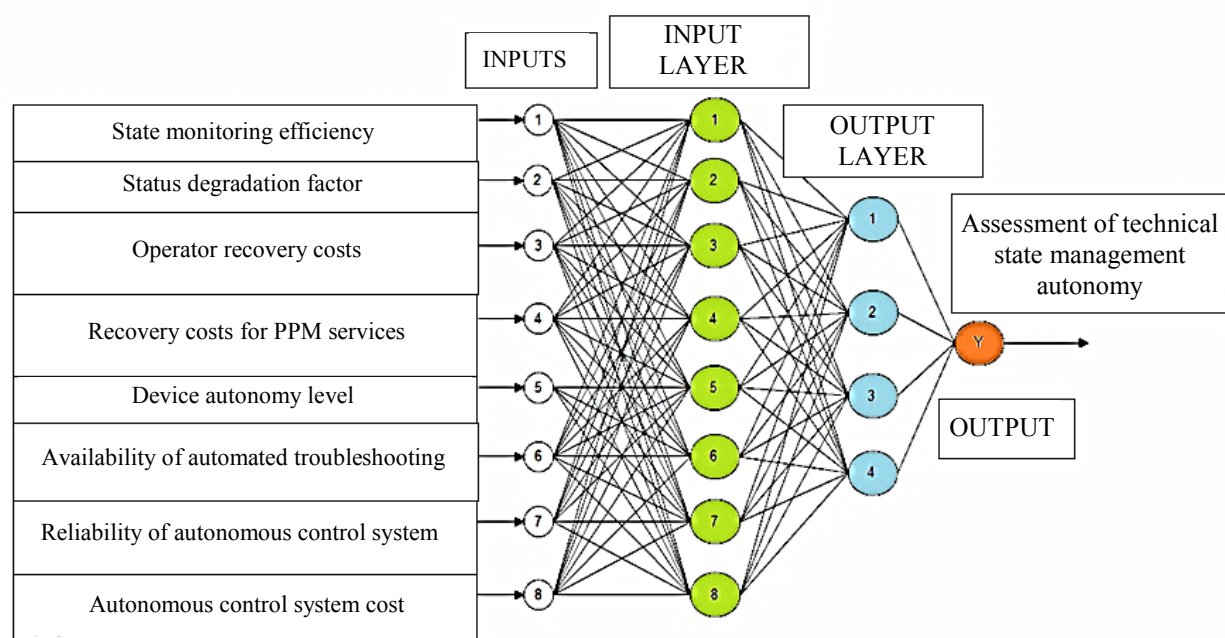

Fig. 3. Structure of neural network assessment of the state management autonomy[1]

Learning efficiency was evaluated with account of the standard error of the deviations of the network outputs from the target values of the training sample [20].

Discussion and Conclusion. The paper presents the basic principles and approaches that provide designing, creating and improving autonomous systems for management of the technical condition of the process facilities. The operation of such systems implies significant uncertainty and limited aprior and current data for decision-making. This necessitates the introduction of state-of-the-art technologies and methods of artificial intelligence.

The authors' view on the role, functions and construction of maintenance systems for MPF and other equipment is presented. The proposed approach is based on the application of digital information processing and decision-making technologies, which is due to the growing complexity of MPF automation. In each process system, the principles of openness, autonomy, and control of fine movements are implemented to one degree or another. This should be considered when designing workpart procedures and when implementing processes to maintain the equipment operability.

---

[1] PPM — preventive and predictive maintenance.

References

1. Mal'tsev AI, Mal'tsev AA. Monitoring tekhnicheskogo sostoyaniya krupnykh mashin [Monitoring the technical condition of large machines]. Elektrostal: DAMO; 1998. 62 p. (In Russ.)

2. Nikitin YuR, Abramov IV. O postroenii sistemy diagnostirovaniya stankov s CHPU [Designing of CNC machines, diagnosing system]. Mechatronics, Automation, Control. 2011;4:32–35. (In Russ.)

3. Muller A, Suhner M-C, Iung B. Formalisation of a new prognosis model for supporting proactive maintenance implementation on industrial system. Reliability Engineering and System Safety. 2008;93(2):234–253. URL: https://ideas.repec.org/a/eee/reensy/v93y2008i2p234-253.html (accessed 15.05.2020).

4. Lee J, Ni J, Djurdjanovic D, et al. Intelligent prognostics tools and e-maintenance. Computers in Industry. 2006;57:476–489.

5. Djurdjanovic D, Lee J, Ni J. Watchdog Agent — an infotronics-based prognostics approach for product performance degradation assessment and prediction. Advanced Engineering Informatics. 2003;17(3):109–125.

6. Moore WJ, Starr AG. An intelligent maintenance system for continuous cost-based prioritisation of maintenance activities. Computers in Industry. 2006;57:595–606.

7. Kruglova TN, Glebov NA. Diagnostirovanie i prognozirovanie tekhnicheskogo sostoyaniya mekhatronnykh modulei dvizheniya tekhnologicheskogo oborudovaniya [Diagnosis and prediction of the technical condition of mechatronic motion modules of technological equipment]. Novocherkassk: Izd-vo YURGTU (NPI); 2011. P. 119. (In Russ.)

8. Emmanouilidis C, Jantunen E, Gilabert E, et al. E-Maintenance update: the road to success for modern industry. COMADEM: proc of the 24th International Conference on Condition Monitoring and Diagnostic Engineering Management, 30 May - 1 June 2011. Norway, Stavanger. ResearchGate: URL: https://www.researchgate.net/publication/258006515_e-aintenance_update_the_road_to_success_for_modern_industry (accessed 15.05.2020).

9. Wang P, Vachtsevanos G. Fault prognostics using dynamic wavelet neural networks. Artificial Intelligence for Engineering Design, Analysis and Manufacturing. 2001;15:349–365.

10. Zhang W, Halang W, Diedrich C. An agent-based platform for service integration in E-maintenance. Industrial technology: proc. of IEEE international conference. Slovenia, Maribor. 2003;1:426–433. ResearchGate: URL: https://www.researchgate.net/publication/4070917_An_agent-based_platform_for_service_integration_in_E-maintenance (accessed 15.05.2020).

11. Lee J. E-manufacturing: fundamental, tools, and transformation. Robot. Comput.-Integr. Manuf. 2003;19(6):501–507.

12. Mitchell J, Bond T, Bever K, et al. MIMOSA — four years later. Journal of Sound and Vibration. 1998;11:12–21.

13. Lee L, Wu F, Zhao W, et al. Prognostics and health management design for rotary machinery systems — reviews, methodology and applications. Mechanical Systems and Signal Processing. 2014;42:314–334.

14. Cao X, Jiang P. Development of SOA Based Equipments Maintenance Decision Support System. Intelligence Robotics and Applications: Proc. First International Conference, ICIRA. China, Wuhan October 15–17, 2008. Berlin; Heidelberg: Springer-Verlag; 2008. Part II;5315:576–582.

15. Rissland EL, Skalak DB. Combining case-based and rule-based reasoning: A heuristic approach. In: Proc. 11th International joint conference on Artificial intelligence (IJCAI-89). Michigan, Detroit. Vol. 1:524–530. URL: https://www.researchgate.net/publication/220816256_Combining_Case-Based_and_Rule-Based_Reasoning_A_Heuristic_Approach (accessed 15.05.2020).

16. Bangemann T, Reboul D, Scymanski J, et al. PROTEUS — An integration platform for distributed maintenance systems. Computers in Industry. Special issue on E-maintenance. 2006;57(6):539–551.

Information technology, computer science, and management

17. Karray MH, Chebel-Morello B, Lang C. A component based system for S-maintenance. ResearchGate : URL: https://www.researchgate.net/publication/252048503_A_component_based_system_for_S-maintenance (accessed 15.05.2020).

18. Muller A, Marquez C, Iung B. On the concept of e-maintenance: Review and current research. Journal of Reliability Engineering and System Safety. 2008;93:1165–1187.

19. Tugengol'd AK, Voloshin RN, Yushchenko SV. Modul' E-Mindmachine v intellektual'noi sisteme monitoringa stanka [E-Mindmachine module in the intelligent machine monitoring system]. International Research Journal. 2008;9(40), pt. 2:100–102. (In Russ.)

20. Tugengol'd AK, Voloshin RN, Dimitrov VP, et al. Upravlenie tekhnicheskim sostoyaniem stankov [Machine condition management]. STIN. 2018;7:8–15. (In Russ.)

21. Tugengol'd AK, Voloshin RN. Gibkii monitoring mekhatronnykh tekhnologicheskikh mashin [Flexible monitoring of mechatronic technological machines]. Vestnik of DSTU. 2016;4:51–58. (In Russ.)

22. Tugengol'd AK, Dimitrov VP, Izyumov AI, et al. Monitoring and Control of Tools in Multifunctional Machine Tools. Russian Engineering Research. 2017;37(5):440–446.

23. Tugengol'd AK, Dimitrov VP, Voloshin RN, et al. Monitoring of Machine Tools. Russian Engineering Research. 2017;37(8):440–446.

24. Push VE, Pigert R, Sosonkin VL. Avtomaticheskie stanochnye sistemy [Automatic machine systems]. Moscow: Mashinostroenie; 1982. 320 p. (In Russ.)

25. Tugengol'd AK, Dimitrov VP, Borisova LV, et al. Autonomous Maintenance of Digital Equipment. Russian Engineering Research. 2019;39(6):510–515.

26. YadchenkoAV, Solomykin MYu, Tugengol'd AK, Voloshin RN. Struktura i algoritm raboty sistemy diagnostiki sostoyaniya mnogooperatsionnogo stanka [The structure and algorithm of the system for diagnosing the state of a multioperational machine]. Sovremennye nauchnye issledovaniya i razrabotki. 2017;8(8):232–237. (In Russ.)

27. Tugengol'd AK, Voloshin RN. Kriterii kritichnosti pri analize sostoyaniya tekhnologicheskikh mashin [Criteria of criticality in the analysis of the state of technological machines]. In: Proc. 10th Int. Sci.-Pract. Conf. within framework of the 20th Int. Agroindustrial Exhibition "Interagromash-2017". Rostov-on-Don: Izd-vo DGTU; 2017. P. 288–292. (In Russ.)

About the authors:

Tugengol'd, Andrei K., professor of the Robotics and Mechatronics Department, Don State Technical University (1, Gagarin sq., Rostov-on-Don, 344000, RF), Dr.Sci. (Eng.), professor, ResearcherID: E-5707-2018, ORCID: https://https://orcid.org/0000-0003-0551-1486, akt0yandex.ru

Luk`yanov, Evgenii A., Head of the Robotics and Mechatronics Department, Don State Technical University (1, Gagarin sq., Rostov-on-Don, 344000, RF), Cand.Sci. (Eng.), associate professor, ORCID: https://orcid.org/0000-0001-6147-2907, r.voloshin2909@gmail.com

Voloshin, Roman N., postgraduate student of the Robotics and Mechatronics Department, Don State Technical University (1, Gagarin sq., Rostov-on-Don, 344000, RF), ORCID: https://orcid.org/0000-0002-6363-6511, lukevgan@gmail.com

Bonilla, Venegas F.V., associate professor of the Mechatronics Department, University of Technology (UTE) (Occidental y Mariana de Jesus St., Quito, EC170528, Republic of Ecuador), Cand.Sci. (Eng.), associate professor, ScopusID 57195722104, ORCID: https://orcid.org/0000-0001-6542-9666, vbonilla@yahoo.com

Claimed contributorship

A.K. Tugengol'd: concept development; research objectives and tasks setting; mathematical rationale of problems; theoretical description of solutions; development of state management levels; assessment of the state management autonomy using a neural network. E.A. Luk'ynov: mathematical calculations; building block diagrams; rationale for using different management levels; conclusion formulation. R.N. Voloshin: writing a review on the topic; text processing; assessment of criticality; work with standards; building the neural network structure. F.V. Bonilla: work with foreign sources; text processing; building dependences based on the neural fuzzy ANFIS system in MATLAB.

All authors have read and approved the final manuscript.

INFORMATION TECHNOLOGY, COMPUTER SCIENCE, AND MANAGEMENT

Artificial intelligence in data storage systems

V. V. Zhilin[1], O. A. Safar'yan[2]
[1] Budenny Military Academy of Communication (St. Petersburg, Russian Federation)
[2] Don State Technical University (Rostov-on-Don, Russian Federation)

Introduction. The artificial intelligence (AI) performance in data storage systems is considered. When working with data, the advantage of its use both in economic terms and for security is determined. The work objective is the introduction of artificial intelligence in data storage systems. The key tasks involve the description of methods for data separation, organization of its storage and counteraction to security threats.

Materials and Methods. The data that should be fed into the drives is divided into parts so that it can be restored without one of the parts. This is necessary to be able to access and recover information in the event of a software or hardware failure.

Results. The AI performance under detecting security threats is considered. Since the model implies the interaction of users with data, it was found out how the data access control is carried out and the keys are stored.

Discussion and Conclusions. The use of AI in organizing a data warehouse will speed up the system. Artificial intelligence with built-in machine-learning algorithms will provide responding to a situation that affects the state of the system. Analysis of the state of the drives will avoid a possible hardware or software failure. Minimization of the human factor in the system operation contributes to the improvement of its work.

Keywords: artificial intelligence, threshold separation, threat, machine learning, storage organization, dynamic change, key, encryption, backup, attack, hash.

Introduction. At the present stage of development of information and telecommunication technologies, a person comes across various kinds of information. The data storage in a safe place is an urgent issue. The science that deals with the storage of information in an encrypted form is cryptography. It studies how to hide data and provide its confidentiality[1].

The information is static in all data storage implementations. That is, the data will be where it was for the first time. Information can get to another disk or another sector only after removing it from its original location. However, this fact may be regarded as weakness of existing algorithms.

To increase the protection effectiveness, it is recommended to share data [1] in order to store their parts. This provides organizing fault-tolerant storages for information recovery algorithms in the event of any fault, failure of one of the drives, as well as with loss of one or more parts of the data.

If an attacker has access to the disk, he will be able to obtain the necessary information. In case of static storage, if an illegitimate user gains access to several such disks, he can recreate information. Separated data storage increases information security. In addition, in large storages, as a rule, hard disk drives are used, whose running speed (reading and writing operations) is significantly lower than that of solid state disks (SSD) and flash drives[2]. In this regard, you have to choose between the volume used and the operation speed.

The work objective is to describe the performance of artificial intelligence (AI) in data storage systems. The task is to describe the AI operation algorithms when performing the following operations:

• data recording on drives;

---

[1] Ryabko BYa, Fionov AN. Kriptografiya v informatsionnom mire [Cryptography in the Information World]: Goryachaya liniya-Telekom; 2018. 305 p URL: https://www.techbook.ru/book.php?id_book=1001 (accessed 04.05.2020).
[2] Sravnenie SSD i HDD diskov v real'nykh usloviyakh ispol'zovaniya [Comparison of SSD and HDD drives under real-time conditions of usage]. Habr. URL: https://habr.com/ru/post /394135/ (accessed 04.05.2020).

• referral from users;

• data warehouse analysis;

• in case of information security threats.

Artificial intelligence impact on the storage system quality. In modern devices, such as smartphones and computers, developers give special consideration to the implementation of artificial intelligence. In these technologies, machine learning algorithms are implemented, which increases the operation speed and reduces the response time to conducting frequently repeated information. It should be considered how the introduction of artificial intelligence and machine learning into storage systems can significantly improve the quality of their operation [2].

Currently, large companies and organizations are starting to implement AI in their data warehouses. A widespread adoption of machine learning and artificial intelligence technologies helps to improve the operating quality at the management level. This facilitates the work of network and data warehouse administrators through constantly diagnosing the causes of traffic overload and reduction. This will allow them to identify potentially vulnerable segments of the model beforehand.

Artificial intelligence involves the use of integrated deep learning algorithms that can predict the state of the entire system and respond quickly to possible changes. This will significantly reduce the cost of eliminating the consequences caused by equipment failure. In addition, the introduction of artificial intelligence in the organization of fault-tolerant storages will allow for their automation [3]. This implies an analysis of the system state and processing of incoming data in dynamic mode.

Artificial intelligence and machine learning provide minimizing the likelihood of data loss. Together with redundant arrays of independent disks, such a system increases the availability and speed of overcoming forced downtime thanks to intelligent data recovery, a backup strategy and the transfer of necessary data [4].

Data distribution by input parameters. To store data in a shared form, threshold separation methods can be applied. In classical algorithms, the in parameters are static values, which is a major disadvantage. Gaining access to one data through selecting input parameters threatens safety of all other data in the system.

Thus, the greatest preference in terms of information security is given to the algorithm that uses various input parameters for threshold sharing. These parameters can be randomly generated according to a certain algorithm or depend directly on the input data, which will be analyzed accordingly to select the most preferred parameters. The generation of such parameters will be handled directly by artificial intelligence. At the same time, it should consider the number of users to whom this information is available. Threshold sharing parameters and the location of the first share are stored in the database. This database is encrypted on the keys of specific users, which corresponds to the application of an asymmetric cryptoalgorithm.

Parameters of the proposed algorithm for data reliability. When distributing data among drives, artificial intelligence uses the following parameters: drive speed, availability, free volume and reliability index. At the same time, AI uses the data value parameters, size and frequency of accesses to it for calculation.

The algorithm for the distribution of data shares across drives is based on the calculation of drive coefficients. To determine the speed of the drive S, it is required to find the arithmetic average of the writing speed $s_{зап}$ and read rate $s_{чт}$:

$$S = \frac{s_{зап} + s_{чт}}{2}.$$

Drive accessibility A has 3 levels: 0 — unavailable, 1 — frequent situation of drive unavailability, 2 - rare situation of drive unavailability, 3 — anytime available. The exponential coefficient of the drive can be expressed by the formula:

$$K_{н} = S \cdot A \cdot V \cdot R,$$

where V is disk capacity; R is reliability, it is ranked from 1 to 10 points; A is the number of file accesses in a given period of time.

The significance factor of the file $K_{ф}$ depends on the value level (1 — low, 2 — medium, 3 — high). Based on the known attributes, this parameter can be calculated from the formula:

$$K_{ф} = S \cdot V \cdot A.$$

Consider the technique of selecting a storage drive for the remaining files. To determine the priority of the drive, we use the file number n_1 in the sorted table in descending order of the parameter $K_{ф}$. Then the disk number N_1 participating in the sample for storing the first share of the data is found from the formula:

$$N_1 = round\left(\frac{d \cdot n_1}{f}\right) mod \; n_2,$$

where d is the number of disks used for storage; f is the number of files in the system; n_2 is the number of drives; *round* is rounding to the nearest integer.

In the same way, drive N_2 is determined, which may be selected as a drive for storing the first share:

$$K_{first} = K_ф \cdot K_{d.max},$$

where $K_ф$ is the split file ratio; $K_{d.max}$ is maximum drive coefficient.

Next, the drive, whose difference in the coefficients K_{first} and $K_н$ is the smallest, is selected as N_2. To store the first share, one of the found disks N_1 and N_2 is randomly selected.

Advantages of the considered algorithm of data distribution among storage devices. Classically, disks combined into one data array (*RAID*-array) operate according to a static algorithm. That is, when the first share of data is detected, a search procedure for the second share can be performed. Each time, upon detection of the next share, the probability of determining a specific distribution algorithm increases. In the proposed algorithm, the distribution is based on information data and drives. In other words, the task of finding all the data shares is *NP*-complete, that is, it cannot be solved in polynomial time. It follows that the use of this algorithm increases the reliability of the information storage system.

However, users do not create a key; it is generated automatically and stored on the devices of the users themselves. Thus, when trying to decrypt data, a specific key must be used, otherwise this operation fails. The location of the keys changes dynamically over time. Such changes can occur at certain hours, or at specific time intervals [5]. Artificial intelligence is responsible for the key location with account of the availability of all devices connected to the system. This complicates the work of an attacker whose goal is to access information stored on drives [6].

Since the information in the repository is operated by users, it should be determined who of them is allowed to conduct operations with data, in other words, how to differentiate the data access.

Access comparison is performed according to the hash-sum table[1]. If a user has access to data, then they are restored. If there is no entry in the database on granting access rights, the entity requesting access to the object is denied.

In addition, an attempt to gain access will be recorded in the log file, and the subject who owns the information stored in the system will be informed about the access attempt by an illegal user or subject. In this case, artificial intelligence analyzes the actions of each user to make decision in the event of a specific situation. For example, it determines whether the query is invalid, or it has any purpose [2].

Fig. 1 shows an example of granting access to data recovery and access denial with recording the event in a log file and the user notice.
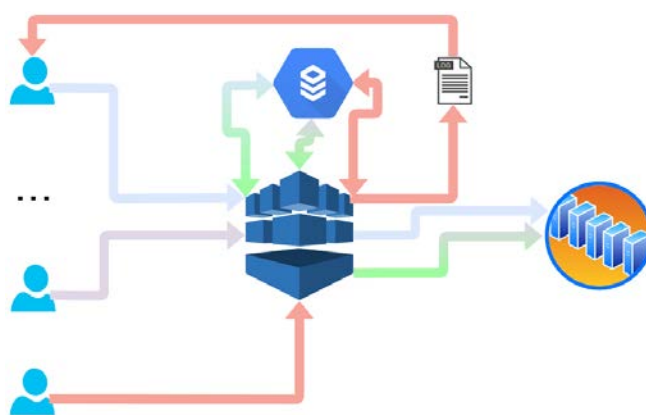

Fig. 1. Granting and denial of access to data recovery

Consider the access control function. Since the primary subjects in the system are users, the issue of providing access to data is particularly topical. Full control over user operations is very important. The decision to provide access to data is made by a distribution device with support of artificial intelligence. In this case, the use of AI will increase the

---

[1] Legkii sposob poddelki kontrol'noi summy s pomoshch'yu kollizii [Easy way to fake checksum using collisions]. xakep.ru. Available from: https://xakep.ru /2012/11/22/light-fake-checksum/ (accessed 04.05.2020).

user's data handling speed. This is achieved through transforming the most commonly used information, which avoids waiting for the response time to the sent data recovery request.

We consider dynamic change of storage. In certain cases, artificial intelligence controls the transfer of data and is responsible for data backup and restore including the time-based ones. In this case, the data migrates from one disk to another, and the information in the database also changes. This minimizes the likelihood of predicting the system state at a specific time. Since all keys are generated on the ground of previous sequences using hash sums, the task of finding a key designed to decrypt a database is an *NP*-complete problem [7]. In this case, artificial intelligence analyzes the state of drives, as well as the system as a whole. When a malfunction is detected, data is transferred from those drives on which failures are noticed. This minimizes the likelihood of information loss.

When a threat is detected, artificial intelligence analyzes the attack to determine its target. If the final goal is the storage object, then the data from it is transferred to another drive. Thus, in the event of a successful attack, AI will take effective actions to hide information [8].

As users work with data, the human factor plays an important role. Therefore, the system is designed so that only users with access can work with the data. There is an analogy with the mandatory access control model. An exception is that the distribution of access is controlled by the user who has created the information in the system and is its owner.

Conclusion. Thus, the use of artificial intelligence increases the system speed under organizing a data warehouse. Restricting user access to the algorithm of the system operation improves information security. Artificial intelligence with built-in machine learning algorithms provides a quick response to any situation affecting the state of the system. Analysis of the state of the drives avoids a possible hardware or software failure. Minimization of the human factor in the system operation helps to improve its functioning and a deeper analysis of user queries. In addition, the collection of information on possible attacks enables maintaining the system security at a proper level.

References

1. Mogilevskaya NS, Kul'bikayan RV, Zhuravlev LA. Porogovoe razdelenie failov na osnove bitovykh masok: ideya i vozmozhnoe primenenie [Threshold file sharing based on bit masks: concept and possible use]. Vestnik of DSTU. 2011;11(10):1749–1755. URL: https://vestnik.donstu.ru/jour/article/ view/912/907 (accessed 04.04.2020). (In Russ.)

2. Nikolenko SI, Kadurin AA, Arkhangel'skaya EV. Glubokoe obuchenie. Pogruzhenie v mir neironnykh setei [Deep learning. Immersion in the world of neural networks]. St. Petersburg: Piter; 2018. 481 p. (In Russ.)

3. Dubrova E. Fault-Tolerant Design. Springer; 2013. 185 p.

4. Flakh P. Mashinnoe obuchenie [Machine Learning]. Moscow: DMK Press; 2015. 400 p. (In Russ.)

5. Zhilin VV, Drozdova II, Cherkesova LV, et al. Trekhmernaya model' bezopasnosti komp'yuternykh sistem [Three-dimensional model of computer systems security]. Young Researcher of the Don. 2018;5:30–37. URL: http://mid-journal. ru/upload/iblock/f81/6_620_ZHilin_30_37.pdf (accessed 04.05.2020). (In Russ.)

6. Parloff R. Why Deep Learning Is Suddenly Changing Your Life. Fortune. 2016. Retrieved 13 April, 2018.

7. Cormen Th, Leiserson Ch, Rivest R. Algoritmy: postroenie i analiz [Algorithms: construction and analysis]. Moscow: Vil'yams; 2006. 1296 p. (In Russ.)

8. Hutson M. Missing data hinder replication of artificial intelligence studies. Science. 15 February, 2018. doi:10.1126/science.aat3298.

About the authors:

Zhilin, Viktor V., student of the Cybersecurity of IT Systems Department, Military Academy of Communication of S.M. Budenny (3, Tikhoretsky Av., K-64, St. Petersburg, 194064, RF), ORCID: https://orcid.org/0000-0001-6277-3795, zhilin95@inbox.ru

Safar'yan, Olga A., associate professor of the Cybersecurity of IT Systems Department, Don State Technical University (1, Gagarin sq., Rostov-on-Don, 344000, RF),   Cand.Sci. (Eng.), associate professor, ScopusID 57210832767, ORCID: https://orcid.org/0000-0002-7508-913X, safari_2006@mail.ru

Claimed contributorship

V. V. Zhilin: collection and analysis of literature data; determination of research techniques; task setting. O. A. Safar'yan: academic advising; basic concept and the paper structure formulation.

All authors have read and approved the final manuscript.